Forschungszentrum Jülich
IBG-2: Institute for Bio- and Geosciences – Plant Sciences

Combining Fluorescence and Reflectance to Quantify Dynamics in Photosynthetic Regulation

Dissertation

zur Erlangung des Grades

Doktor der Agrarwissenschaften (Dr. agr.)

der Landwirtschaftlichen Fakultät
der Rheinischen Friedrich-Wilhelms-Universität Bonn

von

Kelvin Acebron

aus
San Pablo City, Laguna, Philippines

Bonn, 2021

Gutachter: Prof. Dr. Uwe Rascher
Zweiter Gutachter: Prof. Dr. Michael Frei

Tag der mündlichen Prüfung: 06.10.2021

Angefertigt mit Genehmigung der Landwirtschaftlichen Fakultät der Universität Bonn

All rules for study are summed up in this one:
learn only in order to create.
- *Friedrich Schelling*

SUMMARY

Photosynthesis in the field is anything but steady-state. Because environment is unsteady, understanding the photosynthetic activity *in situ* is challenging. Measurement of solar-induced fluorescence (SIF), along plant spectral reflectance (ρ), provides novel opportunity to understand the dynamic regulation of photosynthesis in the field. However, the interpretation of SIF is complicated by the complex relationship between photochemical and non-photochemical energy use in plant leaves. This thesis was aimed to establish a theoretical framework to link SIF and ρ with the photochemical and non-photochemical quenching (NPQ) of chlorophyll fluorescence (ChlF) at leaf level in order to elucidate the photosynthetic regulation in field conditions. First, I investigated the photosynthetic response of Chl-deficient soybean mutant during dark-to-light transition. Second, I traced SIF and ρ on a young canopy of turf grass after the application of Dicuran herbicide. Third, I probed the effect of different NPQ mechanisms on SIF and ρ using *Arabidopsis thaliana* having mutation on NPQ components that resulted to reduced NPQ capacity. And finally, I compared the photosynthetic response of glasshouse- and field-grown cassava plants in outdoor condition using active ChlF technique, passive SIF and ρ. As a result, I showed that Chl-deficient soybean mutant had lower NPQ, lower apparent F_{yield}, higher internal F_{yield} (Φ_f), lower fraction of open reaction centre (qL) and lower electron transport rate (ETR) as compared to wild type. On the other hand, no difference in PSII efficiency (Φ_{PSII}) was observed. The decrease in NPQ and ETR was likely resulted from the reduced PSII connectivity. While the increase in Φ_f is likely resulted from the reduction in NPQ, the decrease in apparent F_{yield} (or brightness) might have directly resulted from lower Chl concentration in the leaves of soybean mutant. I also showed that, SIF and photochemical reflectance index (PRI) significantly increased when photosynthesis was blocked using herbicide, indicating a degree of sensitivity of both SIF and PRI to the build up in lumenal pH. Furthermore, the results in Arabidopsis *npq* mutants showed that decrease in NPQ had similar increase in SIF regardless of the impaired NPQ mechanisms. Analysis of diurnal ρ strongly suggests that diurnal change in ρ during summer is connected to the activity of the xanthophyll cycle and not the PsbS-mediated conformational changes. When plants were suddenly exposed to cold, the onset of photoinhibition strongly quenched SIF in all Arabidopsis lines. Overall, the results I showed here covers the strength and limitations of remote sensing signals to quantify dynamic regulation in leaf photosynthesis and NPQ in the field and its contribution to the canopy productivity. In the future, parallel SIF and ρ measurements can be potentially used to test hypothesis on the functional role of NPQ in photosynthetic carbon gain in plants.

ZUSAMMENFASSUNG

Im Feld ist die Photosynthese alles andere als im Gleichgewicht. Da die Umgebung unstetig ist, ist das Verständnis der photosynthetischen Aktivität *in situ* eine Herausforderung. Die Messung der solar-induzierten Fluoreszenz (SIF), zusammen mit der spektralen Reflexion (ρ) der Pflanze, bietet eine neue Möglichkeit, die dynamische Regulierung der Photosynthese im Feld zu verstehen. Die Interpretation der SIF wird jedoch durch die komplexe Beziehung zwischen photochemischer und nicht-photochemischer Energienutzung in Pflanzenblättern erschwert. Ziel dieser Arbeit war es, einen theoretischen Rahmen zu schaffen, um SIF und ρ mit dem photochemischen und nicht-photochemischen Quenchen (NPQ) der Chlorophyll-Fluoreszenz (ChlF) auf Blattebene zu verknüpfen, um die photosynthetische Regulation unter Feldbedingungen zu erklären. Zunächst untersuchte ich die photosynthetische Reaktion von Chl-defizienten Sojabohnen-Mutanten während des Übergangs von Dunkelheit zu Licht. Zweitens verfolgte ich SIF und ρ in einem jungen Grasdach nach der Anwendung des Herbizids Dicuran. Drittens untersuchte ich den Effekt verschiedener NPQ-Mechanismen auf SIF und ρ unter Verwendung von *Arabidopsis thaliana* mit Mutationen an NPQ-Komponenten, die zu einer reduzierten NPQ-Kapazität führten. Schließlich verglich ich die photosynthetische Reaktion von Gewächshaus- und Freilandpflanzen unter Freilandbedingungen mit Hilfe der aktiven ChlF-Technik, passivem SIF und ρ. Als Ergebnis zeigte ich, dass die Chl-defiziente Sojabohnenmutante im Vergleich zum Wild type eine geringere NPQ, einen geringeren scheinbaren Ertrag, einen höheren internen Ertrag (Φ_f), einen geringeren Anteil des offenen Reaktionszentrums (qL) und eine geringere Elektronentransportrate (ETR) aufwies. Auf der anderen Seite wurde kein Unterschied in der PSII-Effizienz (Φ_{PSII}) beobachtet. Die Abnahme der NPQ und der ETR wurde wahrscheinlich durch die reduzierte PSII-Konnektivität verursacht. Während der Anstieg von Φ_f wahrscheinlich aus der Verringerung von NPQ resultiert, könnte die Verringerung der scheinbaren F_{yield} (oder "Helligkeit") direkt aus der geringeren Chl-Konzentration in den Blättern der Sojabohnen-Mutante resultieren. Ich habe auch gezeigt, dass der SIF und der photochemische Reflexionsindex (PRI) signifikant anstiegen, wenn die Photosynthese mit einem Herbizid blockiert wurde, was auf eine gewisse Empfindlichkeit von SIF und PRI gegenüber dem Aufbau des lumenalen pH-Wertes hinweist. Darüber hinaus zeigten die Ergebnisse in Arabidopsis *npq*-Mutanten, dass eine Abnahme des NPQ unabhängig von den beeinträchtigten NPQ-Mechanismen zu einem ähnlichen Anstieg des SIF führte. Die Analyse des täglichen Rhythmik von ρ deutet stark darauf hin, dass während des Sommers mit der Aktivität des Xanthophyll-Zyklus und nicht mit den PsbS-vermittelten Konformationsänderungen zusammenhängt. Als die Pflanzen plötzlich Kälte ausgesetzt wurden, löschte die einsetzende Photoinhibition die SIF in allen Arabidopsis-Linien stark ab. Insgesamt decken die hier gezeigten Ergebnisse die Stärke und die Grenzen von Fernerkundungssignalen ab, um die dynamische Regulation der Blattphotosynthese und der NPQ im Feld zu quantifizieren und deren Beitrag zur Kronenproduktivität zu bestimmen. In der Zukunft können parallele SIF- und ρ-Messungen möglicherweise verwendet werden, um Hypothesen über die funktionelle Rolle der NPQ bei der photosynthetischen Kohlenstoffgewinnung in Pflanzen zu testen.

ABBREVIATIONS

A	antheraxanthin
A	CO_2 assimilation rate
ADP	adenosine diphosphate
APAR	absorbed photosynthetically active radiation
ATP	adenosine triphosphate
BetaCar	beta carotene
CAM	crassulacean acid metabolism
Chl	chlorophyll
Chl*	chlorophyll in excited state
Chla	chlorophyll *a*
Chl_{a+b}	chlorophyll *a* and *b*
Chlb	chlorophyll *b*
ChlF	chlorophyll fluorescence
C_i	intercellular CO_2 concentration
CP22	PsbS protein
Cyt b_6f	cytochrome b_6f complex
DCMU	3-(3,4-dichlorophenyl)-1,1-dimethylurea
ETR	electron transport rate
F'_0	minimal fluorescence yield from PAM device measured using modulated light in light-adapted state
F'_m	maximal fluorescence yield from PAM device measured after saturating flash in light-adapted state
F_0	minimal fluorescence yield from PAM device measured using modulated light in dark-adapted state
F680	solar-induced fluorescence emission at 680 nm
$F680_{yield}$	solar-induced fluorescence yield at 680 nm (F680 normalised by PAR)
F760	solar-induced fluorescence emission at 760 nm
$F760_{yield}$	solar-induced fluorescence yield at 760 nm (F760 normalised by PAR)
fAPAR	fraction of absorbed photosynthetically active radiation
FCVI	fluorescence correction vegetation index
Fd	ferredoxin

Abbreviations continued...

F_{II}	fraction of absorbed light directed to photosystem II
FLEX	fluorescence explorer satellite mission of the European space agency
FLOX	Fluorescence Box, developed by JB Hyperspectral Devices (Düsseldorf, Germany)
F_m	maximal fluorescence yield from PAM device measured after saturating flash in dark-adapted state
FRR	fast-repetition rate principle in LIFT
F_s	steady-state fluorescence yield
F_v/F_m	maximum efficiency of the photosystem II for photochemistry
F_{yield}	fluorescence yield
GPP	gross primary productivity
g_{sw}	stomatal conductance to water vapour
I	irradiance
iFLD	improved Fraunhofer Line Depth method
IRGA	infra-red gas analyser
J_a	electron transport rate estimated by gas-exchange parameters
LHCII	light-harvesting antenna complex of photosystem II
LIFT	light-induced fluorescence transients
Lut	lutein
NADPH	nicotinamide adenine dinucleotide phosphate
NCHU	National Chung Hsing University in Taiwan
NDVI	normalised difference vegetation index
Neo	neoxanthin
NIRv	near infra-red reflectance of vegetation
NPQ	non-photochemical quenching
NSA	non-stress acclimated (glasshouse-grown plants)
PAM	pulse-amplitude modulation
PAR	photosynthetically active radiation
PC	plastocyanin
PI	photoprotective index
PQ Pool	plastoquinone pool

Abbreviations continued...

PRI	photochemical reflectance index
PSI	photosystem I, also called P700
PSII	photosystem II, also called P680
Q_A	platoquinone A
qE	energy-dependent quenching component of NPQ
qI	photoinhibitory quenching component of NPQ
qL	fraction of photosystem II that are open
qLd	value of qL in the dark during photodamage
qN	percentage of non-photochemical quenching
qP	extent of photochemical quenching
qPd	value of qP in the dark during photodamage
qT	state-transition
qZ	zeaxanthin-dependent quenching component of NPQ
R	reflectance, also synonymous to ρ
R_d	dark-respiration rate
REIP	red edge inflection point
ROI	region of interest
Rubisco	ribulose biphosphate carboxylase-oxygenase
SA	stress acclimated (field-grown plants)
SCOPE	soil-canopy observation, photosynthesis, and energy balance
SE	standard error
SFM	spectral fitting method
SIF	solar-induced fluorescence
SIF_{down}	downwelling SIF emission
SIF_{tot}	total solar-induced fluorescence (upwelling plus downwelling SIF emission)
SIF_{up}	upwelling SIF emission
SIF_{yield}	solar-induced fluorescence yield (SIF normalised by PAR)
T	transmittance
UTC	coordinated universal time
V	violaxanthin

Abbreviations continued...

VAZ cycle	violaxanthin-antheraxanthin-zeaxanthin cycle
V_{cmax}	maximum carboxylation efficiency
VDE	violaxanthin de-epoxidase
VIS-NIR	visible and near infra-red region
VPD	vapour pressure deficit
WT	wild type
WT_{At}	wild type *Arabidopsis thaliana*, also called Col-0 ecotype
WT_{sb}	wild type soybean, also called Eiko cultivar
Z	zeaxanthin
α	absorbance
Γ	CO_2 compensation point
$\Delta\rho$	change in spectral reflectance
η	efficiency for energy transfer
ρ	spectral reflectance
ρ_{adj}	adjusted spectral reflectance
σ_{PSII}	functional absorption cross section of photosystem II
Φ_{CO2}	efficiency for CO_2 assimilation
Φ_D	efficiency for basal heat dissipation
Φ_f	efficiency for fluorescence emission
$\Phi_{f,D}$	efficiency for fluorescence emission and basal heat dissipation
Φ_{int}	internal fluorescence yield, equivalent to F_{yield} or Φ_f
Φ_{NPQ}	efficiency for regulated heat dissipation
Φ_{ovl}	apparent fluorescence yield, equivalent to brightness
Φ_P	photochemical yield
Φ_{PSII}	effective quantum efficiency of the photosystem II, also called simply as photosystem II efficiency

TABLE OF CONTENTS

Parts of this thesis is published in Behmann et al. (2017), Pinto et al (2020) and Acebron et al. (2020) through the course of the PhD program and is hereby cited in Boxes mentioned in the Methods, Results and Discussion sections. My contributions for each paper are listed in Chapter 6 of this thesis.

1. INTRODUCTION

Photosynthesis is fundamental for plants' growth. Because of unstable availability of the substrates (i.e. water, carbon dioxide (CO_2) and light), the active process of photosynthesis is anything but steady-state. This makes it challenging to understand the dynamic regulation of photosynthesis in the field condition. Consequently, this creates a knowledge gap between plant physiology and agricultural production, ecophysiology and plant functional ecology. The dynamics of photosynthesis can be explored by looking at the conversion of solar energy to chemical energy in a process called photochemical reaction. Fluorescence emission can be used to understand the changes in the efficiency for photochemistry and heat dissipation. That is, due to limited photochemical energy conversion, fluorescence photons are emitted and heat is dissipated. Despite this link, the regulatory balance among the three processes is not yet fully understood.

1.1. Light-Dependent Reaction of Photosynthesis

Before the solar energy is absorbed and converted into chemical energy, photons of light that reaches the leaf surface are either reflected or transmitted. This primary light partitioning mostly rely on the energy (wavelength) of the photons and the absorption features of the pigment molecules. Light energy in the range of 400 to 700 nm wavelength (also called photosynthetically active radiation, PAR) are selectively absorbed by plant pigments (Chls and carotenoids). From here, photons of light have three fates: photochemistry, fluorescence emission, and heat dissipation (Butler, 1978). Photochemistry, the process of converting light energy to chemical energy, is a rate limited process (Sukenik et al., 1987) which when slowed down, creates feedback effect to the efficiency of photosystem II (Φ_{PSII}) that subsequently forces the excited Chl molecules (Chl*) to immediately redirect and dissipate excess energy through fluorescence or heat dissipation (also called non-photochemical quenching, NPQ) (Genty et al., 1989). The series of electron transport starts from the excited P680 (P680*) molecule which has free electron capable of donating its electron to pheophytin (Fajer et al., 1975; Allakhverdiev et al., 2010). The electron then reduces the primary quinone type electron acceptor called plastoquinone A (Q_A), and in a slower rate, reduces Q_B (Diner et al., 1991). When Q_B receives two electrons

from Q_A, it binds to the plastoquinone pool (PQP) and passes the electron through the cytochrome b6 and f (Cyt b_6f; Hill & Bendall, 1960), next to plastocyanin (PC) and ultimately to photosystem I (PSI) (for overview of the Z-scheme, see Shevela & Björn, 2017). On one end of the reaction chain, the highly oxidant $P680^+$ instantly accepts another electron from the donor Z (a tyrosine residue of the D1 protein) which is oxidised by the splitting of H_2O molecule through the oxygen-evolving complex (OEC) situated at the lumen side of the photosystem II (PSII; McEvoy & Brudvig, 2006). The splitting of H_2O by OEC is driven by the unstable state of PSII as a result of trapping excitonic energy transfer from the absorbed PAR (APAR).

The electron transport can both occur in a linear and cyclic pattern (Bendall & Manasse, 1995). The linear electron flow happens when the electron is transferred from H_2O to $NADP^+$ via the PSII and PSI scheme while cyclic electron flow occurs from the recycling of electrons from reduced ferrodoxin (Fd) or NADPH through the plastoquinone shuttle (Hill & Bendall, 1960). As a result, linear electron flow produces both the NADPH and ATP while cyclic electron flow is only involved in the production of ATP. Thus, NADPH is produced from the series of electron transfer from H_2O to NADPH while ATP is produced by building pH gradient across the thylakoid membrane from the oxidation of H_2O molecule and pumping H^+ protons through the plastoquinone shuttle (see review from Allen, 2003). Both NADPH and ATP will then be used in the fixation of the CO_2 via the ribulose bisphosphate carboxylase-oxygenase (Rubisco) in the Calvin cycle to form sugar molecules (see mini-review from Raines, 2003).

1.2. Fates of Absorbed Light in the Antenna System and the Reaction Centre

Chlorophyll molecules surround photosystems which serve as antennae for light capture (Bassi et al., 1987). Primarily, the absorption of energy from the light occurs specifically at the “head” of the Chl molecule which contains double bonds and a Magnesium (Mg^{2+}) core. These double bonds have π conjugated systems containing delocalised electrons that can be easily excited by photons turning the electron of the Chl molecule from ground state to higher state once energy is absorbed. The excited electron is short-lived and can lead to three different fates: (1) transfer the energy either to a

neighbouring Chl molecule through the resonance of excited electron or directly transferring the electron to an electron acceptor, (2) relaxation of Chl molecule through heat dissipation, (3) emission of fluorescence with lower energy level (higher wavelength) as the electron undergoes interconversion from 1st excited singlet state to the ground state (see review from Porcar-Castell et al., 2014).

Chlorophyll molecules are embedded in a protein complex called the light-harvesting complex and are arranged such that excitons migrate through the Chl molecules via resonance energy transfer (see review from Sener et al., 2011). As the plant absorbs more light energy, the rate of photochemistry becomes limiting and absorbed energy will be re-emitted at a longer wavelength via fluorescence emission or dissipated as heat (see next sub-chapter on NPQ). Hence, the three fates of absorbed light serve as competing relaxation avenues of Chl* molecule such that a decrease in the rate of photochemistry will have a relative increase in the rate of fluorescence and/or heat dissipation. This relationship however is non linear and difficult to separate. Nevertheless, the process of photochemistry begins within picoseconds (10^{-12} sec) making it a more favoured downhill reaction as compared to the fluorescence emission that occurs in shorter scale nanoseconds (10^{-9} sec). Fluorescence spectrum ranges from 650 to 800 nm wavelengths with peaks at ~685 and 740 nm emitting from PSII and single peak at 740 nm for PSI. On the other hand, heat dissipation or NPQ serves as a photo-protective mechanism (i.e. photosystem II efficiency) to excessive high light condition and can be activated in seconds or minutes depending on the NPQ component that is operating (see Ruban, 2016).

1.3. Non-Photochemical Quenching (NPQ)

Plants have developed the mechanism to protect themselves from harsh environments. For instance, as a response to high light condition, leaves dissipate heat through different mechanisms of NPQ. Thus, the nature of thermal dissipation of excess absorbed energy occurs in molecular level, albeit the exact mechanisms is still a matter of scientific debate. When leaves experience changes from low to high light conditions, thylakoid lumen becomes acidic. The accumulated H^+ protonates PsbS protein, while violaxanthin de-epoxidase (VDE) is activated, resulting to the conversion of violaxanthin (V)

to zeaxanthin (Z) via antheraxanthin (A), i.e. the VAZ cycle (Yamamoto et al., 1999; Li et al., 2000; Li et al., 2004). Consequently, conformational changes of the light harvesting complex of photosystem II (LHCII) antenna is induced, switching the mode from light harvesting to heat dissipation (for review, see Horton et al., 1994; Müller et al., 2001; Ruban, 2016). In addition, VDE also plays a role in converting lutein epoxide to lutein in some species where lutein cycle operates (García-Plazaola et al., 2007).

Different components of NPQ are identified by their relaxation kinetics during leaf darkening. Namely they are: energy-dependent quenching (qE), zeaxanthin-dependent quenching (qZ), state-transitions (qT) and photoinhibitory quenching (qI). Rapidly inducible and reversible qE is the predominant form of NPQ. It occurs from seconds to minutes and responds to light fluctuations during warm conditions (Müller et al., 2001). qE is mainly associated with light-induced proton transport into the thylakoid lumen which results in acidification of the lumen (Krause et al., 1982). PsbS protein (CP22) is considered as an important component of dissipating excess light energy. It is a ubiquitous pigment-binding protein associated in PSII. Studies involving *Arabidopsis thaliana* mutants without qE component revealed lack of PsbS protein (*npq4*) and consequently showed no conformational change of the LHCII complex (Li et al., 2000). Yet, *npq4* mutant had normal xanthophyll cycle (Roach & Krieger-Liszkay, 2012). In the same report, *npq4* mutants generated higher singlet oxygen ($^1O_2$) in chloroplasts which accompanies a higher extent of PSII photoinhibition. Over-expression of PsbS protein (*oePsbS*) protects more the PSII from $^1O_2$ under high light condition while the PSI damage is more expressed compared to wild type and *npq4* mutants.

In addition, NPQ is dependent to Z (Demmig-Adams, 1990; Demmig-Adams et al., 1990), which was eventually termed as qZ type (Jahns & Holzwarth, 2012). It was argued that Z is either capable of quenching the singlet excited Chl molecules (Owens et al., 1992) or directly controlling the conformational structure of the LHCII (Horton et al., 1991). Nonetheless, this component responds slower than qE and occurs in few minutes to an hour. Successful genetic dissection of photoprotection in Arabidopsis was reported by Niyogi et al. (1997) in which they used Arabidopsis *npq1* mutant to study xanthophyll-dependent photoprotection in plants. This mutation affects structural gene encoding the enzyme VDE which subsequently unable to form Z and consequently resulted to lower levels of qE as well

as less photoprotective capacity (Havaux & Niyogi, 1999). In the same conference reported by Niyogi et al. in 1997, they found out that this mutant still exhibit substantial amount of pH-dependent NPQ, suggesting that there is a component of NPQ independent from the xanthophyll cycle. On the other hand, another *npq* mutant (*npq2*) reported by the same group showed constitutive Z accumulation. Because of this mutation, *npq2* mutant showed faster NPQ induction compared to wild type and *npq1* mutant.

The physical migration of LHCII antenna between the two photosystems is called state transitions (qT) which involved a reversible phosphorylation of LCHII driven by thylakoid kinase STN7. State-transition is said to be only important in low light levels (see review of Dietzel et al., 2008). Experimental evidence showed changes in fluorescence emission at 77K in Arabidopsis mutants having mutations in state transitions. Arabidopsis *stn7* mutant which showed no state transitions (LHCII stays in PSII) showed decrease in fluorescence intensity at the peak between 730 nm and 750 nm (Bellafiore et al., 2005). In contrast, *stn7oe* mutants (LHCII presumably stays in PSI) showed increase in fluorescence intensity in the same spectral region (Wunder et al. 2013).

Finally, qI type is a slowly reversible component of NPQ. It is also known as sustained NPQ which takes several hours to relax and is also associated with reduced maximal efficiency of photochemistry (F_v/F_m parameter). This affects the PSII efficiency of the leaf. Reduced F_v/F_m is strongly linked to damaged photosystem II (PSII) reaction centre, as well as major reorganisation of pigment-protein complex in the thylakoid membrane leading to photoinhibition of photosynthesis, and ultimately resulting to down-regulation of carbon fixation (Powles, 1984; Krause, 1988; Aro et al., 1993). As a result, plants reduce the efficiencies of PSII (Φ_{PSII}) and CO_2 assimilation (Φ_{CO_2}) which in turn reduces the quantum yield of leaf photosynthesis (Long et al., 1994). Furthermore, qI is associated with Z accumulation (Demmig-Adams & Adams, 2006). Incidentally, qE and qZ are compounding with qI. The quenching mechanism changes depending on the prevailing environmental condition (Verhoeven, 2014).

1.4. Measurements of Fluorescence Emission and Spectral Reflectance

Measurement of the intensity and kinetics of ChlF has become the working benchmark in detecting photosynthetic activity *in situ* of plants as well as stress physiology, ecophysiology and phytopathology (Enriquez & Borowitzka, 2010; Maxwell & Johnson, 2000). This is either with the use of pulse-amplitude modulation (PAM; Baker, 2008) or with light-induced fluorescence transient (LIFT; Kolber et al., 2005). However, despite the theory that NPQ is a form of heat dissipation, thermal measurements at leaf level is complicated due to greater contribution of stomatal control to heat exchange. And, precise measurement of heat dissipation had only been done by measurement of thermal photo-acoustic signals (see review from Buschmann, 1999). More commonly, heat dissipation can be estimated using the NPQ parameter from PAM ChlF which is calculated by comparing the maximal fluorescence in a dark-adapted and light-adapted states (Bilger & Björkman, 1990). While in remote sensing, photochemical reflectance index (PRI) is used to track changes in the xanthophyll cycle and further used to predict light-use efficiency (Gamon et al., 1990; Peńuelas et al., 2011). Formation of Z changes the absorbance in 505 nm, while changes in LHCII conformation consequently alters the absorbance in 535 nm (Krause, 1973; Bilger & Björkman, 1994). This opened opportunities to measure leaf spectral reflectance (ρ) to monitor pigment changes that resulted from light adjustments (Gamon & Surfus, 1999). However, recent study by Rahimzadeh-Bajgiran et al. (2012) showed that this parameter was highly influenced by plant pigments and can be more correlated to Chl content than to NPQ and xanthophylls. Recently, sensitivity of PRI to NPQ was validated in situ using Arabidopsis *npq1* and *npq4* mutants. Kohzuma & Hikosaka (2018) verified that PRI is capable of tracking qZ but not the total NPQ activity yet also demonstrated the sensitivity of PRI to changes in pH. Previous reports already stated that the limitation of PRI rests on the changes in pigment pools, leaf albedo (Busch et al., 2009; Wong & Gamon, 2015) and canopy structure (Barton & North, 2001; Garbulsky et al., 2011). Nevertheless, Nichol et al. (2006) argued that PRI can potentially account for 70% of total NPQ processes based on the fact that Z synthesis is necessary for 70% of the total NPQ. In addition to this, van Wittenberghe et al. (2019) argued that fast and slow changes in ρ during light induction may be attributed to a structural change involving both carotenoids and Chl which opens new opportunity to relate changes in ρ to other mechanisms of photoprotection.

Despite of the uncertainty on understanding the NPQ in canopy level, there has been successful works that modifies the NPQ response of plant to maximise the photosynthetic potential. Kromdijk et al. (2016) have demonstrated that by increasing the recovery of photoprotection in tobacco plants, a higher photosynthesis is achieved which was translated to higher biomass production in the field. However, a contrasting result was observed when a similar gene construct was inserted in Arabidopsis plants. One question that is of paramount interest to plant scientists is whether NPQ is optimised (Horton et al., 2008; Johnson et al., 2008). Thus understanding the regulation of NPQ in canopy scale can provide insights in solving this question.

1.5. Dynamic Regulation of Photosynthesis

PAM fluorometers are widely used to probe the mechanistic interplay between fluorescence yield (F_{yield}), NPQ, and effective quantum yield of PSII (Φ_{PSII}) (Quick & Horton, 1984; Krause & Weis, 1991; Maxwell & Johnson, 2000). At leaf level, there is a clear inverse relationship between NPQ and Φ_{PSII} in a course of a day, protecting plants from light stress (i.e. photoprotection). Studies done in non-stressful conditions showed that the Φ_{PSII} decreases while NPQ increases with increasing light intensity. This relationship is tightly linked with the de-epoxidation state of the xanthophyll cycle (Demmig-Adams et al., 1995). In the winter, sustained NPQ predominates especially during overwintering of evergreen plants (Öquist & Huner, 2003; Verhoeven, 2014). Under a bright and clear sky, light intensity and temperature are low in early morning and late in the afternoon and reach the peak during noon. This trend has been shown to have significant effect on photosynthetic regulation. To illustrate, measurement on a fully-developed leaf of a tea plant (*Camellia sinensis* (L.) O. Kuntze) done by Mohotti & Lawlor (2002) showed that maximum CO_2 assimilation (A) increases in the morning as the light intensity increases between 8:00 am to 10:00 am. Similarly, both the intercellular CO_2 concentration (C_i) and the stomatal conductance to water vapour (g_{sw}) were high in the morning, while leaf temperature is cooled and vapour pressure deficit (VPD) is small. During noon time where light intensity, leaf temperature and VPD is high, NPQ can reach maximum and consequently reduces A, g_{sw} and photochemical quenching (qP). The activation of NPQ helps protect the photosynthetic apparatus from photo-damage. Nevertheless, Mohotti & Lawlor (2002) have

found a recovery in g_{sw} and C_i while A remains low. Similar response of photosynthetic rate where found in wheat fields while both water-use and radiation-use efficiencies calculated diurnally showed bimodal behaviour with maximum values in early morning and late in the afternoon (Evrendilek et al., 2008).

Leaves adopted to either sun or shade environment largely differ in photosynthesis (Boardman, 1977). Differences in photosynthetic rates between sun and shade leaves can be comparatively measured using ChlF technique as previously demonstrated in the study conducted by Lichtenthaler et al. (2007b). For instance, the chloroplasts of shade-adapted leaves have large grana stacks which may contain as many as 160 thylakoids per granum and can change the fluorescence intensity as observed in the thylakoids suspended in basic medium (Jia et al., 2012). *In situ*, fluorescence signal can be affected by the reabsorption of photons within the leaf (Porcar-Castell et al., 2014). A study conducted by Nobel in 1976 demonstrated the change in photosynthetic rates of sun vs shade leaves and showed that sun-adapted leaf was shorter in length compared to shade leaf yet the sun leaf had higher Chl content per unit area, thicker mesophyll cells and higher ratio of internal to external leaf area. Also, Malkin & Fork (1981) found higher photosynthetic unit size (number of Chl per reaction centre) in shade plants compared to sun plants. Furthermore, plants grown under high light had higher mesophyll cell area and total mesophyll cell volume per unit leaf area compared to plants grown to low light condition. This translated to higher photosynthetic rates under sunny conditions yet some studies show similar rates under shaded condition (Yun & Taylor, 1986). The same trend of increased photosynthetic rate at sun leaf was observed in some broadleaf trees which is also characterised by higher levels of total Chl_{a+b} and total carotenoids (Lichtenthaler et al., 2007a). Furthermore, leaves also acclimate at low and high light condition by redistributing its chloroplast within the cell. It is known that the chloroplasts move in order to avoid photodamage from excess light (Kasahara et al., 2002). During high light condition, chloroplast are redistributed on the lateral side of the cell to avoid excessive light exposure. Under low light, chloroplasts are redistributed on top and bottom part of the cell to efficiently capture low light for energy conversion. However, the importance of redistribution of the chloroplasts at the bottom side of the cell is still unknown.

Age of the leaf can influence the photosynthetic rates at various ways and leaf senescence is a major aspect. One of the major factors that changes photosynthetic rates at

ageing leaf is the degradation of Chls. In estimating plant productivity at canopy level, it is important to know how much of its leaf parts are still contributing to photosynthetic carbon gain (Harper, 1989). In pioneer trees, photosynthetic rates decrease as the leaf ages (Kitajima et al., 2002). Study of grapevine leaves under natural environment showed that base leaf (older) had lower total Chl and soluble proteins per leaf mass. Likewise, base leaf showed significant inhibition of PSII and whole chain while slight inhibition was observed in PSI activity. Minimal fluorescence yield (F_0) was higher while F_v/F_m was lower compared to middle and apical leaves (Bertamini & Nedunchezhian, 2002). Also in another study of Bertamini & Nedunchezhian (2003) under controlled condition, younger leaves of grapevine showed lower Chl_{a+b} per area basis and higher amount of total carotenoids. In contrast to their previous studies, there was a greater decline in PSII activity and whole chain in young leaves under high light condition compared to older leaf. The theory of optimal leaf longevity states that a tree is expected to shed off its leaves once its no longer contributing to the net carbon gain (Givnish, 1978; Chapin, 1980).

Clearly, the biophysical and biochemical efficiency of photosynthesis is actively regulated by prevailing environmental conditions and is exhibited at different spatial and temporal scales. Photosynthetic regulation is influenced by the photoprotective processes (Demmig-Adams & Adams, 1992; Murchie & Niyogi, 2011) as well as the leaf status that resulted from the long-term acclimation of developing leaves to the sudden changes in environmental conditions (Walters et al., 1999; Walters, 2005; Athanasiou et al., 2010). These regulatory processes were usually and mainly observed and studied at leaf scale. Understanding the dynamic regulation of photosynthesis in the field still remains a challenge (Rascher & Nedbal, 2006), particularly in the capability to conduct phenotyping strategies that will account dynamic changes in environment (Murchie et al., 2018). Exploring and understanding these variations in a plant canopy scale is of paramount importance for plant research as it can provide (1) insights on plants' evolution, (2) fundamental knowledge to breed crops that are efficiently responding to the present fluctuating environments (Horton, 2000) and (3) understanding of plants' adaptation in future global environmental conditions (Schurr et al., 2006).

1.6. Solar-Induced Fluorescence (SIF)

Fluorescence emission originates from the Chl molecules, resulting from de-excitation when the high-energy electrons from singlet excited state is transformed back to a ground state. Chls are embedded in a protein matrix serving as a light-harvesting antenna, including other pigments (or protein subunit) that may directly control fluorescence quenching or may change the structural configuration of LHCII antenna. This results to the change in the balance among efficiency for fluorescence emission, heat dissipation and photochemistry at photosystem level, *in situ*.

SIF is a passive fluorescence signal that can reflect the status of photosynthesis of leaves (and potentially whole plant) under natural condition. Several research have already linked SIF signal to dynamic photosynthesis (Frankenberg et al., 2011; Joiner et al., 2011; Guanter et al., 2014; Rossini et al., 2015) as well as to a variety of plant traits that responds to major abiotic stress (Ać et al. 2015) occurring both in short term (diurnal) and long term (seasonal) regulation. Such plant traits is not only limited to photosynthetic efficiency (Rossini et al., 2015; Pinto et al., 2016; Pinto et al., 2020; Maguire et al., 2020), but also APAR (Yang et al., 2015; Zeng et al., 2019) and NPQ (Acebron et al., 2020; Magney et al., 2019; van Wittenberghe et al., 2020), providing a holistic overview on plant light-use efficiency under natural conditions. Hence understanding mechanisms at leaf level can also provide explanation on the dynamic relationship between SIF, Φ_{PSII} and NPQ at a homogeneous canopy (especially that in the case of mono-cropping system in agricultural fields).

Because of this novelty, FLuorescence EXplorer (FLEX, Drusch et al., 2016) has been selected as the eight earth explorer satellite mission of the European Space Agency (ESA) dedicated to provide a timely global maps of SIF to quantify photosynthetic activity of the terrestrial vegetation. Despite of this great potential, there are several challenges on how to mechanistically link SIF to photosynthesis both at leaf and canopy level. Earth satellite map of ChlF largely requires understanding the functional meaning of SIF (Frankenberg et al., 2011; Joiner et al., 2011). This is best done at leaf level. Furthermore, more research has to focus on correcting the retrieved SIF signal at canopy level before we can use this signal on understanding diversity in plant functional traits (Aasen et al., 2019). In the past, more studies has been conducted at the leaf level (van Wittenberghe et al., 2013;

Vilfan et al., 2019; Magney et al., 2017), top of canopy (Pinto et al., 2016), airborne (Zarco-Tejada et al., 2000; Rascher et al., 2015), and satellite platforms (Frankenberg et al., 2011; Joiner et al., 2011) providing a comprehensive understanding on how SIF signal changes across important spatial and temporal domains. Moreover, this also provides increasing opportunities to understand not only photosynthesis of plants under natural environment at different scales (Rascher et al., 2009) but also plant structure, biophysical traits and light use efficiency that may contribute to overall productivity of the plant. Although SIF is not as informative as the active fluorescence signal, its novelty lays on the potential mapping of SIF on a large scale.

Linking SIF to the dynamics, kinetics and instantaneous status of photosynthesis require understanding the excitonic energy transfer in the LHCII as well as the basal and regulatory nonphotochemical quenching processes (Porcar-Castell et al., 2014). The concept of excitons in LHCII antennae complex is an extension from a classical solid-state physics to chemical physics and biophysics. This means that the properties observable at the leaf level result from their atomic- and molecular-scale properties. To understand relationship of SIF to photosynthesis at leaf level is of paramount importance. Because of the fundamental relationship of ChlF, photochemistry, and heat dissipation is dynamic, linking SIF to photosynthesis would need a holistic understanding of the interplay of NPQ mechanisms operating in the field conditions. Although technologies that exploit SIF signal to model photosynthesis are reaching maturity, the inherent nature of ChlF quenching is complicated by the antagonistic nature of photochemical and non-photochemical processes.

Because SIF signal has distinct characteristics, several properties of it can be quantified that is linked to some important plant traits. Among the properties of SIF, the ratio of red to far-red SIF are well documented for studying its relation to stress, canopy structure (reabsorption) and gross primary productivity (GPP, Mohammed et al., 2019). There are also techniques on how to normalise SIF in order to link to other more inherent plant traits. Such techniques involved quantifying absorbed PAR and escape probability of fluorescence photon from the canopy (Yang et al., 2020; van der Tol et al., 2019).

1.7. Linking SIF and Reflectance to Photosynthesis

SIF signal is a mixture of biophysical (structural) and biological (physiological) phenomenon that occurs at the sub-cellular, cellular, leaf, and canopy as well as their interaction to environment. To link SIF signal to changes in photochemical and nonphotochemical energy use, it is vital to account the structural component and its effect onto SIF emission as well as its detection. Meaning, it is necessary to disentangle the contribution of biophysical parameters from leaf to canopy in order to remain the contribution of physiology to changes in SIF intensity across the fluorescence spectra. Unfortunately, this is not easily achievable. Because of the complexity and the high-computing capacity required for modelling the probabilistic path of fluorescence photon from the leaf component to the whole canopy, understanding the link of SIF to photosynthesis requires leaf level observation. At this level, the factors for fluorescence emission is narrowed down into: (1) the amount of light absorbed, (2) the excitonic energy transfer within the LHCII antenna, (3) the efficiency of the PSII and the rate of photosynthetic electron transport, and (4) different regulatory and non-regulatory NPQ mechanisms that could be operating in a wide range of environmental conditions.

SIF can be used to improve the modelling of diurnal courses of GPP which can be tightly linked to the carbon fixation (Damm et al., 2010). However, because SIF reflects both photochemical and non-photochemical events, it does not linearly correlate to photosynthesis. Furthermore, nitrogen content, Chls *a* and *b* concentration, maximum carboxylation capacity (V_{cmax}) and canopy structure changes the relationship between GPP and fluorescence in the far-red region (F760) (Migliavacca et al., 2017); and combining SIF with PRI improves the diurnal modelling of GPP (Schickling et al., 2016). Using numerical simulations, Atherton et al. (2016) showed that combining SIF with PRI can predict the dynamics of photochemical and non-photochemical activities at leaf level. In the context of the FLEX satellite mission, it is necessary to understand the influence of NPQ on SIF and ρ in order to correctly interpret these signals in terms of apparent photosynthesis or GPP (Drusch et al., 2016). Hence, it is crucial to understand to which extent the Φ_{PSII} and NPQ are modulating SIF under given environmental conditions to where the leaf is exposed. Although modelling has been greatly improved by integrating leaf gas-exchange parameters, its application is still limited to healthy and not chronically photoinhibited leaves (Hikosaka & Noda, 2018). Recent efforts linking active and passive fluorescence signals, together with

CO_2 uptake, led to the development of tools which aid in understanding the relationship of SIF to photosynthetic functions of a leaf (Magney et al., 2017; Vilfan et al., 2019).

Pinto et al. (2016) provided a proof of concept that SIF images on top of canopy showed variability resulting from the spatial and temporal patterns in leaves that differ in photosynthetic efficiency. Since canopy photosynthesis is a totality of its individual leaf parts, understanding spatial and temporal variation of photosynthesis at leaf level is vital. To upscale leaf level SIF signal to the canopy, the escape probability of fluorescence photon from the plant canopy must be accounted. Moreover, SIF signal also must be corrected to the amount of light absorbed (in the PAR region) as well as the amount of fluorescence photon re-absorbed from within the leaf and within the plant canopy, both can be potentially measured in plant reflectance signal. Because measuring SIF on top of canopy is highly related to incoming radiation, scattering effect and leaf angularity also has to be considered. When all these parameters are considered at canopy level, other plant traits related to its response to major abiotic stresses can be quantified other than photosynthesis. For example, Rascher et al. (2009) reported that the leaf level measurements of fluorescence using active approaches and the canopy level using SIF on corn canopy provided proof of the changes of SIF at 760 nm related to stress. Similarly, it was shown in previous studies that fluorescence in both red and far-red region and their ratio changes at different vegetation type due to differences in leaf and canopy structure (Rossini et al., 2016). Moreover, Wieneke et al. (2016) demonstrated the sensitivity of both red and far-red region to physiological changes in plants. In particular, the intensity of red and far-red signals reduces at water-stressed plants while low temperature increases both signals (Ač et al., 2015). Furthermore, studies demonstrating SIF sensitivity to track diurnal and seasonal changes in plant canopy scale has been widely explored (Cogliati et al., 2015; Migliavacca et al., 2017; Liu et al., 2017; Pinto et al., 2016; Rascher et al., 2009; Rossini et al., 2015; Wieneke et al., 2016; Yang et al., 2015). Despite of these, variations in SIF in a plant canopy scale are mainly attributed to large variability of surface illumination caused by canopy structure and sun position (Pinto et al., 2016). Short-term changes in SIF and SIF_{yield} (SIF normalised by APAR) can be mainly attributed in changes in APAR while long-term changes is highly affected by phenological changes such as changes in pigmentation and leaf area (Daumard et al., 2012; Rossini et al., 2010). In terms of actual photosynthetic efficiency, both Rossini et al. (2015) and Pinto et al. (2016; 2020) clearly demonstrated the change in SIF with DCMU-treated grass plots

inferring that the transient change in SIF is related to photosynthetic status and protection mechanism in plants.

Several modelling concepts aim to quantify structural and physiological contribution on top-of-canopy SIF signal to further quantify and understand the energy balance from leaf to ecosystem level. To do this, simultaneous quantification of SIF, photochemistry and NPQ at the leaf is essential. Remarkably, the quantitative link between photosynthesis, SIF, and NPQ is usually sparse and inconclusive, mainly due to the compounding nature of different modes of NPQ. To further improve existing models, it is important to outline the factors that can affect the SIF estimation. There are also efforts to link leaf level photosynthesis model to the canopy fluorescence model by considering radiative transfer model from the leaf to the canopy. Nevertheless, it has been widely shown that SIF (especially the far-red signal) is correlated with GPP which has been shown to be due to the incident light and the total light absorption by the Chls in the plant canopy (Joiner et al., 2014; Goulas et al., 2016; Yang et al., 2015).

The Soil-Canopy Observation, Photosynthesis, and Energy Balance (SCOPE) model from van der Tol et al. (2014) has been widely used to link leaf level fluorescence to photosynthesis by also integrating the photosynthesis model of Farquhar et al. (1980). Using (SCOPE) model, van der Tol et al. (2014) demonstrated the effect of relative light saturation on the relationship between F_{yield} and photochemical yield. In low light, the relationship between photochemical yield and F_{yield} is inversely proportional. During this scenario, the decrease in F_{yield} is controlled by the photosynthetic induction. While in high light, this relationship becomes directly proportional due to the regulation of NPQ. Under severe stress, a further decrease in photochemical yield is equivalent to increase in F_{yield}. Furthermore, the relationship between F_{yield} and photochemical yield is temperature dependent, i.e. temperature above 35°C generally shifts this dynamic correlation. Although the relative light saturation may indicate the level of NPQ although no mechanistic studies has been done so far in order to illustrate the effect of difference components of NPQ to SIF – photosynthesis relationship. Nonetheless, the strength of SCOPE model was shown to predict net photosynthesis of a canopy with the use of SIF retrieved at O_2A and O_2B bands Verrelst et al. (2016).

1.8. Aim of the Study

The purpose of this thesis is to understand the spatio-temporal dynamics of photosynthesis using SIF and ρ. More specifically, the objective is to provide a theoretical framework on the photochemical and non-photochemical interpretations of SIF and ρ signals measured on plant leaves under field condition. To approach this, the following questions were asked:

1. What happens to PSII efficiency and NPQ when leaf is transitioned from dark to light? And can we use this to understand the energy balance in the leaf during fluctuating light?

2. How dynamic is the relationship of F_{yield} to NPQ and PSII efficiency in the field condition? How is SIF_{yield} related to intrinsic F_{yield} and APAR?

3. How related is PRI to NPQ? And how can we track NPQ activity in the field using spectral reflectance? and;

4. How do we relate the temporal dynamics of SIF and PRI to dynamic interplay of photosynthesis and NPQ in the field?

2. MATERIALS AND METHODS

This section provides a detailed description of the materials and methods conducted in this thesis. The sub-sections are organised in order to minimise redundancy of methodological descriptions while maintaining the fluidity and relevance to the overall structure of the research. First, plant materials and their growing conditions were described together with the experimental setup and the main treatment effects. Second, active and passive fluorescence measurements were compared both in terms of physical (or engineering) as well as the physiological interpretations of the parameters derived from each technique. Third, mathematical and physiological descriptions of the relevant parameters which were acquired from the fluorescence, spectral reflectance and gas-exchange measurements were summarised with reference to the previously published studies.

2.1. Plants Materials and Experimental Setup

2.1.1. Soybean Chlorophyll-Deficient Mutant versus Wild Type

To investigate the effect of light absorption on $F_{yield,}$ Φ_{PSII} and NPQ regulation during photosynthetic light induction, two soybean varieties (*Glycine max* L.) were used in this study with different Chl content: the pale mutant Minngold which is Chl-deficient (Campbell et al., 2015); and the green Eiko, a wild type cultivar (WT_{Sb}; Fig. 1). The plants were sown in a 3 L pots and grown inside a growth chamber with three different light regimes: (1) constant light, (2) diurnal with non-fluctuating light, and (3) diurnal with fluctuating light. In constant light chamber, the light was set to 650 µmol m^{-2} s^{-1} throughout the entire day. In diurnal with non-fluctuating light setup, the intensity of light changed so that it simulated the daily profile of the solar intensity, reaching a maximum of 650 µmol m^{-2} s^{-1} at mid-day. For diurnal with fluctuating light, the light fluctuated every 2 minutes (with a duty cycle of 1 minute) from 520 to 780 µmol m^{-2} s^{-1} and vice versa. The plants were grown in the summer 2019.

Fig. 1. Soybean wild type (Eiko also labelled WT_{Sb}, left) and chlorophyll (Chl)-deficient mutant (Minngold, right) and sown in pots and grown inside the growth chamber with constant illumination throughout the day.

Over the course of a day, lights were turned on from 5:00 until 19:00 (UTC + 2:00). Temperature was set to 20 °C at night and 27 °C during the day, while the relative humidity was set to 70% at night and to 50% during the day. Eight plants for each genotype were placed inside one chamber (4.5 m^3) representing one replicate, except for constant light setup which had 4 plants per genotype. Total of 3 replicates per treatment (fluctuating, non-fluctuating and constant light) were used in this study. Throughout the growing cycle, the plants were watered using Hoagland nutrient solution while the soil was composed of mainly sand type. A 100% Hoagland solution was composed according to the following mixture of ingredients: 900 mL of Potassium nitrate (KNO_3), 900 mL of Calcium nitrate ($Ca(NO_3)_2$), 360 mL of Magnesium sulfate ($MgSO_4$), 180 mL of Monopotassium phosphate (KH_2PO_4), 180 mL of Spuren element, 180 mL of Fe-EDTA and H_2O was finally added resulting in 180 L of solution. When used for watering plants, the solution was diluted to 50%, and 312 mL of such a solution were used to water each plant on a weekly basis. In the case of drought stress, plants were not watered two days prior to photosynthesis measurements.

Young fully expanded trifoliate leaves of soybean were selected for each plant type (Chl-deficient mutant and WT_{Sb}) to simultaneously trace fluorescence and gas-exchange parameters during photosynthetic light induction. First, plants were dark-adapted overnight.

In the next day, measurements were conducted in a dark room and performed using LI-6800 (Licor Biosciences, Nebraska, USA) equipped with Infra-Red Gas Analyser coupled with PAM fluorometer to simultaneously measure the rate of CO_2 assimilation (A), stomatal conductance to water vapour (g_{sw}), intercellular CO_2 concentration (C_i), dark respiration (R_d), NPQ, Φ_{PSII}, and F_{yield} during either constant or fluctuating light. For details, see Chapter 2.2.1 for PAM fluorescence protocol and 2.3 for gas-exchange protocol.

Lastly, the average and standard error (SE) of four plants per genotype were calculated in WT_{Sb} and Chl-deficient mutant for all the variables measured during the light induction (either using constant or fluctuating light) across time. Pairwise mean comparison between Chl-deficient mutant and WT_{Sb} was performed using student's t-test in R software (R Core Team, 2013).

2.1.2. Turf Grass Seedlings Treated with DCMU

To investigate the link between photosynthesis, SIF and ρ, the response of turf grass after treating with Dicuran herbicide was measured within 3 hours after treatment. Turf grass (*Poa pratense*) seeds were kindly provided by Deutsche Saatveredelung AG (Lippstadt, Germany). Seedlings were grown in a small tray (Fig. 2) filled with ~3 cm thick layer of commercial garden soil (Typ Pikier, Einheitserde, Germany). The seedlings were grown until 32 days prior to herbicide treatment. Different doses of Dicuran 700 FW (Syngenta AG), a commercial formulation of Chlortoluron (3-(3-Chloro-4-methylphenyl)-1,1-dimethylurea), was used block the PSII photochemistry in turf grass prior to SIF and ρ measurements. The herbicide blocks the electron flow from Q_A to Q_B and thereby inhibiting re-oxidation of Q_A in PSII reaction centres. The doses used were 1.6 mL per L of H_2O (D1.6), 6 mL per L of H_2O (D6) and 24 mL per L of H_2O (D24), while distilled H_2O was sprayed in control plots.

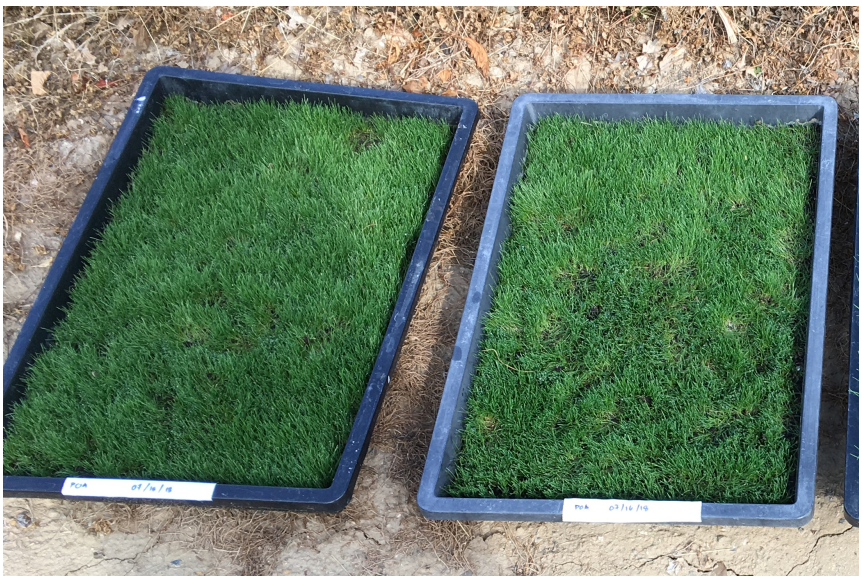

Fig. 2. Seedlings (15-day old) of turf grass (*Poa pratense*, L.) grown on a tray with commercial garden soil medium. Each tray was divided into two sections to accommodate two treatments (i.e. doses of Dicuran herbicide).

Seedlings of turf grass were sprayed with different doses of Dicuran herbicide prior to SIF and ρ measurements. The downwelling fibre optics of FLOX device was placed ~ 30 cm on top of the grass carpet (Fig. 3). Each measurement cycle lasted for about 2 minutes and different treatments were repeatedly measured for 2.5 hours upon Dicuran herbicide application. SIF at O_2B band was retrieved using spectral fitting method (SFM; Meroni et al., 2010).

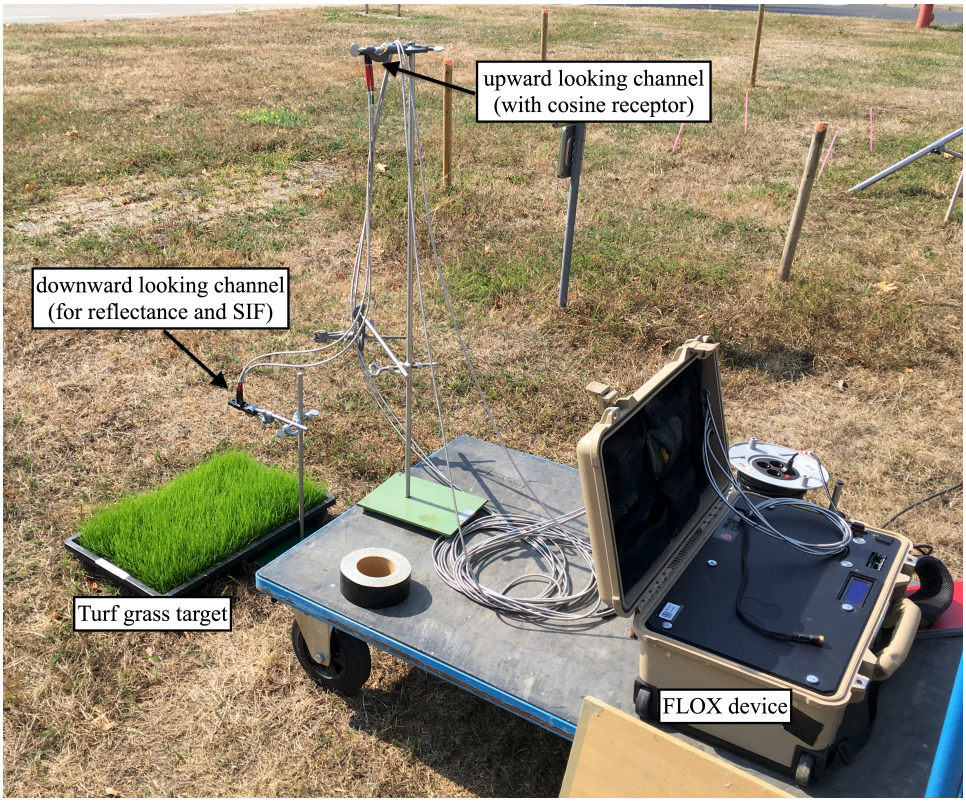

Fig. 3. Measurement setup on tracing solar-induced fluorescence (SIF) and change in spectral reflectance (ρ) on turf grass (*Poa pratense*, L.) upon application of DCMU treatment. Simultaneous measurements of SIF and ρ was performed using Fluorescence Box (FLOX) device from JB Hyperspectral Devices (Düsseldorf, Germany).

2.1.3. Arabidopsis *npq* Mutants and Wild Type

To investigate the effect of different NPQ mechanisms on SIF and ρ, we compared the response of *Arabidopsis thaliana npq* mutants and wild type at different setup. Seeds of Columbia 0 (Col-0) ecotype as wild type (WT_{At}), as well as the mutants derived from either ethyl methanesulfonate or fast-neutron bombardment, were sown and transplanted into small pots (0.34 cm^3) containing *Dachstaudensubstrat* soil type (Hawita, Germany). The mutants were deficient in VDE (*npq1;* Niyogi et al., 1998) or in PsbS protein (*npq4*; Li et al., 2000), both leading to a reduced NPQ capacity. Arabidopsis seeds were sown in seedling trays and grew inside a growth chamber until seedling stage, then were transferred to the glasshouse at the IBG-2 Plant Science, Forschungszentrum Jülich, Germany (50°54'35.1"N, 6°24'47.4"E). The growth chamber had a condition of 12-h day-night light regime (100 µmol m^{-2} s^{-1}) with temperature set to 20°C day / 15°C night while the relative humidity was maintained at 60%. The seedlings were transferred to the glasshouse ~20 days after sowing. Fig. S1 summarises

the recorded light and temperature where plants were grown prior to diurnal field measurements.

Prior to diurnal field measurements, the effect of field exposure to Arabidopsis plants grown in the glasshouse condition was investigated using portable hyperspectral imaging sensor (Behmann et al, 2018). To do this, we compared plants grown in the glasshouse (non-stress acclimated, NSA) versus grown in the field (stress acclimated, SA) with 3 plants from each genotype. Hyperspectral image was taken inside the glasshouse (see chapter 2.4.1 and Behmann et al., 2018). To select the pixels within the image that represents plant parts, the normalised difference vegetation index (NDVI, Eqn 6) was computed and used as a basis to classify region of interest (Jackson et al., 1983). In August of the summer 2017, plants were placed outside of the glasshouse for at least two consecutive days before measurements. In February of the winter 2018, plants were directly exposed outside and diurnal measurements were conducted for two consecutive days of measurements, while plants were moved back to the glasshouse at night.

Fig. 4. *Arabidopsis thaliana* Col-0 ecotype (wild type, WT_{At}, left), violaxanthin de-epoxidase (VDE)-deficient *npq1* mutant (middle) and PsbS-deficient *npq4* mutant (right) showing no distinct morphological differences except mutation that leads to deficiency in NPQ.

Arabidopsis *npq* mutants were investigated both using active and passive fluorescence technique in the controlled and diurnal field condition. In controlled setup, plants were initially dark-adapted for at least 30 mins and traces of active fluorescence using PAM and LIFT were recorded during photosynthetic light induction for a duration of 5 mins. In the field condition, parallel measurement of active and passive fluorescence, along with hyperspectral point sensing, were done in the summer and winter conditions. In the summer, the plants were exposed in the field under clear sky for at least 2 successive days prior to diurnal field measurement. In the winter, the greenhouse grown plants were directly exposed in the cold winter days under clear sky condition.

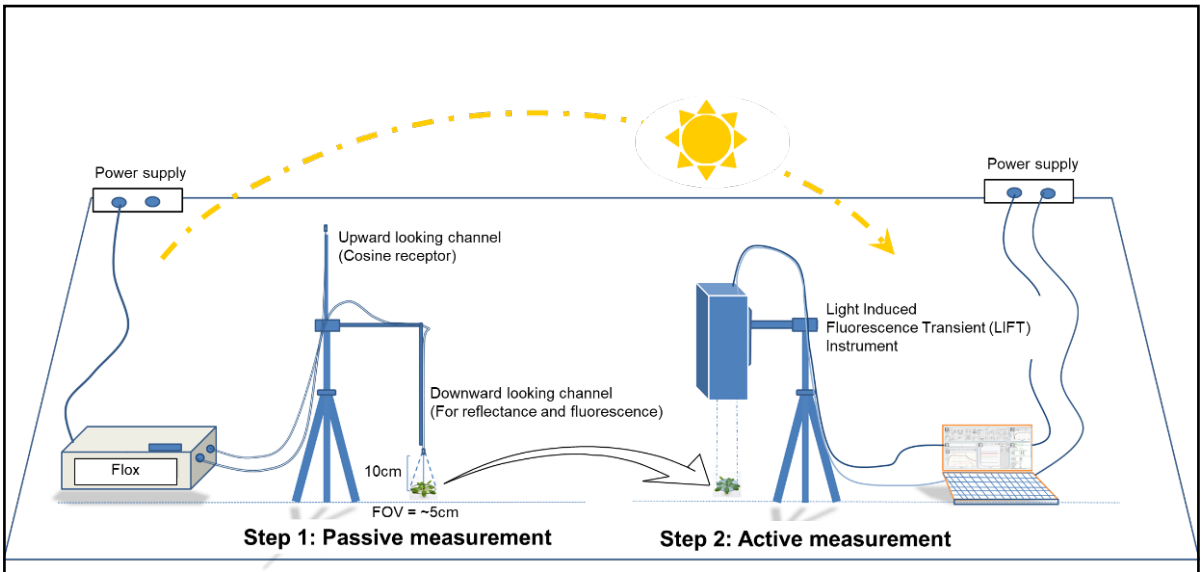

Fig. 5. Illustration of diurnal measurement combining both active and passive fluorescence detection on Arabidopsis plant.

This image was taken from Supplementary Figure 2 in Acebron, K., Matsubara, S., Jedmowski, C., Emin, D., Muller, O., & Rascher, U. Diurnal dynamics of non-photochemical quenching in Arabidopsis *npq* mutants assessed by solar-induced fluorescence and reflectance measurements in the field. *New Phytologist*. 05.Oct.2020

Prior to all measurements, the top layer of soil was carefully scraped-off in order to eliminate mosses which may provide fluorescing background signal. On the one hand, light induction was done in laboratory condition on five plants for each type in a completely randomised design using both the Imaging PAM and LIFT. Before turning on the actinic

light during light induction, saturating flash was triggered to record variable (F_v) and F_m to quantify F_v/F_m (Eqn. 1). When actinic light was turned on, F'_m and steady-state fluorescence (F_s) were recorded every 20 s to quantify Φ_{PSII} (Eqn. 2) and NPQ (Eqn. 3). This protocol was sustained for 5 min for each plant. A total of 4 plants for each type were measured using this assay. Similarly, field measurement of $SIF_{spectra}$ and SIF_{yield} on a single detached leaf was done on 3 plants for each plant type in a randomised manner. On the other hand, parallel measurements using LIFT and FLOX device were conducted diurnally in summer and winter climate were performed using Repeated Measures Design at which 3-4 plants per type were completely randomised per time point. In addition, plant ρ were also measured integrated within the FLOX system. The measurement setup is illustrated in Fig. 5. In the summer, 9 measurement time points were spanned across the day (from 07:34 to 16:04 UTC). While in winter, 19 and 30 measurement time points were done in Day 1 (from 09:37 to 16:50 UTC) and Day 2 (from 07:00 to 16:30 UTC), respectively. We randomised all the plant types for each measurement window to take into account the temporal changes that may affect both optical and biological response of plant within the measurement time point. The recorded diurnal light intensity and temperature in both summer and winter conditions are shown in Fig. S1. For active fluorescence measurement using LIFT device, an average of the two sequential Q_A flashes was used to quantify both the Φ_{PSII} and NPQ of light-adapted plant.

In order to verify the photoinhibition as the cause of the decline in the quantum yield of the PSII, the recovery of the F_v/F_m was traced in the greenhouse condition on plants exposed in the winter stress. The three plants from each plant type were transferred in the greenhouse on the next day after winter stress. The plants were dark-adapted for at least 30 minutes prior to measurement, and the measurement was done every ~45 mins for the duration of 3.5 hours. Similar to the laboratory and field measurement, Q_A flash protocol was used in the LIFT device to estimate the F_v/F_m parameter.

2.1.4. Glasshouse versus Field-Grown Cassava Plants

Stem cuttings of cassava (*Manihot esculenta,* Crantz) plants were either grown in pots inside the glasshouse or under field conditions (Fig. 6). Two cultivars were compared, the model cassava plant 60444 and the farmer-preferred Nigerian landrace TME7. In glasshouse setup, 2 to 3 plants from each line were planted on single pots and grown from 27 November 2018 to 3 May 2019 and 3 May 2019 to October 2020. The glasshouse is located at the Technical University of Kaiserslautern in Germany (49°25’36.0"N 7°45’16.4”E). There were a total of 13 plant replicates from 60444 in glasshouse. Artificial light inside the glasshouse was set to ~300 µmol m^{-2} s^{-1} over the top of the canopy.

Fig. 6. Cassava plants grown in pots and inside the (left) glasshouse at the Technical University of Kaiserslautern in Germany and (right) in the field at the National Chung Hsing University (NCHU) in Taichung City, Taiwan.

In the field setup, a total of 14 plant for TME7 and 14 plants for 60444 were grown and randomly transplanted in the field with 1.2 m distance between and within rows. Plants were grown from 18 March to 4 December 2019 located at the National Chung Hsing University (NCHU) in Taichung, Taiwan (24°04'41.9"N, 120°42’56.1”E).

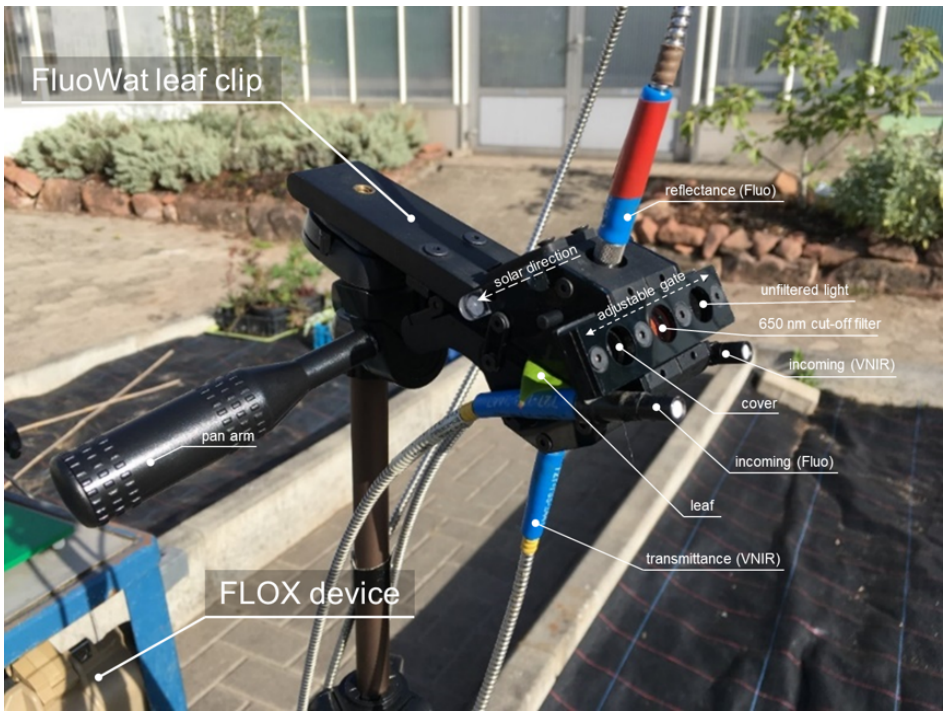

Fig. 7. Hybrid setup between FluoWat Device coupled with spectrometers from Fluorescence Box (FLOX). The measurement setup was used to quantify solar-induced fluorescence spectra as well as spectral transmittance simultaneously on cassava leaves in the field condition.

MiniPAM device was used to either conduct point measurements of F_v/F_m, NPQ, and Φ_{PSII}. During point measurements, the whole plant canopy was profiled by measuring individual leaves on its original position and orientation. Prior to day measurement, F_m were recorded for each leaf (3 segments per leaf) during pre-dawn measurements. During the light measurements, care was taken to not alter the light condition where the leaf was naturally exposed. PAM parameters, such as F'_m and F_s, including the incident PAR and temperature were recorded for each leaf on the same spot were F_m were also previously measured. Each measurement points were noted on which leaf number, in relation to the position within the canopy, it was recorded.

To continuously trace NPQ adjustments during fluctuating light, actinic light was changed from 2,000 µmol m^{-2} s^{-1} to 200 µmol m^{-2} s^{-1} every 2 minutes using LI-6800. This cycle was repeated for 6.5 cycles on a leaf which is dark-adapted for at least 30 minutes. In the glasshouse grown plants, the potted plants are brought to the dark room while in the case of field-grown plants, the leaf are cut with a sharp cutter and immediately dip the cut tip in

the water then transferred to the dark room. The leaf sampling was done in the afternoon and left overnight in the dark room for dark adaptation. Pigment analysis was performed by Plant Physiology group in Technical University of Kaiserslautern (Kaiserslautern, Germany) using HPLC technique. Levels (in picomole per mg of fresh weight) of neoxanthin, violaxanthin, antheraxanthin, zeaxanthin, Chl *a*, Chl *b*, lutein and β-carotin were among the pigment data quantified. The deepoxidation state (DEPS) was calculated based on Thayer & Björkman (1990) expressed as (0.5 antheraxanthin + zeaxanthin) / (violaxanthin + antheraxanthin + zeaxanthin). NPQ adjustments were measure the next day. PAM fluorescence parameters along with CO_2 gas-exchange parameters were recorded every 20 s during light fluctuations.

Diurnal field measurement in cassava leaves were conducted by integrating FLOX device system with FluoWat device (Fig. 7). By doing so, upwelling and downwelling SIF spectra were able to quantify along with transmittance and ρ, respectively. Furthermore, as the upwelling channel of FLOX device was positioned parallel to the solar tracker, the diurnal measurement of radiance was assumed to be less affected by changes in solar zenith angle.

2.2. Active and Passive Fluorescence Techniques

Chlorophyll fluorescence is a by-product of light absorption, photochemical processes, and non-photochemical events of energy dissipation. Fluorescence are photons of light emitted in the region of far red and the near infrared wavelengths which is only visible to the naked eye through a filtered glass (see Fig. 8 the glow in Arabidopsis plant from the emitted fluorescence and seen through a filtered glass), but can also be quantified by using special fluorometers or high-resolution spectrometers. Several measurement techniques have been established in the past decades for plant research applications but the strategies can be mainly divided into two categories: active and passive fluorescence measurements. In this chapter, I will describe different strategies in measuring ChlF and the key parameters that can be derived.

Fig. 8. Fluorescence emission photographed in *Arabidopsis thaliana* induced by the actinic light of the Imaging Maxi-PAM and viewed from a filtered glass.

2.2.1. Pulse-Amplitude Modulation (PAM) Technique

Active technique for measuring ChlF using Pulse-Amplitude Modulation (PAM) fluorometers was originally described in a patent submitted by Schreiber & Schliwa (1987). The authors described the detection of F_{yield} using pulses of weak LED lights (also known as measuring beam) in order to modulate the fluorescence signal. The measuring beam is incapable of triggering charge separation in the PSII and thus do not drive photochemistry in target leaf. The modulated fluorescence signal then goes to an amplifier which is targeted to detect only the pulses and selects the signal off the background illumination (Schreiber, 1986). This method directly measures the apparent F_{yield} which becomes directly unrelated to the intensity of light but rather related to changes in both photochemistry and NPQ. Under dark-adapted state, the measuring beam produces minimal F_{yield} (F_0). On the other hand, a saturating flash (i.e. high-intensity flash of light) is capable of momentarily reducing the primary electron acceptor in the PSII (Q_A). In combination with measuring beam, F_{yield} under saturating flash is called maximal fluorescence (F_m). The currently existing models of fluorometers (either Walz or Li-Cor systems) are based on this principle.

In this thesis, the PAM technique was done using three different instruments: (1) the standard miniPAM leaf clip from Walz (Effeltrich, Germany, Fig. 9a), (2) the Imaging-PAM M-Series also from Walz (Fig. 9b), and (3) PAM coupled with Infra-Red Gas Analysers

(IRGA, model LI-6800, Fig. 9c) from Li-Cor Biosciences (Lincoln, Nebraska, USA). Both miniPAM and LI-6800 were used to measure single area point in leaves of cassava and soybean plant while Imaging Maxi-PAM was used to image the whole rosette plant of *Arabidopsis thaliana*. The Imaging-PAM M-Series was capable of detecting modulated F_{yield} signal using Charge-Coupled Device (CCD) camera. The actinic light source was built-in the Imaging-PAM system using 300 W LED array with a homogeneous illumination on a 10 x 13 cm area. Measuring light was set to 3 (relative unit, r.u.) with a frequency setting of 1 (r.u.). The gain and damping were set to 4 and 2, respectively.

The active fluorescence signal measured with the PAM devices, as enumerated above, was first calibrated by adjusting the gain and frequency that is later translated to the intensity of the measuring beam. The intensity of the measuring beam was maintained to be less than 1 μmol m^{-2} s^{-1}, which is sufficient to produce F_0 but not enough to trigger first charge separation in photochemical reaction. Saturating flash was set to > 5,000 μmol m^{-2} s^{-1} for 800 ms to momentarily close (reduce) the reaction centres and emit maximal fluorescence in the dark (F_m) or in light-adapted states (F'_m).

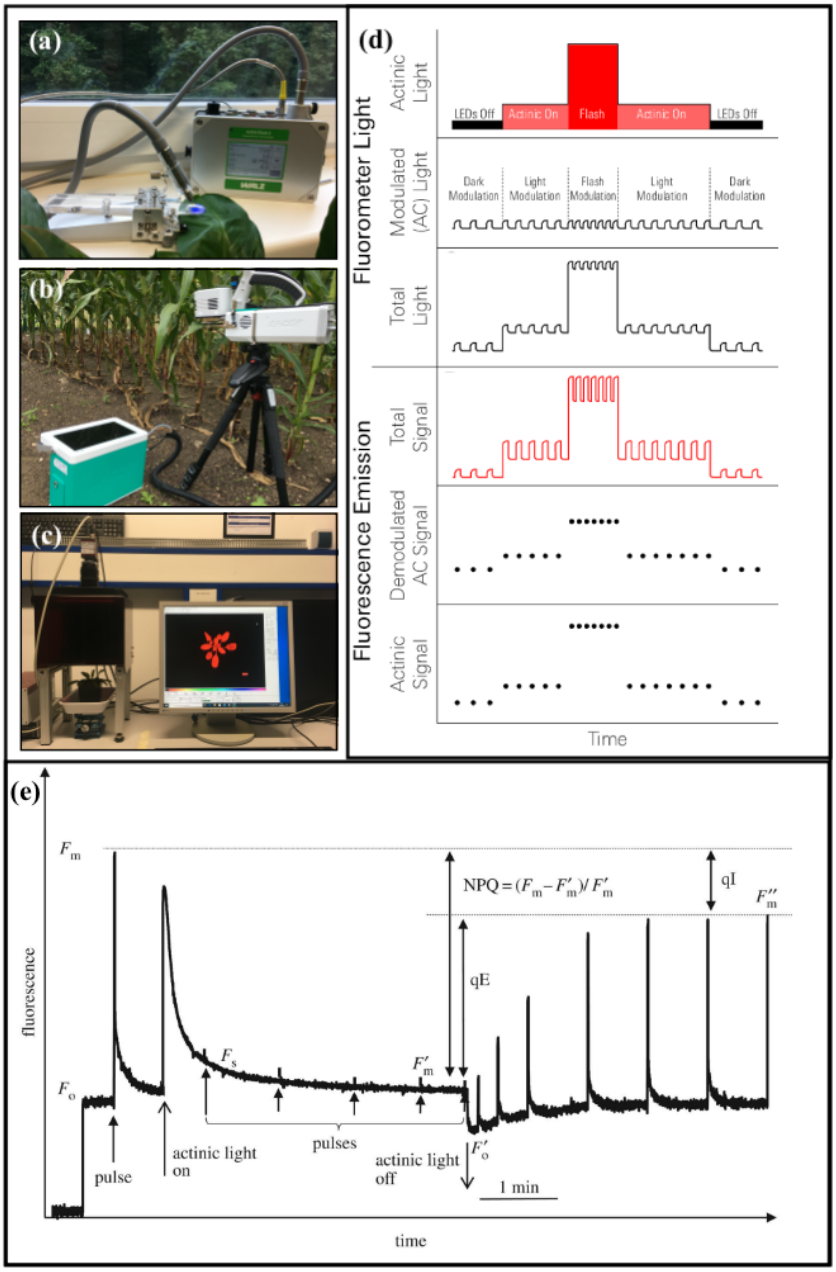

Fig. 9. Pulse-Amplitude Modulation (PAM) Technique using (**a**) PAM fluorometer (mini-PAM from Walz, Effeltrich, Germany) (**b**) PAM fluorometer head coupled on leaf cuvette for gas-exchange measurement (LI-6800, Li-Cor Biosciences, Nebraska, USA) and (**c**) PAM Imaging system (maxi-PAM from Walz, Effeltrich, Germany). (**d**) Simplified illustration of PAM technique showing how fluorescence yield is deconvoluted from the total background light either from actinic light or saturating flash (figure was borrowed from Li-Cor Biosciences, https://www.licor.com/env/support/LI-6800/images/modulated.png). And, (**e**) a typical fluorescence curve from a dark-adapted leaf showing minimal fluorescence (F_0), maximal fluorescence (F_m) in the dark after saturating flash, the steady-state fluorescence yield (F_s) tracking the *Kautsky* effect (Kautsky et al., 1960) as soon as the actinic light is turned on. Saturating flashes under actinic light yields maximal fluorescence (F'_m) lower than F_m. Non-photochemical quenching (NPQ) of chlorophyll fluorescence yield is estimated as $(F_m-F'_m)/F_m$' wherein the fast and reversible energy-dependent quenching (qE) is estimated to relax on the first minute after turning off the actinic light, while photoinhibition (qI) is known to revert in longer time period (figure was taken and modified from Ruban, 2016, p.1905).

2.2.2. Light-Induced Fluorescence Transient (LIFT) Technique

LIFT instrument (Version LIFT-REM, Soliense Inc., Shoreham, NY, USA, http://soliense.com/LIFT_Terrestrial.php; Fig. 10a) utilises the principle of Fast Repetition Rate (FRR; Kolber et al., 1998) to model the variable fluorescence (F_v) from fluorescence transient. FRR technique is composed of a series of sub-saturating excitation flashlets (total excitation power of 18,000 μmol m^{-2} s^{-1} while 1,600 μmol m^{-2} s^{-1} in DC mode). Unlike the measuring beam in PAM technique, a sequence of about 300 sub-saturating flashlets in LIFT is capable of saturating the primary electron acceptor of PSII (Q_A) (Kolber et al., 1998). LIFT instrument was equipped with a pulse-controlled blue LED (445 nm) excitation source that is focused on a 2-cm measuring spot. Fluorescence was detected at 685 (±10) nm in the coaxial optical path of the instrument. Detection of F emission was done by subtracting the signal detected from inter-flashlet periods to the in-flashlet F signal. Finally, F_{yield} (F_{LIFT}) was derived by normalising the F emission against the constant excitation power.

The LIFT technique relies on the established temporal characteristics of a series of redox reaction in photosynthetic electron transport such that the intensity of each fluorescence transients depends on the capacity of the instantaneous photosynthetic electron transport of the leaf. Because photochemistry is a series of redox processes from $Q_A \rightarrow Q_B \rightarrow$ plastoquinone pool (PQ pool) → cytochrome b_6f (Cyt b_6f) → plastocyanin (PC) → photosystem I (PSI), each step in photochemistry provides a resistance to the emission of ChlF. Such that, when the rate of excitation flashlets exceeds the rate of Q_A re-oxidation, the intensity of fluorescence emission increases (Fig. 10b). While, when the rate of excitation flashlets decreases in such a way that the rate of Q_A re-oxidation is faster than the rate of excitation flash, fluorescence emission decreases significantly. For instance, time constant for Q_A re-oxidation depends on the redox level of Q_B and PQ pool, ranging from 150 μs for fully oxidised Q_B and PQ pool to 20 ms for fully reduced PQ pool. The single turnover flash (also known as the Q_A flash protocol, Osmond et al., 2017; Keller et al., 2019) in LIFT produces 300 flashlets from 0.75ms of induction phase and 127 flashlets from 209 ms of relaxation phase (total of 209.75 ms). Each flashlet during induction phase has a length of 1.6 μs with interval between flashlets of 2.5 μs. This increases the fluorescence transients as this rate exceeds the rate of Q_A re-oxidation. Following is a series of 127 flashlets with a similar length (1.6 μs) but the interval is increased by an exponential factor of 1.025. In turn, this reduces the intensity of fluorescence transients as a result of Q_A re-oxidation.

In summary, fluorescence emission increases as the rate of electron transport is exceeded by the energy induced by the repetition rate of excitation flashlets, while decreases as the rate of repetition decreases so that the rate electron transport is higher than the rate of total oxidation state of Q_A pool (Kolber et al., 2005). Due to this nature, fluorescence transient is modelled by Kolber et al. (1998) and therefore can account different photosynthetic signatures such as the functional absorption cross section of PSII (σ_{PSII}), yield of charge separation (Φ_{PSII}), kinetics of electron transport, probability of energy transfer, size of the oxidised portion of PQ pool (PQ_{ox}), carotenoids quenching (CarQ), and donor size quenching ($P680^+Q$). Furthermore, excitation flash in LIFT can be extended to 6,000 extra flashes in order to saturate PQ pool (also known as the PQ flash).

In this thesis, Q_A flash protocol was used which is also described in Keller et al. (2019). LIFT sensor was distanced 60 cm away and approximately in nadir position in reference to the plant target (only used in Arabidopsis plants). In the laboratory, LIFT parameters were traced every 5 seconds for a duration of 5 minutes using Q_A flash protocol while actinic illumination was turned on. Values for traced parameters were averaged every 40 s. In the field, the average of two sequential Q_A flashes was used to quantify Φ_{PSII} and NPQ of light-adapted plant.

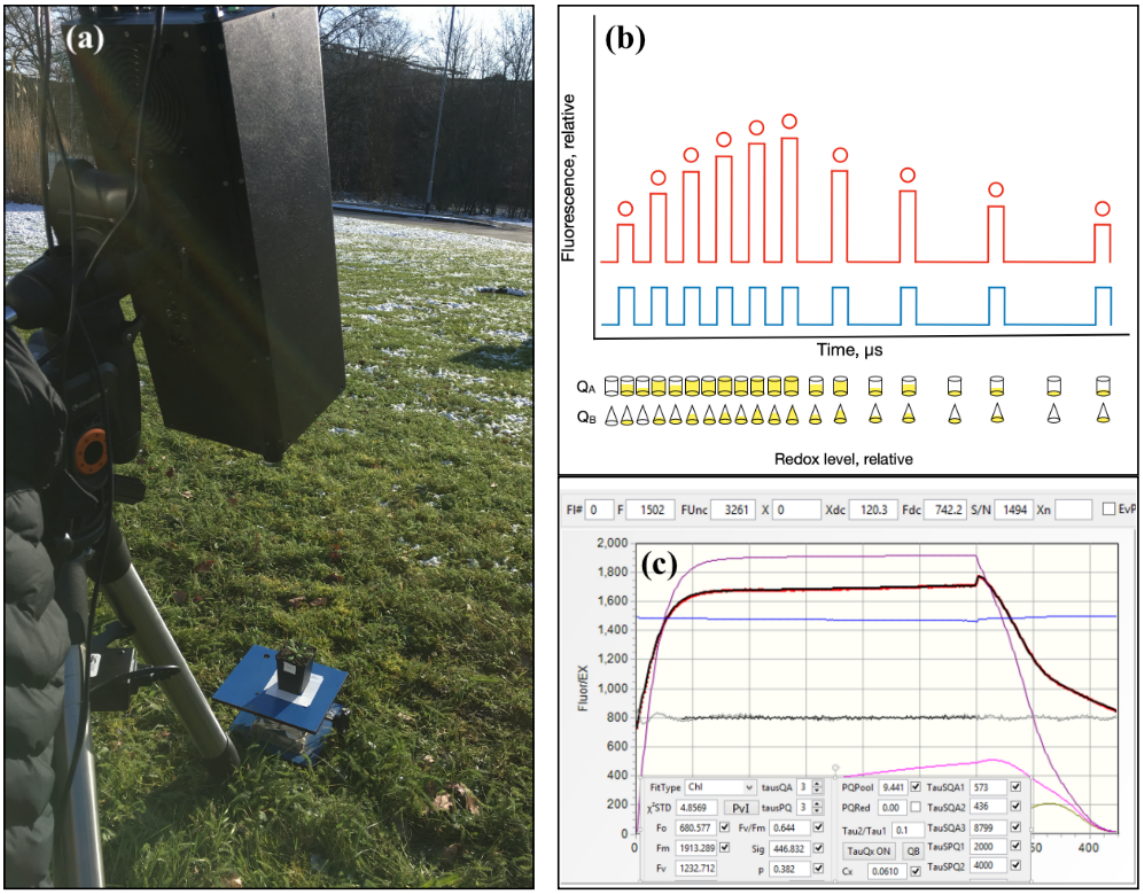

Fig. 10. (**a**) Light-Induced Fluorescence Transient (LIFT) instrument setup measuring *Arabidopsis thaliana* plants in the field condition during winter, (**b**) simplified illustration of fluorescence transients generated by fast-repetition rate protocol and the relative saturation level of reduced Q_A) and (**c**) typical result of fluorescence transients in LIFT from Q_A flash protocol in LIFT fitted in a model developed by Kolber et al. (1998) where different photosynthetic parameters are also fitted.

2.2.3. Solar-Induced Fluorescence (SIF)

Solar-induced fluorescence is a passive emission of ChlF of which the intensity depends on the prevailing light condition (usually under sunlight). SIF signal from a single leaf or a whole plant is detected using high resolution field spectroradiometers such as the ASD FieldSpec® 4 Wide-Res (Malvern Panalytical Lt, Malvern UK). As the SIF emission spectra ranges from 650 to 850 nm, characterised by two dominant peaks at 680 nm and 760 nm, measurement strategies to quantify SIF signal can also vary. In this section, two different strategies of measuring passive SIF signal will be described. One with the use of a leaf clip with short-pass band filter to quantify the full spectra of SIF emission, while the other one is

by exploiting the Fraunhofer lines (or the atmospheric absorption features of the oxygen) to quantify SIF at O_2B band (687 nm, F687) and at O_2A absorption band (760 nm, F760).

2.2.3.1. SIF Detection using FluoWat Device and Measuring APAR

Quantification of the intensity of SIF radiance throughout the spectra (ranging from 650 to 850 nm) can be measured at leaf level with the use of FluoWat Device (van Wittenberghe et al., 2013) coupled with ASD FieldSpec® 4 Wide-Res spectroradiometer. The FluoWat system (Fig. 7) enables filtering of the incoming light at the fluorescence region with the use of a short-pass band filter (> 650 nm) so that the radiating light on leaf surface is purely from fluorescence emission without reflected radiance > 650 nm. The coupled ASD FieldSpec device had a wavelength range of 350-2500 nm with a resolution of 3 nm at 700 nm and 30 nm at 1400/2100 nm. An integral time of 100 milliseconds was used and 10 readings were averaged per log.

The leaf clip is designed with two small slots for the fibre optics of the ASD device located at the top and bottom of the clip which enables the user to position the fibre optics such that it can measure both the upwelling SIF and light reflectance and the downwelling SIF and light transmittance through the leaf. Furthermore, the main aperture for the incoming light is designed such that a user has the option to (1) to provide unfiltered sunlight to the leaf spot, (2) filtered the sunlight (for SIF detection), or completely close the light source (for dark measurements). By combining these features, as well as measuring a white reference panel, the user can correct SIF emission and accurately convert reflected and transmitted radiance to reflectance and transmittance, respectively. The absorbance estimate comes from the unfiltered section of reflected and transmitted radiance (400 to 650 nm) either simultaneously measured, if not with minimal time difference in between. Since the sum of absorbance, transmittance and reflectance is unity, the absorbance from 400 to 650 nm is integrated and used to normalise fluorescence emission. Measurement protocol and calculation of reflectance and transmittance in this thesis were adapted from van Wittenberghe et al. (2013). This protocol was used to detect SIF emission in detached leaves of Arabidopsis plants and in attached leaves of cassava plants diurnally measured in the field condition.

The protocol described in van Wittenberghe et al. (2013) was designed to record SIF signal on the adaxial (upwelling SIF, SIF_{up}) and abaxial (downwelling SIF, SIF_{down}) side of the leaf along with leaf absorbance. Furthermore, total SIF (SIF_{tot}) was estimated by summing up the upwelling and downwelling SIF signal. Apparent F_{yield}, in this case was called $SIF_{yield\ (up,\ down,\ tot)}$, is estimated by normalising SIF_{up}, SIF_{down} and SIF_{tot} by the instantaneous APAR at leaf level. Details on the mathematical derivations of SIF parameters will be described in Section 2.3.

2.2.3.2. SIF Detection using Fraunhofer Lines along with Reflectance Profile

Passive SIF retrieved at ~687 nm (F687) and ~760 nm (F760) was derived with the use of the *Fraunhofer lines* exploiting the O_2B and O_2A absorption bands, respectively. The retrieval technique was either based on the improved Fraunhofer Line Depth (iFLD method, Alonso et al., 2008) or Spectral Fitting Method (SFM; Meroni et al., 2010), which has been widely used in remote sensing applications. Radiance measurements were performed with the use of FLuorescence bOX (FLOX; Fig. 11) device (JB Hyperspectral Devices, Düsseldorf, Germany). This device is capable of simultaneously measuring incoming and reflected radiance due to the two separate optic fibres which are connected to two independent spectrometers. Two optic systems are present: (1) the Fluo module (QE Pro®) that is equipped with high resolution spectrometer (0.3 nm) and spectral sampling interval (SSI) of 0.17 nm with the spectral range of 650 to 850 nm, capable of detecting the contribution of SIF from reflected radiance; and (2) VIS-NIR module (Flame®) that is equipped with a moderate resolution spectrometer (1.5 nm) and SSI of 0.65 nm with the spectral range of 400 to 950 nm, capable of measuring reflected radiance.

The presence of the two modules enables the device to simultaneously measure SIF and ρ in the field condition. Both of the optics had an upwelling and downwelling fibre optic channels with field of view of 25° and 180°, respectively. Fig. S2 shows the field of view characterised from 5 cm on top of the canopy. All measurements conducted in this study were under clear sky conditions in order to eliminate the measurement errors from passing clouds.

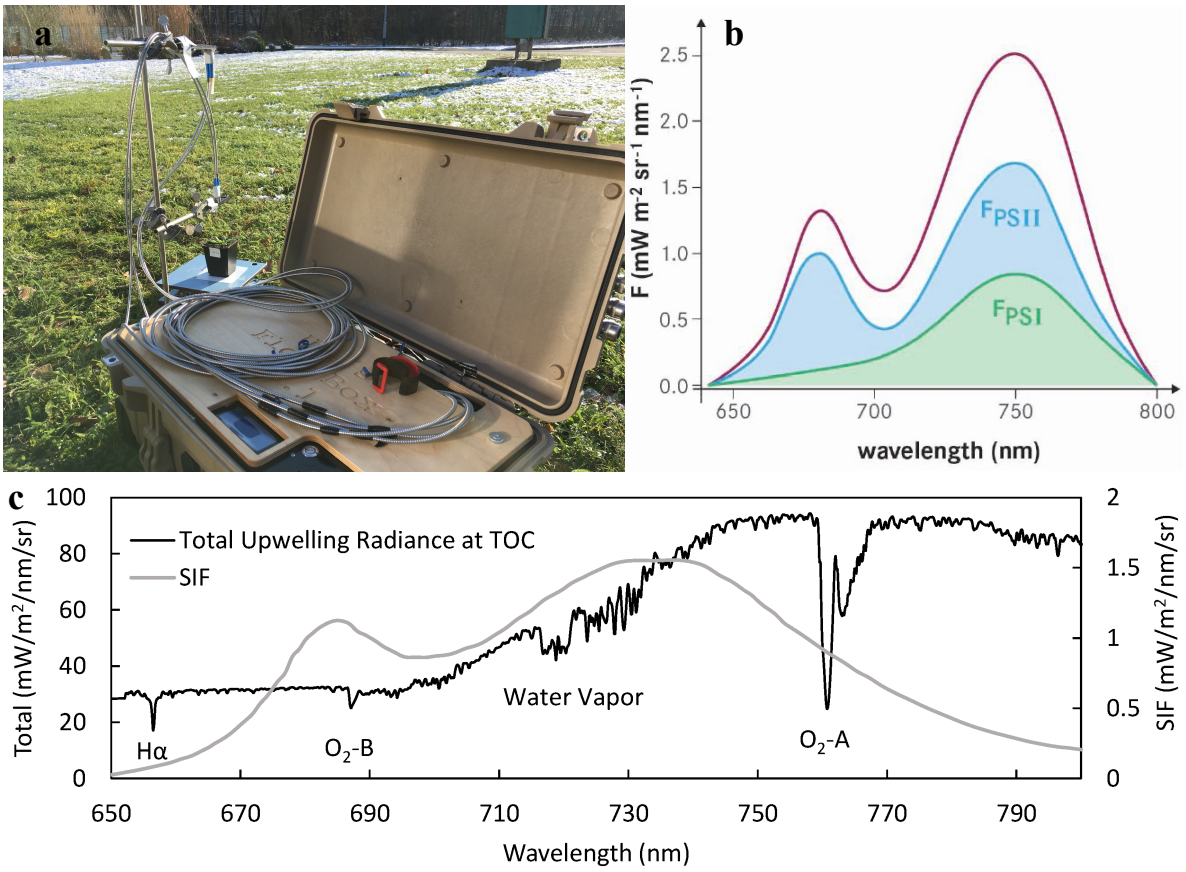

Fig. 11. (a) Fluorescence Box (FLOX) device measuring solar-induced fluorescence (SIF) and spectral reflectance (ρ) in *Arabidopsis thaliana* in the field under clear sky condition. (b) typical SIF spectra showing relative contribution of PSII and PSI (figure was taken from Drusch et al., 2017. p1274). (c) SIF superimposed with total incoming radiance with atmospheric O_2 absorption features to derive F687 (O_2B band) and F760 (O_2A band) (figure was taken from Liu et al., 2015. p10631). In this study, we used improved Fraunhofer Line Depth (iFLD) method developed by Alonso et al. (2008) to estimate F687 and F760 from FLOX device. SIF represents steady-state fluorescence both contributed from PSII and PSI.

2.2.4. Comparison of the Physiological Parameters from PAM, LIFT and SIF Methods

The main difference between PAM, LIFT and SIF is that the first two use active light source to induce changes in F_{yield}, while the latter uses passive light (mostly sunlight). Despite the use of active light source in PAM and LIFT, major differences exist in terms of interpreting fluorescence signals. PAM uses two kinds of active light source: (1) weak modulated signal which is incapable of driving photochemistry and thus unable to carry out first charge separation and (2) saturating flash which is capable of momentarily closing PSII reaction centres. Because of the modulated light, the deconvolution of the fluorescence

signal enables direct measurement of F_{yield} under different actinic light intensity and saturating flashes. The combination of the two different light sources enables clear and accurate quantification of photochemical efficiency and NPQ of ChlF through accurate measurements of F_0 and F_m and thus can measure variable fluorescence (F_v) both under dark and light-adapted states. In contrast, LIFT sensor uses excitation flashes which extrapolates properties of the PSII efficiency upon saturation of electron acceptors in the series of electron transport from PSII to PSI. The model of Kolber et al. (1998) enables placing precise assumptions on the time constants for reducing Q_A, Q_B and PQ Pool and thus estimates the quantum efficiency of PSII as a response to the fluorescence transient excited by series of flashlets. The model rather estimates but not directly measure F_0 and F_m. Nevertheless, despite the fundamental differences in the measurement technique, the estimates of PSII efficiency as well as electron transport rate (ETR) highly correlates well between PAM and LIFT (Kolber et al., 1998, Pieruschka et al., 2014) In addition, the model of Kolber et al. (1998) makes a robust measurement for other parameters such as the σ_{PSII}, energy transfer (Lake vs Puddle model, see review from Stirbet, 2013), the yield of charge separation, and the kinetics of electron transport. While PAM can estimate photochemistry and NPQ parameters as well as basal heat dissipation (Hendrickson et al., 2004).

Lastly, SIF emission highly depends on the incident light. Under field conditions, SIF intensity is directly proportional to the prevailing light intensity. Because of this, quantification of the fraction of APAR (fAPAR) at different spatial and temporal scales is of utmost importance in SIF measurement in order to relate this to photochemical and non-photochemical energy use. In rice, it was shown that SIF is more related to APAR than to photosynthesis (Yang et al., 2018). As the quantification of SIF is derived mostly from spectral measurements, combined ρ measurement can roughly estimate the absorbance of the photosynthetic system. Depending on the complexity of the system (e.g. leaf versus canopy), the estimate of fAPAR may vary significantly from the actual value. When SIF is normalised by the fAPAR, the resulting parameter, SIF_{yield}, becomes more related to photochemical and non-photochemical energy use. The advantage of measuring SIF at different spatio-temporal levels is complicated by a mixed signal from other biochemical and biophysical aspects of SIF emission. For instance, the emission spectra of SIF_{yield} shows contribution from both PSII and PSI. However, since emission spectra is emitted from far-red light, this can also be reabsorbed and thus lowers the level of SIF_{yield} at 680 nm (F680). Furthermore, the

calculation of total SIF at the leaf level (upward and downward SIF emission) can estimate other biophysical events that may influence changes in SIF signal (e.g. chloroplast movement and leaf thickness). The measurement of integrated SIF at the top of canopy enable upscaling the influence of biophysical properties (such as the effect of dense canopies) and the escape probability of fluorescence photon (Lu et al, 2020). The contribution of re-absorbed far-red photon to SIF_{yield} at different spatial and temporal scales is still a matter of active research.

While incident light in the field condition is dynamic, SIF is traditionally compared to the steady-state signal that PAM can derive. More specifically, the SIF emission at 760 nm (F760) is more related to F_{yield} in PAM as most of the PAM devices retrieve fluorescence at 760 nm as it is not sensitive to re-absorption effects.

2.3. Gas-Exchange Measurements

Leaf gas-exchange measurements were conducted on soybean plants using an open gas-exchange system. For each plant replicate, a youngest fully expanded leaf was selected and clipped into the cuvette of LI6800. Prior to illumination, leaf was acclimated in the leaf cuvette for at least 5 mins maintaining CO_2 level at 400 ppm, VPD at 1.8 kPa, fan speed at 10,000 rpm and leaf temperature at 25 °C. (During this time, saturating flash from PAM fluorometer were prompted to record dark-adapted F_v/F_m). To induce photosynthesis from dark-adapted state, the light intensity was turned on to either constant light for the whole 60 min (650 μmol m^{-2} s^{-1}) or fluctuating light. In fluctuating light, the light intensity was changing from 780 μmol m^{-2} s^{-1} for 1 min to 520 μmol m^{-2} s^{-1} for 1 min repeated for 30 cycles. Net CO_2 assimilation rate (*A*), intercellular CO_2 concentration (C_i), transpiration rate *(E*), along with other gas-exchange parameters, were traced for 1 hr with 20 s interval. Recording was operated using the *autoprogram* command in the LI6800, also providing saturating flash from PAM fluorometers every 20 s to induce F_m'. In addition, dark respiration (R_d) - as negative net CO_2 assimilation - was recorded before and after the lights were turned on. The environmental conditions mentioned above maintained throughout the 1-hr light induction protocol up to the 6-mins of dark-relaxation in the end. The rate of

electron transport estimated by gas-exchange parameters was derived based on FvCB biochemical model of photosynthesis (Farquhar et al., 1980; von Caemmerer & Farquhar, 1981, see Eqn. 1). For soybean plants, I used a value of 43.67 ppm for the CO_2 compensation point (Γ) referring to a previous study from Walker & Ort (2015).

(Eqn. 1) $$Ja = (4.5 * (C_i + 7\,\Gamma / 3) / (C_i - \Gamma)) * (A + R_d)$$

2.4. Field Spectroscopy: Imaging and Point Sensors

2.4.1. Specim IQ Camera for Imaging Plant Reflectance

Reflectance image of the plant was taken using Specim IQ camera (Specim Spectral Imaging, Oulu, Finland), while the method was based on Behmann et al. (2018). The IQ camera is a handheld hyperspectral imaging device capable of collecting radiance signals from visible and near infrared region (VNIR 400 to 1000 nm). The acquisition of hyperspectral images were based on the push broom principle with a spectral resolution (full width half maximum) of 7 nm and an image resolution of 512 x 512 pixels. A separate viewfinder RGB camera was integrated in the device in order to help focus the object in which hyperspectral image were taken.

The IQ camera was set up on a tripod to maintain stability while acquiring image. Imaging of plants were for about 1 meter done directly above Arabidopsis plants. Within the field of view, a white reference panel (with 90% reflectance) was included which served as a pixel region for incoming radiance which was later used to normalised reflected radiance and derive reflectance signature for each plant type (see Fig. 12). Throughout the imaging acquisition, the source of illumination was coming from diffused transmitted sunlight inside the greenhouse. Once the focus of the camera was set to the target plants, image was acquired by setting the integration time to 1 s. The acquired images were then transferred on a computer and analysed using ENVI Classic 5.3 software (Harris Geospatial Solutions, Broomfield, USA) or by Matlab 2013a along with the Signal Processing Toolbox 6.19 (The MathWorks, Inc., Natick, USA). The region of interest were selected using NDVI to track pixels that are related to Arabidopsis plants. Each plant was then classified based on their

genotype, while vegetation indices were quantified and the average values for all the pixels for each plant were computed.

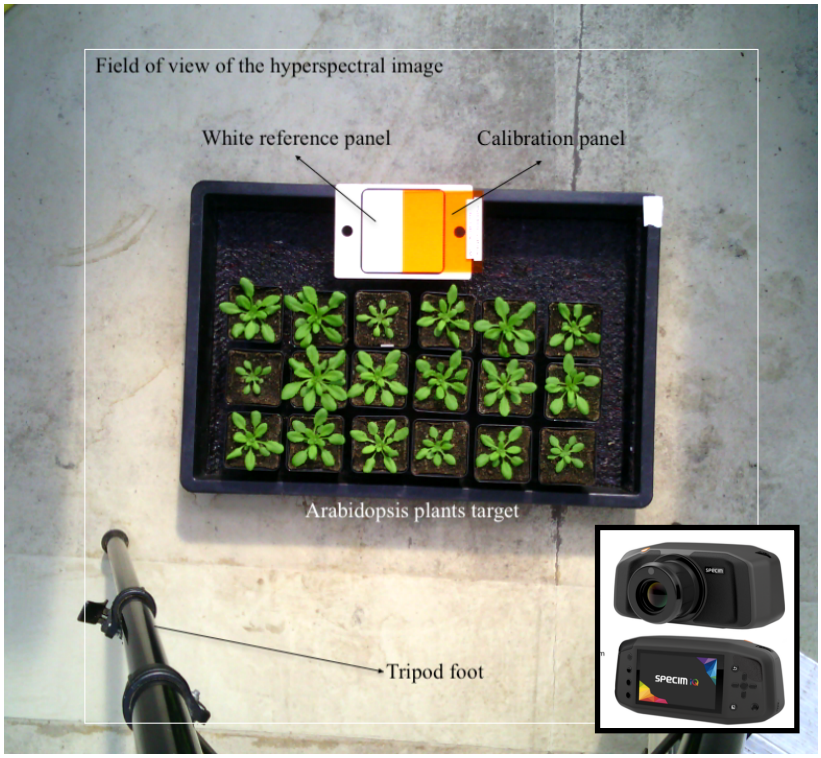

Fig. 12. Field-of-view of the portable Spectral IQ camera (Spectral Imaging Systems, Oulu, Finland) taking hyperspectral image of *Arabidopsis thaliana* wild type and *npq* mutants inside the greenhouse. The inlet image of IQ camera (size is not proportional to the plant) was taken and modified from Figure 1in Behmann, J., Acebron, K., Emin, D., Bennertz, S., Matsubara, S., Thomas, S., ... & Mahlein, A. K. (2018). Specim IQ: evaluation of a new, miniaturized handheld hyperspectral camera and its application for plant phenotyping and disease detection. *Sensors*, *18*(2), 441. 2.Feb.2018

2.4.2. FLOX System for Point Spectroscopy

FLOX device (JB Hyperspectral Devices, Düsseldorf, Germany) was coupled with point spectrometer in the range of 400 to 950 nm with a spectral resolution (FWHM) of 1.5 nm and a spectral sampling interval of ~ 0.65 nm. The radiance signal collected from this optic module was used to calculate vegetation indices. The optic module had a field of view of 25° and 180° for upwelling and downwelling radiance, respectively. Similar to SIF

measurements, the upwelling optic radiance sensors was set up 5 cm on top of Arabidopsis plant (see Fig. 5 for setup and Fig. S2 for the signal intensity in the field of view). Data recording was set to manual in order to better control the signal acquisition during transition from one plant to another. The integration time was automated in the device depending on the intensity of the incoming radiance. Each cycle lasts for about 2 to 3 mins which included the simultaneous acquisition of upwelling radiance and downwelling radiance, then dark measurements for signal to noise correction. The collected diurnal data were analysed by running in a GUI file based on RStudio software V1.0.143 (RStudio, Inc., Boston, USA) and developed by JB Hyperspectral Devices (Dusseldorf, Germany) with the correct calibration file and the list of vegetation indices to be computed.

2.4.3. Calculation of Vegetation Indices from the Reflectance Data

Prior to calculation of vegetation indices, reflectance (ρ) were derived by normalising the reflected radiance from the incoming radiance (Eqn. 21). The ρ signatures of Arabidopsis plants acquired using FLOX device were adjusted based on the minimum and maximum ρ values for each measurement (Eqn. 2). The ρ_{adj} collected diurnally in the summer were averaged per plant type for each window. Then cluster analysis of diurnal ρ data collected in the summer from all Arabidopsis plant types was performed using R software. See chapter 2.6 for details.

Vegetation indices were calculated from the reflectance data gathered from either images acquired from Specim IQ camera or integrated signal from FLOX device. For the hyperspectral reflectance image, the photochemical reflectance index (PRI, Eqn. 3) and normalised difference vegetation index (NDVI, Eqn. 6; Jackson et al., 1983) were calculated using ENVI Classic 5.3 software (Harris Geospatial Solutions, Broomfield, USA), while the red-edge inflection point (REIP, Eqn. 7, Horler et al., 1983) where calculated using Matlab 2013a along with the Signal Processing Toolbox 6.19 (The MathWorks, Inc., Natick, USA). Reflectance data from the spectral image in was smoothed using Savitzky-Golay filtering (Savitzky & Golay, 1964) before calculating the derivative for REIP images. On the other hand, the reflectance signal from FLOX data were processed in a GUI file based on RStudio

software V1.0.143 (RStudio, Inc., Boston, USA) developed by JB Hyperspectral Devices (Düsseldorf, Germany).

(Eqn. 2) $$\rho_{adj} = \frac{\rho_{\lambda} - \rho_{min}}{\rho_{max} - \rho_{min}}$$

Using the adjusted ρ, the PRI was calculated based on Gamon et al. (1992; 1997) (Eqn. 3).

(Eqn. 3) $$PRI_{570} = \frac{\rho_{531} - \rho_{570}}{\rho_{531} + \rho_{570}}$$

(Eqn. 4) $$PRI_{630} = \frac{\rho_{531} - \rho_{630}}{\rho_{531} + \rho_{630}}$$

(Eqn. 5) $$PRI_{670} = \frac{\rho_{531} - \rho_{670}}{\rho_{531} + \rho_{670}}$$

(Eqn. 6) $$NDVI = \frac{\rho_{800} - \rho_{680}}{\rho_{800} + \rho_{680}}$$

(Eqn. 7) $$REIP = 700 + 40\frac{\frac{\rho_{670} - \rho_{780}}{2} - \rho_{700}}{\rho_{740} - \rho_{700}}$$

2.5. Calculations of Active and Passive Fluorescence Parameters

2.5.1. Active Fluorescence Parameters

The quenching of active ChlF parameters is a function of both the photochemical and non-photochemical events. The degree of which the two events quench ChlF is difficult to distinguish but the two processes can be differentially expressed using mathematical equations. Each derived and calculated parameter aims to describe specific physiological event or state of the leaf. For instance, the maximal efficiency of the PSII photochemistry was denoted as F_v/F_m (Eqn. 8; Genty et al., 1989) is widely used in measuring the leaf health (Baker, 2008). In this thesis, this parameter was used to investigate the physiological status

of soybean, Arabidopsis and cassava leaves. Moreover, the operating efficiency of the PSII during light was expressed as Φ_{PSII} (Eqn. 9) and was used to track changes in the quantum yield of the PSII at different light scenarios. In this thesis, photosynthetic efficiency was mostly estimated by this parameter despite the fact that other measures are possible and may differ significantly from Φ_{PSII} (e.g. CO_2 assimilation and V_{cmax}). Moreover, the NPQ parameter based on Stern-Volmer relationship (Eqn. 10; Bilger & Björkmann, 1990) was used to estimate the regulated thermal dissipation that can coarsely estimate sum of independent NPQ mechanism: energy-dependent quenching (qE), zeaxanthin-dependent quenching (qZ), photoinhibitory quenching (qI) and state-transitions (qT). Table 1 summarises all the fluorescence parameters used in this thesis together with their physiological descriptions and mathematical derivations. In the case of LIFT technique, the derivations for F_v/F_m, Φ_{PSII} and NPQ were similarly derived to that in PAM except that the minimal and maximal F_{yield} were based on a model developed by Kolber et al. (1998) and extended by Keller et al. (2019).

Table 1. List of fluorescence parameters together with their mathematical and physiological descriptions.

Parameters	Derivations	Descriptions	References
F_v/F_m (Eqn. 8)	$(F_m - F_o) / F_m$	maximum quantum efficiency of PSII photochemistry measured in the dark-adapted state; maximum yield of primary photochemistry; quantum efficiency of open PSII reaction centres	Kitajima & Butler, 1975; Genty et al., 1989; Maxwell & Johnson, 2000; Baker, 2008
Φ_{PSII} (Eqn. 9)	$(F'_m - F_s) / F'_m$	estimates the operating efficiency of PSII photochemistry; efficiency at which light absorbed by PSII is used for Q_A reduction; also equivalent to $\Delta F/F'_m$ or F'_q/F'_m	Genty et al., 1989; Hendrickson et al., 2004; Baker, 2008
NPQ (Eqn. 10)	$(F_m - F'_m) / F'_m$	estimates the non-photochemical of ChlF or the regulated heat dissipation from PSII	Bilger & Björkman, 1990; Baker, 2008
ETR (Eqn. 11)	$I*A_{leaf}*fraction_{PSII}*\Phi_{PSII}$	electron transport calculated by fluorescence. Whereas I = incident light; $fraction_{PSII} = 0.5$; $A_{leaf} = 0.55$ and 0.78 for Minngold and Eiko, respectively	Krall & Edwards, 1992
qN (Eqn. 12)	$(F_m - F'_m) / F_m$ or $1 - F'_v/F_v$	percentage of non-photochemical quenching similar to the calculation of efficiency of PSII. The three components of NPQ can be separated in qE, qT and qI	Roháček, 2010; Schreiber et al., 1986; Ruban, 2017

Table 1. Continued...

Parameters	Derivations	Descriptions	References
qP (Eqn. 13)	$(F'_m - F_s) / (F'_m - F'_o)$	extent of photochemical quenching; mathematically identical to PSII efficiency factor, F'_q/F'_v; this relates the maximum PSII efficiency to the PSII operating efficiency via a non-linear proportion of PSII reaction centres that are open (Q_A oxidised)	Schreiber et al., 1986; Genty et al., 1989; van Kooten & Snel, 1990; Kramer et al., 2004; Baker, 2008; Ruban, 2017
qL (Eqn. 14)	$(F'_q / F'_v) / (F'_o / F_s)$ or qP (F'_o / F_s) or $[(F'_m - F_s) / (F'_m - F'_o)] * F_o/F_s$ or $(1/F_s - 1/F'_m) / (1/F_o - 1/F_m)$	fraction of PSII centers that are open (Q_A oxidised) on the basis of lake model	Kramer et al., 2004; Baker, 2008; Kasajima et al., 2009
Φ_{NPQ} (Eqn. 15)	$(F_s / F'_m) - (F_s / F_m)$	estimates the fraction of absorbed light by PSII that is dissipated as heat via ΔpH and/or the xanthophyll cycle; efficiency at which light absorbed by PSII is used for regulated heat dissipation	Cailly et al., 1996; Hendrickson et al., 2004
$\Phi_{f, D}$ (Eqn. 16)	F_s / F_m	sum of fraction of absorbed light that is lost by either fluorescence emission or constitutive heat loss	Hendrickson et al., 2004
Φ_f (Eqn. 17)	F / S $(F - F_o) / (F_m - F_o)$	efficiency for fluorescence emission where F is the apparent F_{yield} measured in PAM fluorometer while S is the sensitivity factor in PAM	Paillotin, 1976; Kramer et al., 2004; Stirbet, 2013

Table 1. Continued...

Parameters	Derivations	Descriptions	References
PI (Eqn. 18)	$[(F'_m - F'_o) / F'_m] / [(F'_m - F'_{o\_calc}) / F'_m]$	photoprotection index or the efficiency of photoprotection assuming no photoinhibitory effect on theoretical F'_{o_calc}	Kromdijk et al., 2016
qPd (Eqn. 19)	$(F'_m - F'_{o,\,act}) / (F'_m - F'_{o,\,calc})$	value of qP in the dark during photodamage	Ruban & Murchie, 2012; Ruban, 2017
qLd (Eqn. 20)	qPd (F'_{o_calc} / F'_{o_act})	value of qL in the dark during photodamage	In this thesis

2.5.2. Passive Fluorescence Parameters

Emission spectra of passive SIF was quantified using FluoWat device in mW m^{-2} s^{-1} units. Likewise, reflected and transmitted radiance were measured together with the incoming radiance. The ρ and transmittance were derived by normalising the reflected and transmitted radiance, on the incoming radiance estimated in white reference measurements (Eqn. 21 and 22, respectively). Whereas, the absorbed light was calculated using Eqn. 25. Furthermore, the yield of SIF spectra (SIF_{yield}) was derived by normalising SIF intensity for each wavelength by the amount of light absorbed from 400 to 700 nm or APAR (Eqn. 26).

(Eqn. 21) $$Reflectance(R) = \frac{ReflectedRadiance}{Irradiance(I)}$$

(Eqn. 22) $$Transmittance(T) = \frac{TransmittedRadiance}{Irradiance(I)}$$

(Eqn. 23) $$PAR = \int_{400}^{700} I \bullet d\lambda$$

(Eqn. 24) $$fAPAR = \int_{400}^{700} (1 - R - T) \bullet d\lambda$$

(Eqn. 25) $$APAR = fAPAR x PAR$$

(Eqn. 26) $$SIF_{yield} = \frac{\uparrow SIF + \downarrow SIF}{APAR}$$

SIF intensity estimated based on the iFLD method (Alonso et al., 2008) and was performed using R software. The equation for retrieval is summarised in Eqn. 27 where E and L are the incoming and reflected radiance, respectively. In O_2B band, F687 was retrieved by utilising 757.6 nm wavelength outside the O_2B band (λ_{out}) while 760.7 nm was used inside the O_2B absorption band (λ_{in}). In contrary, F760 was retrieved using radiance values at 686.2 nm as outside the O_2A band (λ_{out}) while 687.7 nm was used inside the O_2A band (λ_{in}). The yield of SIF retrieved at O_2B ($F687_{yield}$) and O_2A bands ($F760_{yield}$) were calculated by normalising SIF intensity to the incoming radiance at 760 nm.

(Eqn. 27) $$F = \frac{E(\lambda_{out}) \bullet L(\lambda_{in}) - L(\lambda_{out}) \bullet E(\lambda_{in})}{E(\lambda_{out}) - E(\lambda_{in})}$$

2.6. Statistical Analyses

2.6.1. Analysis of Variance and Mean Comparison

Statistical analyses were performed in fluorescence and reflectance data acquired in soybean, Arabidopsis and cassava plants. In soybean, comparison of mean values between WT_{Sb} and Chl-deficient mutant were performed using simple t-test in R software. In Arabidopsis, traces of PAM and LIFT fluorescence parameters during photosynthetic induction were performed on the basis of completely randomised design. First, the measured parameters were fitted in a linear mixed model where parameter was a function of the interaction between plant type and time after induction plus having plant replicate as a random effect (see below model, Eqn. 28). The analysis of variance (ANOVA) from the

model effect was performed using anova() function in R software (R Core Team, 2013). Similarly, the pairwise mean comparison was performed using *lsmeans* function in the same computer program.

(Eqn. 28)

$$Parameter_{PAM\ or\ LIFT} \sim plant\ type + time\ after\ light\ ON + plant\ type * Time + (1 \mid plant\ replicate)$$

Likewise, the parallel measurements of active and passive fluorescence diurnally measured in the field were performed using Repeated Measures Design and was analysed using model below (Eqn. 29) and tested for significant effects similarly in the induction protocol.

(Eqn. 29) $$Parameter_{LIFT\ or\ SIF} \sim plant\ type * time\ of\ day + (1 \mid plant\ replicate)$$

2.6.2. Cluster Analysis

In Arabidopsis, reflectance data acquired diurnally in the summer were adjusted based on the maximum value (see Eqn. 2) and statistically clustered. Firstly, the adjusted ρ data previously discussed were pooled consisting of individual measurement from 4 plants for each plant type from Window 1 to 9. Secondly, the dissimilarity between data points were computed using Pearson's r^2 in the '*dist*' function in R (RStudio software V1.0.143 (RStudio, Inc., Boston, USA)). Thirdly, the hierarchical clustering was done using '*hclust*' function in R using ward.D method. Lastly, the generated cluster graph was annotated based on the time it was measured as well as the expected xanthophyll activity.

In cassava, correlation coefficients among fluorescence data, vegetation indices and pigment data were clustered using dissimilarity index. First, correlation analysis was performed using *cor()* function in R package called 'stats v3.6.2' for: (1) PAM fluorescence parameters (NPQ, Φ_{PSII} and F_{yield}; see chapter 2.5.1), (2) passive fluorescence parameters (F680 and F760; see chapter 2.5.2), (3) vegetation indices (NDVI and PRI, see chapter 2.4.3), (4) PAR and (5) pigment data. Second, dissimilarity distance between data points was calculated using Euclidean method in the *dist* function in the same programming software. This enabled generating dendogram using the *heatmap()* function in R.

2.6.3. Developing the Input Values for the Schematic Model

The effect of different NPQ mechanisms on SIF_{yield} under different environmental conditions were summarised in a schematic model and illustrated using Sankey diagram generated using Phyton Matplotlib Sankey package. To see detailed method on how we derive the input values, see Note S1 in Acebron et al., 2020). Prior to this, the following assumptions were listed based on the data observed diurnally in the summer and winter spell in Arabidopsis wild type and *npq* mutants.

Assumptions:

1. F_{yield} is synonymous to SIF_{yield} and thus the effect of reduced NPQ to F_{yield} is similar to the effect in SIF_{yield}.

2. Both *npq1* and *npq4* mutants had similar rates of NPQ under low light.

3. Under low light condition, efficiency for PSII photochemistry among all plant types are typically the same.

4. To simplify the model, the contribution of non-regulated heat dissipation is assumed to be constant and similar to all plant types and across different conditions.

5. When SIF_{yield} was fully quenched during high light and cold spell, the value of SIFyield was set to a minimum of 3% of the total energy dissipation.

First, the values of Φ_{NPQ} and Φ_{PSII} in the morning (~8:00 am) and mid-day (~12:00 nn) for WT_{At} and *npq* mutants were used as a reference point to further derive changes in NPQ and Φ_{PSII} form low to high light condition. To derive values for SIF_{yield}, the contribution of photochemical and non- photochemical events was normalised in such a way that the sum of Φ_{PSII} and Φ_{NPQ} is maximally at 90% of total energy dissipation, setting the contribution of SIF_{yield} to 10%. In the absence of photoinhibition, the contribution of qE and qZ to NPQ were set to 50%. While, in the presence of photoinhibition, its contribution is set to residual. Such that:

(Eqn. 30) $$qI = 1 - \Phi_{PSII} - \text{PSBS-dependent} - \text{Z-dependent} - SIF_{yield}$$

3. RESULTS

3.1. Dynamics of Energy Partitioning in Chlorophyll-Deficient Soybean Mutant

3.1.1. Response of Chlorophyll-Deficient Mutant during Photosynthetic Induction

To investigate the effect of Chl-deficiency in photosynthetic light-use at photosystem level, I examined the efficiency for fluorescence emission, photochemistry, basal heat dissipation and NPQ during the photosynthetic induction phase until the steady-state condition was reached. From dark-adapted state, the proportion for energy dissipation of absorbed light varied significantly during the induction phase and the steady-state conditions as well as between the two plant types. Fig. 13 showed that the Chl-deficient mutant reached the steady-state condition in a slower manner than the WT_{Sb}, that is internal fluorescence yield (Φ_f) in mutant and in WT_{Sb} reached the steady-state at ca 30 and 15 mins, respectively. Further, the mutant also showed a higher Φ_f and lower efficiency for NPQ (Φ_{NPQ}) as compared to the WT_{Sb}, consistent under both constant and fluctuating light scenarios. In turn, no significant difference in Φ_{PSII} and Φ_D was observed between the two plant types. The significant differences were quantified by calculating the area of the curve for each efficiency pathway and was shown in Table S1.

At leaf level, the Chl-deficient mutant had lower leaf absorbance as compared to green WT_{Sb} (Sakowska et al., 2018). In turn, the mutants had significantly lower apparent F_{yield} traced by PAM fluorometer at leaf level and lower NPQ under steady-state but similar F_v/F_m when grown under non-stressed (Table 2). Moreover, the mutant had a significantly lower PI and qLd while higher qPd during dark following 1 hour of moderate light (650 μmol m^{-2} s^{-1}), albeit a small increase. The trends in of F_v/F_m, PI and qPd were similar in constant and fluctuating light conditions (Tables S2 and S3).

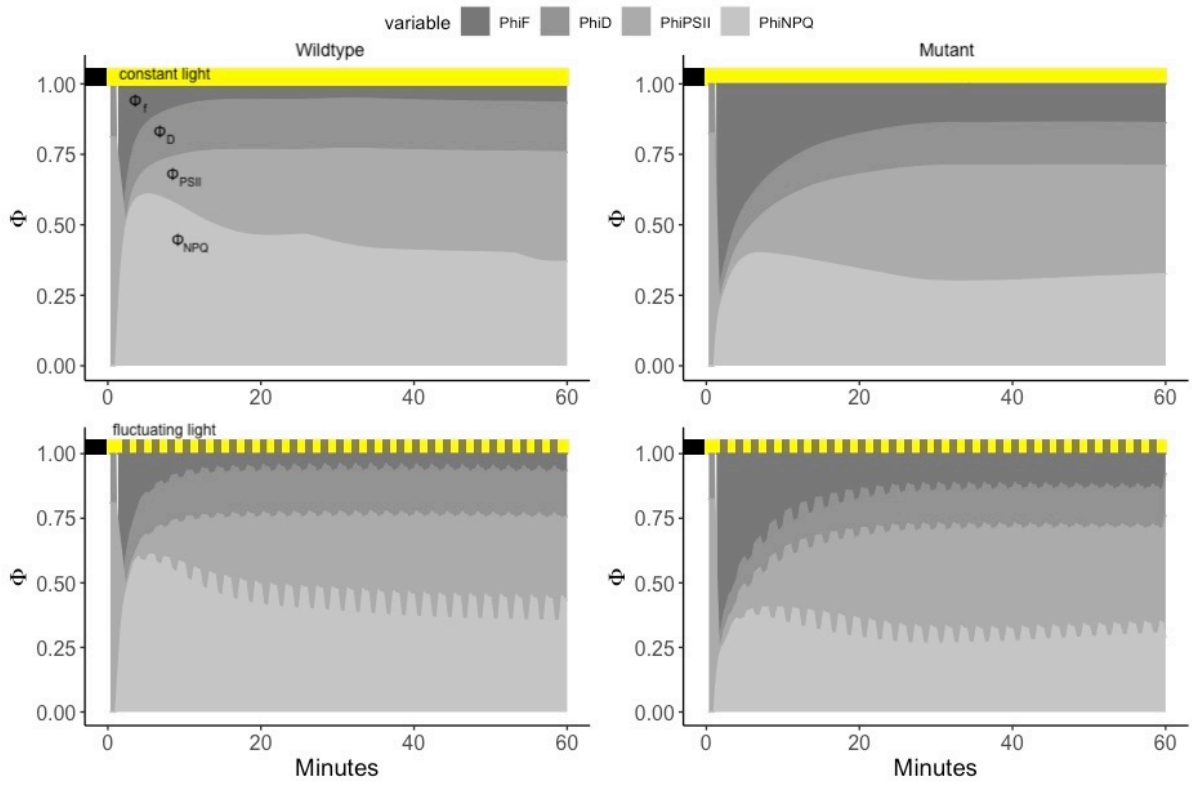

Fig. 13. The efficiency for fluorescence emission (Φ_f), basal heat dissipation (Φ_D), photochemistry (Φ_{PSII}) and regulated non-photochemical quenching (Φ_{NPQ}) traced during photosynthetic induction using a constant light (650 µmol m^{-2} s^{-1}) and fluctuating light (high light 720 µmol m^{-2} s^{-1} to low light 580 µmol m^{-2} s^{-1}) in green soybean cultivar (Eiko also defined here as WT_{Sb}) versus pale mutant (Minngold). The values are average of four plant replicates measured on the youngest fully expanded leaf.

Table 2. Differences in the steady-state of active fluorescence parameters measured between green Eiko Soybean (WT_{Sb}, Wild type) cultivar and Chl-deficient mutant.

Fluorescence Parameters	Wild type	Mutant
F_{yield}	956.0 ± 2.4[a]	688.1 ± 3.0[b]
NPQ	1.70 ± 0.01[a]	1.08 ± 0.01[b]
F_v/F_m	0.812 ± 0.00[a]	0.825 ± 0.00[a]
PI	0.828 ± 0.008[a]	0.790 ± 0.007[b]
qP_d	0.903 ± 0.014[a]	0.944 ± 0.006[b]
qLd	0.658 ± 0.009[a]	0.606 ± 0.012[b]

different letters indicate significant difference at α 0.05 comparing the mean of WT_{Sb} and mutant

3.1.2. Quenching Analysis during Photosynthetic Induction

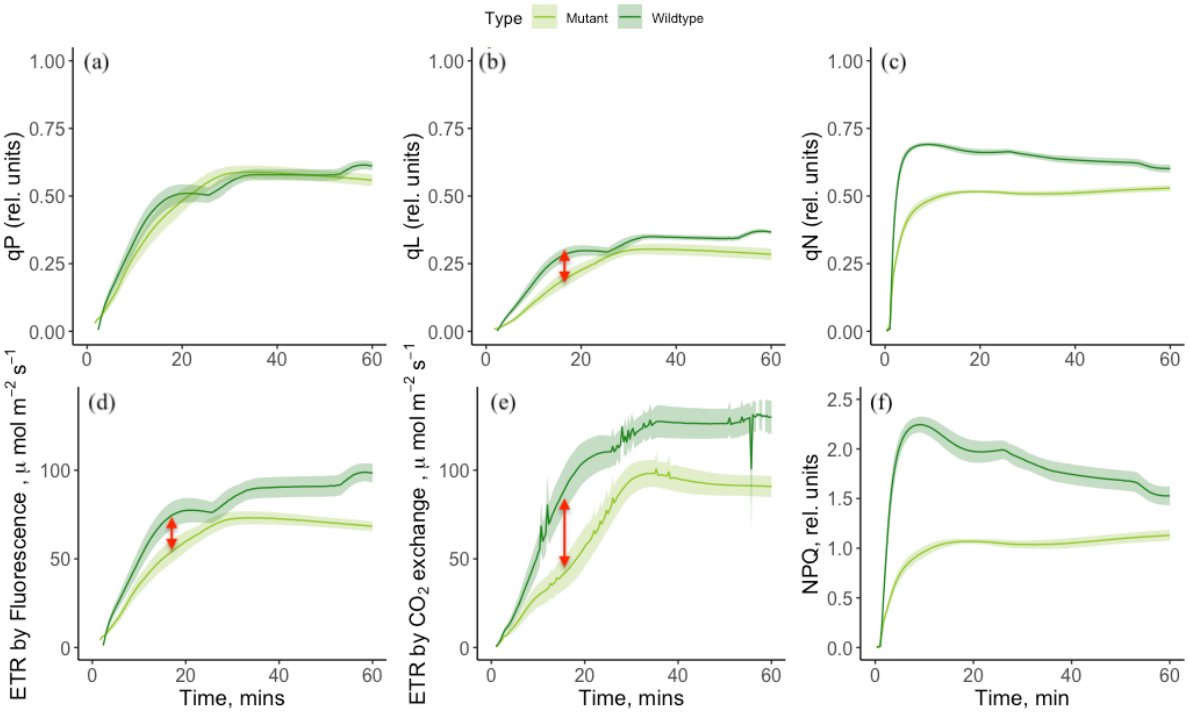

Fig. 14. Quenching analysis during photosynthetic induction on dark-adapted leaves comparing wild type (Eiko, also defined here as WT_{Sb}) and Chl-deficient mutant (Minngold). (**a**) photochemical quenching on the basis of puddle model, (**b**) fraction of open reaction centre on the basis of lake model, (**c**) percentage of non-photochemical quenching, (**d**) electron transport estimated using fluorescence parameters, (**e**) electron transport estimated using CO_2 gas-exchange, and (**f**) non-photochemical quenching calculated based on Bilger & Björkmann (1990). Red arrows emphasise the difference between wild type and mutant during the induction phase. Plants are grown in either constant or fluctuating light condition and dark-adapted overnight prior to measurement. During the induction, light is maintained at constant intensity (650 µmol m^{-2} s^{-1}).

To investigate the consequence of Chl-deficiency on the excitonic energy transfer, I analysed the quenching of ChlF by (1) photochemical quenching parameters based on puddle and lake model, (2) NPQ parameters, and (3) electron transport by fluorescence and CO_2 gas-exchange. Fig. 14a showed that the efficiency for photochemical quenching (qP) based on the puddle model was identical between WT_{Sb} and Chl-deficient mutant further supporting the similar PSII efficiency for both plant types (Fig. 13). On the other hand, the fraction of open reaction centres (qL) was observed to be lower in the mutant compared to WT_{Sb} (Fig. 14b). This parameter was based on the lake model where the PSII units are assumed to share the light-harvesting antennae. Notably, the difference in qL seemed parallel to the difference

in electron transport calculated using fluorescence parameter (Fig. 14d). Furthermore, the difference between WT_{Sb} and mutant during the induction phase was higher when the rates of electron transport was calculated based on CO_2 gas-exchange (Fig. 14e). During the induction phase in mutant, the estimated ETR by CO_2 exchange was lower than that estimated using fluorescence (red arrow in Fig. 14d & 14e), while in WT_{Sb}, this was not true. Moreover, the ETR estimated by gas-exchange exceeds that of fluorescence for both plant types during steady-state (> 30 mins; Fig. 14d, 14e & 16). Lastly, a lower qN was observed in the mutant as compared to WT_{Sb}, while this difference was more prominent in NPQ parameter (Fig. 14c & 14f).

3.1.3. Kinetics of NPQ and Φ_{PSII} during Light Fluctuations

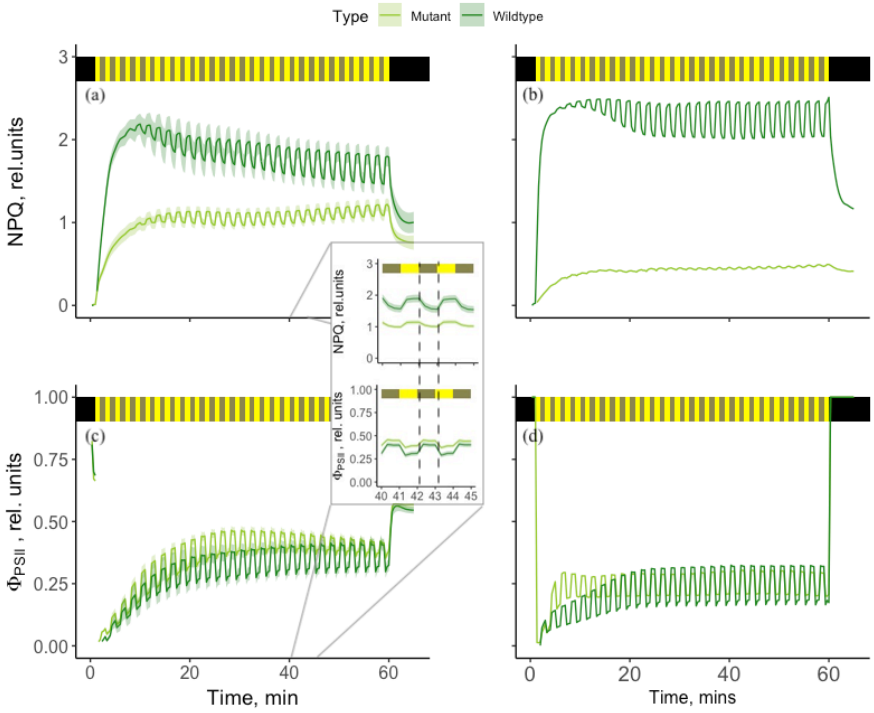

Fig. 15. Capacity and kinetics of non-photochemical quenching (NPQ) and the operating efficiency of photosystem II (Φ_{PSII}) traced during light fluctuations upon dark-to-light transition comparing wild type (WT_{Sb}; Eiko cultivar) and Chl-deficient mutant (Minngold) measured on non-stressed (**a, c**) and stressed (**b, d**) conditions. Graph shows NPQ kinetics (**a, b**) and Φ_{PSII} (**c, d**) measured on a dark-adapted leaf. The insert shows a magnified response of NPQ and Φ_{PSII} during transition from high (bright yellow) to low (dark yellow) light.

To investigate whether Chl-deficiency had affected the kinetics of NPQ, we traced the NPQ adjustments during fluctuating light both on plants which were healthy and stressed (after drought treatment). Pale mutants had consistently lower NPQ capacity which was more pronounced when in drought stress (Fig. 15a & 15b). The bigger difference was due to much lower NPQ in the mutant and a slightly higher NPQ in WT_{Sb} in stressed plants compared to non-stressed plants. Although fluctuations in NPQ seemed greater in WT_{Sb} than in mutant, NPQ derivatives (data not shown**)** revealed that the kinetics in non-stressed plants were identical when NPQ induction and relaxation were normalised to its amplitudes. In contrast, the pale mutant, when stressed, showed slower induction and relaxation (Fig. 15b). A replicated measurement confirmed that NPQ adjustments in the mutant were slowed down when stressed (Fig. S3). Generally, while NPQ increased from low to high light, Φ_{PSII} decreased. On the other hand, a change from high to low light decreased NPQ while increased the Φ_{PSII} (see insert in Fig. 15).

3.1.4. Comparing Electron Transport Rates by CO_2 Gas-Exchange and Fluorescence

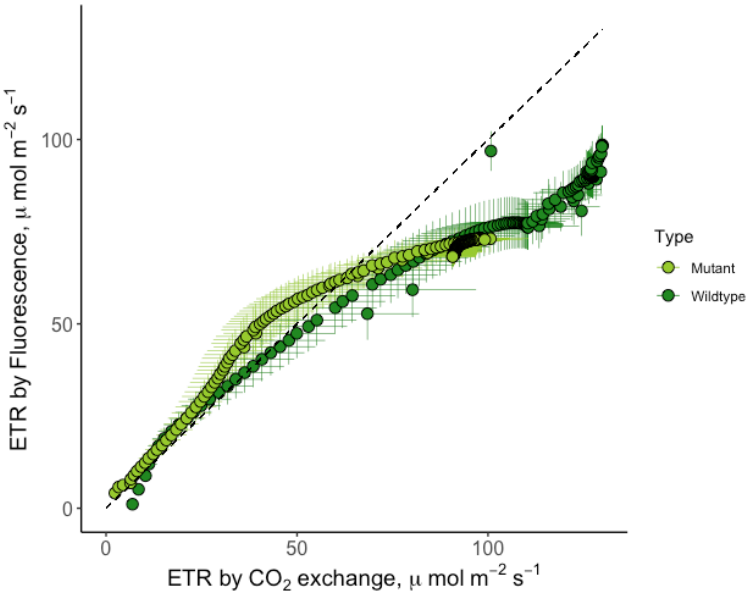

Fig. 16. Correlation between the rates of electron transport (ETR) estimated using CO_2 gas-exchange and fluorescence. The points derived from measuring green wild type soybean (Eiko; $WT_{Sb;}$ dark green) and Chl-deficient Minngold mutant (light green). Points further show mean values and standard error of 3 replicates collected during photosynthetic induction under constant illumination (650 µmol m^{-2} s^{-1}). Dash line shows 1:1 relationship.

The relationship between ETR by fluorescence and by CO_2 gas-exchange diverged from 1:1 for the two plant types at values above ca. 75 µmol m^{-2} s^{-1} (Fig. 16). Fig. 14d–e showed that these values (75 µmol m^{-2} s^{-1}) were achieved after ~30 mins of illumination. From this point, the ETR estimated by CO_2 exchange was higher than that estimated by fluorescence for both WT_{Sb} and Chl-deficient mutant. On the other hand, the ETR by fluorescence was higher than that of CO_2 exchange during the induction phase (10 to 20 mins), remarkably only in the case of the Chl-deficient mutant and not in WT_{Sb}.

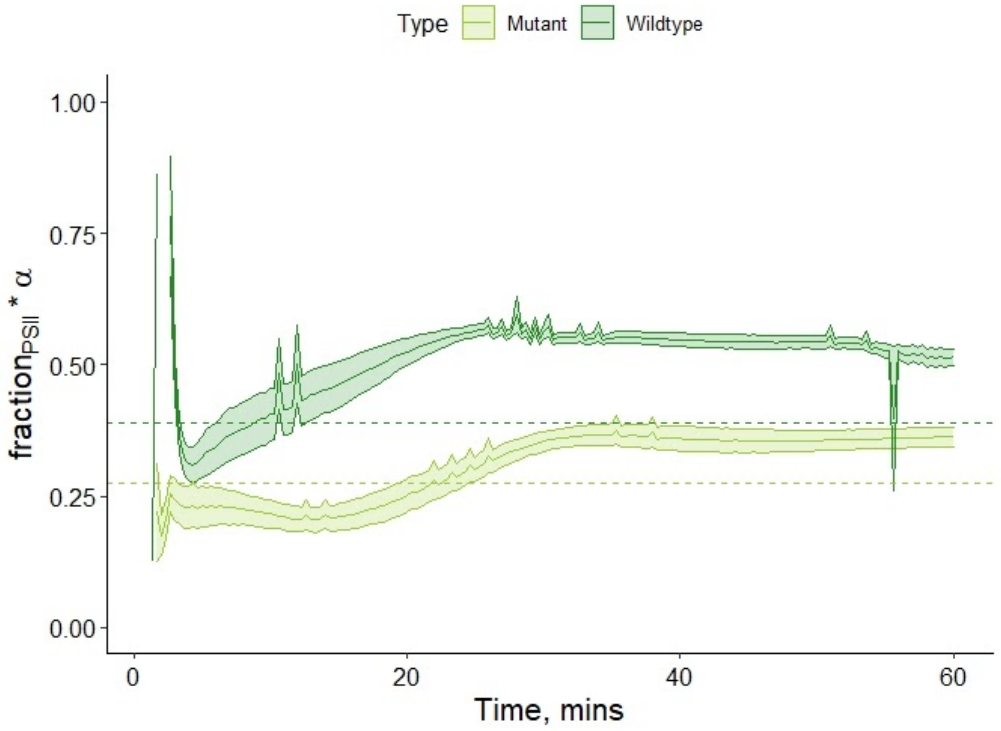

Fig. 17. Time course of the product of absorbance (α) and the fraction of light directed to PSII (F_{II}) during the 60 min photosynthetic induction under constant illumination (650 µmol m^{-2} s^{-1}). Line graphs are comparing the average and standard error in wild type (WT_{Sb}) and Chl-deficient mutant. The dashed lines indicate the constant value that is usually assumed in fluorescence-based ETR calculations.

The product of α x F_{II} changed dynamically particularly during the first 30 mins of photosynthetic induction as the actinic light was turned on (Fig. 17). The dynamic change was characterised by a steep decline for the first ~ 4 mins, then followed by a slow increase before reaching a steady-state (ca. 30 mins). The Chl-deficient mutant had consistently lower $\alpha \cdot F_{II}$ than the WT_{Sb}. The mutant also reached steady condition slower than the WT_{Sb} (WT_{Sb} ~ 25 mins, mutant ~ 30 mins).

3.2. Relationship among NPQ, Φ_{PSII} and F_{yield} at the Leaf Level

3.2.1. Relationship during Non-Steady-State Conditions

Fluorescence yield was maximum when NPQ and Φ_{PSII} were close to zero (Fig. 18). During moderate light intensity (650 μmol m^{-2} s^{-1}), F_{yield} was initially being quenched by regulated heat dissipation along with small increase in Φ_{PSII}. At saturating level of NPQ, F_{yield} was continually quenched by the increase in Φ_{PSII}. In the case of green WT_{Sb}, further increase in Φ_{PSII} consequently reduced NPQ level, while NPQ in Chl-deficient mutant remained at its peak (Fig. 18a). The degree of which the relationship shifted from direct to inverse proportionality between NPQ and Φ_{PSII} changed with respect to the amount of light absorbed, guided by red arrow (Fig 18a). Specifically, the curvature of the arrow was more pronounced in WT_{Sb} compared to Chl-deficient mutant, thus comparing the relative amount of light absorbed (i.e. WT_{Sb} has higher APAR than the mutant).

Likewise, cassava leaf exposed to high light fluctuations (90% decrease or 100% increase in light intensity), showed that the direction of F_{yield} quenching was towards the drastic increase in NPQ during high light scenario (2,000 μmol m^{-2} s^{-1}), while quenching was towards the increase in Φ_{PSII} at low light setting (200 μmol m^{-2} s^{-1}, Fig. 18b). Furthermore, when fluorescence was mostly quenched by NPQ, the maximal fluorescence in high light (F'_m) was very low (data not shown) – close to the value of steady-state F_{yield} – thus leading to low estimate of Φ_{PSII}. It is worth noting that under high light, Φ_{PSII} regulation was minimal, while regulation of NPQ was maximised. Under low light, both were regulated in a comparable degree.

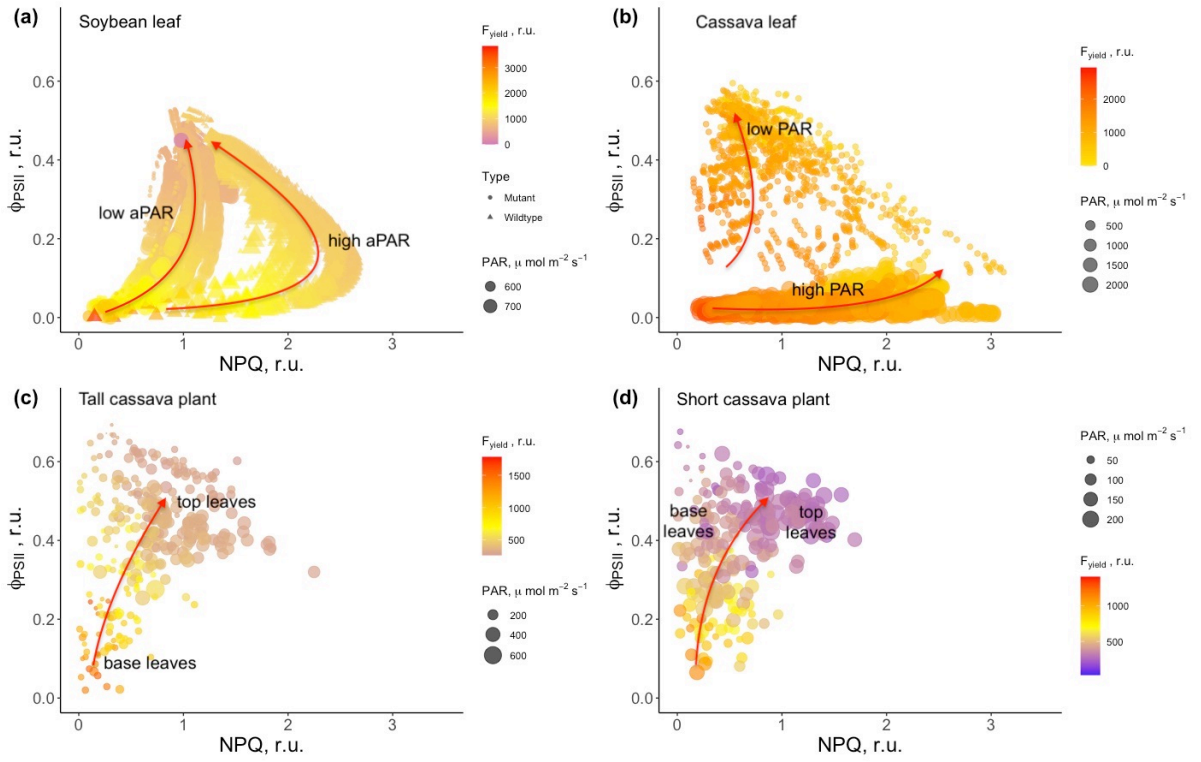

Fig. 18. Relationship between non-photochemical quenching (NPQ) and the operating efficiency of the photosystem II (Φ_{PSII}) effecting decrease in F_{yield} measured in (**a**) dark-adapted Soybean leaves comparing green cultivar (Eiko, WT_{Sb}) and Chl-deficient (Minngold, mutant) during induction using constant but moderate light intensity (650 µmol m^{-2} s^{-1}) or in fluctuating light scenario (780 µmol m^{-2} s^{-1} to 520 µmol m^{-2} s^{-1}), (**b**) dark-adapted cassava leaf during light fluctuations from high (2,000 µmol m^{-2} s^{-1}) to low light (200 µmol m^{-2} s^{-1}), (**c**) light-adapted tall cassava plant measured for all leaves, and (**d**) light-adapted small cassava plant measured for all leaves. The arrows indicate the direction of fluorescence decrease. Horizontal direction follows non-photochemical quenching measured as NPQ = (F_m – F'_m) / F'_m while vertical direction follows photochemical quenching measured as Φ_{PSII} = (F'_m – F_s / F_s).

3.2.2. Relationship during Steady-State Conditions

Similar to the induction phase, the level of F_{yield} on different leaves of a plant under more steady conditions was inversely proportional to the increasing NPQ and Φ_{PSII} (Fig. 18c & 18d). However, the relationship between NPQ and Φ_{PSII} changed depending on the light intensity incidental to the leaf and its corresponding intensity of F_{yield}. At high F_{yield}, Φ_{PSII} increased with increasing NPQ and incoming PAR. At low F_{yield}, Φ_{PSII} decreased with increasing NPQ and incoming PAR. This was true for both tall and small plants, albeit less pronounced in small plants.

At the top leaves, level of F_{yield} was in quenched state whilst, the decline in the level of Φ_{PSII} seemed to be regulated by the increase in NPQ activity. On the other hand, the base leaves received less incident light and thus showed both low level of Φ_{PSII} and NPQ with unquenched level of F_{yield} (Fig. 18c). From bottom leaves to the top, the level of F_{yield} decreased, while the relationship between NPQ and Φ_{PSII} changed from direct to inverse – an observation that was more pronounced in tall cassava plants. At low light, Φ_{PSII} ranges from 0.1 to 0.7 while NPQ remained less than 0.5. This was likely because the bottom leaves received low light and tended to be older which could be accentuated in taller canopy. In short plants however, the relationship between NPQ and Φ_{PSII} was generally directly proportional, except at higher Φ_{PSII} (> 0.4) where increase in NPQ seemed to decrease Φ_{PSII}. The base leaves in short plants had lower NPQ capacity but still had high Φ_{PSII}. Older leaves in cassava plants seemed to contribute less in overall photosynthetic efficiency of the plant.

3.3. Response of Turf Grass upon Application of DCMU Herbicide

Application of DCMU herbicide on turf grass immediately changed the ρ and SIF emission (Fig. 19). $F760_{yield}$ was instantly increased and continued until around 1 hr after application of DCMU. The increase in $F760_{yield}$ was similar to all doses of DCMU sprayed on grass carpet (Fig. 19a). Likewise, PRI also increased upon application of DCMU but reached a steady-state half an hour earlier than the $F760_{yield}$ (Fig. 19b). Also, the increase in PRI was similar to all doses of DCMU applied. In contrary, NDVI values dropped down upon application to DCMU. Albeit small decrease, the heaviest dose (D24) had the sharpest decline, while less steep in decline for lower doses of DCMU application (Fig. 19c).

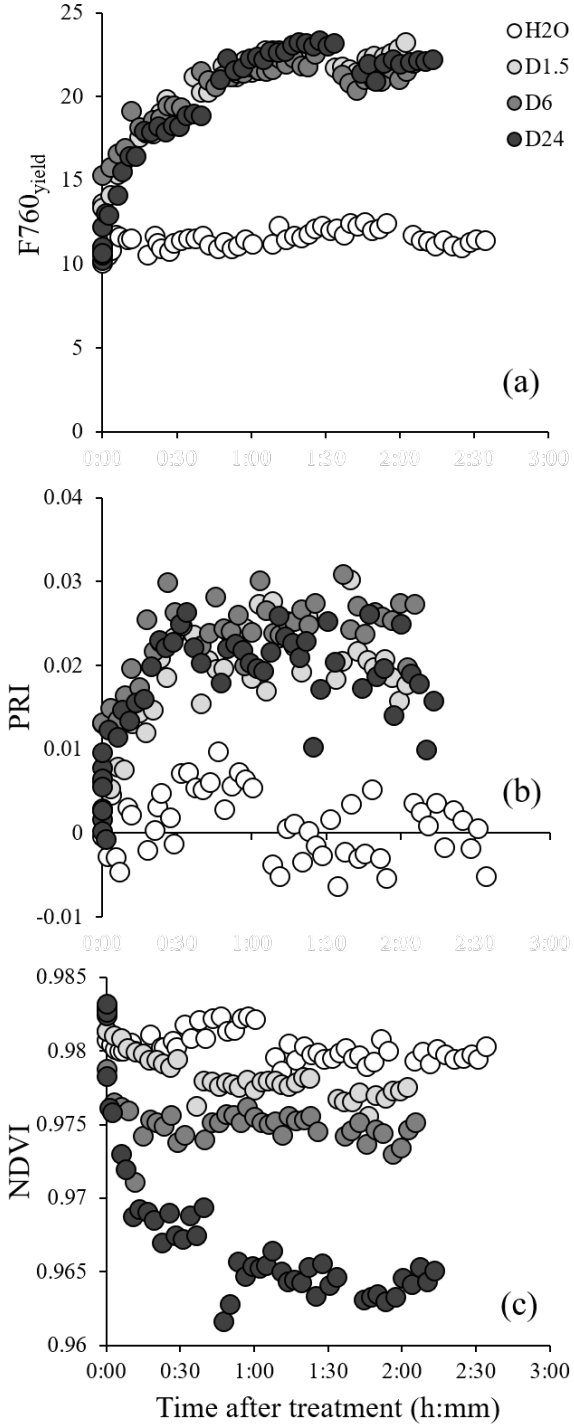

Fig. 19. Responses of (**a**) solar-induced fluorescence yield yield retrieved at O_2B band (760_{yield}) using Spectral Fitting Method (SFM), (**b**) photochemical reflectance index (PRI) and (**c**) normalised difference vegetation index (NDVI) measured on turf grass (*Poa pratense*) after treatment of different doses of DCMU. Measurement was performed at a regular interval for the duration of 2.5 hours. Different doses of DCMU (D1.5 – 1.5 mL of DCMU per L of H_2O; D6 – 6 mL DCMU per L of H_2O; and D24 – 24 mL of DCMU per L of H_2O) were compared with control treatment which was only sprayed with H_2O.

Figures **a** and **b** were modified from Figure S4 published in Pinto, F., Celesti, M., Acebron, K., Alberti, G., Cogliati, S., Colombo, R., ... & Panigada, C. (2020). Dynamics of sun-induced chlorophyll fluorescence and reflectance to detect stress-induced variations in canopy photosynthesis. *Plant, Cell & Environment.* 13.March.2020

The response of the ratio of F687 to F760 upon DCMU application was different when retrieval technique was based on iFLD method versus SFM (Fig. 20). In iFLD method, the SIF ratio of DCMU treated grass did not differ from that of control (H_2O). In contrast, SFM technique measured a slightly increased SIF ratio uniformly for all doses of DCMU treatment compared to control. This increase was more visible for the first 30 mins upon DCMU application. Notably, the SIF ratio on control plot showed slightly increasing trend

throughout the 2.5 hours of observation, making indistinguishable difference between DCMU and water treated plot after 1 hr.

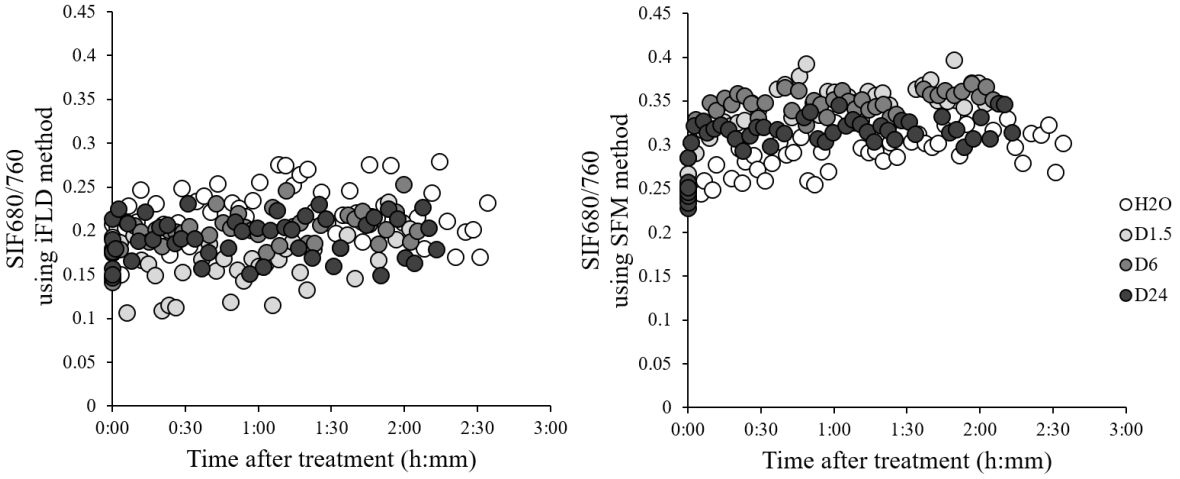

Fig. 20. The ratio of F687 and F760 retrieved either using improved Fraunhofer Line Depth (iFLD method, left) and Spectral Fitting Method (SFM, right) and traced upon application of DCMU herbicide on turf grass (*Poa pratense*). Measurement was performed at a regular interval for the duration of 2.5 hours. Different doses of DCMU (D1.5 - 1.5 mL of DCMU per L of H_2O, D6 - 6 mL DCMU per L of H_2O and D24 - 24 mL of DCMU per L of H_2O) were compared with control treatment which was only sprayed with H_2O.

3.4. Understanding Temporal Changes of NPQ using SIF and Spectral Reflectance in Arabidopsis *npq* Mutants

3.4.1. Effect of Reduced NPQ on Active Fluorescence Parameters

Fluorescence yield in both *npq* mutants was higher as compared to WT_{At}, more prominently towards reaching the steady-state condition (Fig. 21a). In contrast, Φ_{PSII} was similar in mutants and WT_{At} plants (Fig. 21b), while the degree of NPQ for both *npq* mutants was lower (Fig. 21c). Moreover, *npq1* had the level of NPQ abruptly increasing while *npq4* showed a gradually increasing trend. Results from PAM and LIFT were comparable despite differences in measurement approach of the two active methods. Despite the difference in F_{yield}, no morphological differences in size and greenness were observed between WT_{At} and *npq* mutants (Fig. 4).

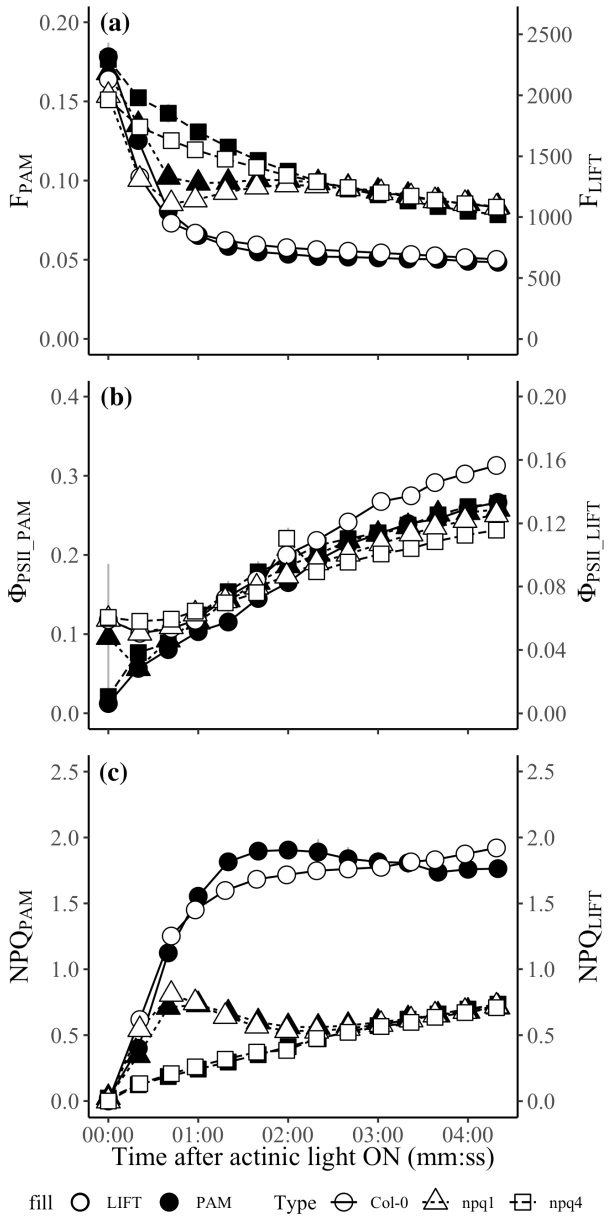

Fig. 21. Fluorescence dynamics after turning on the actinic light (370 µmol m^{-2} s^{-1}), measured in the dark-adapted *Arabidopsis thaliana* wild type (WT_{At}) and non-photochemical quenching (NPQ)- deficient (*npq*) mutants, using active fluorescence measurement techniques. Lines show 4.5-min induction of (**a**) the fluorescence yield from pulse-amplitude modulation technique (F_{PAM}) or light- induced fluorescence transients technique (F_{LIFT}); (**b**) the effective quantum yield of photosystem II (Φ_{PSII}); and (**c**) non-photochemical quenching (NPQ) of the Columbia 0 (Col-0) ecotype (circles), and mutants *npq1* (violaxanthin de-epoxidase (VDE)-deficient; triangles) and *npq4* (PsbS-deficient; squares). Measurements were taken using either pulse-amplitude modulation (PAM, closed symbols) or light-induced fluorescence transients (LIFT, open symbols) techniques. Points indicate the average ± standard error of five plants from each type, measured at room temperature with controlled illumination.

Image was taken from Figure 1 in Acebron, K., Matsubara, S., Jedmowski, C., Emin, D., Muller, O., & Rascher, U. Diurnal dynamics of non-photochemical quenching in Arabidopsis *npq* mutants assessed by solar-induced fluorescence and reflectance measurements in the field. *New Phytologist*. 05.Oct.2020

3.4.2. Diurnal Trend of PSII Efficiency, NPQ, and SIF in the Summer and Winter Conditions

During the summer day, Φ_{PSII} for all plant types was inversely proportional (Fig. 22a), whereas NPQ was directly proportional (Fig. 22b), to the incoming irradiation. The Φ_{PSII} was lowest in the midday when light intensity was at peak while NPQ was highest. At the end of the day, Φ_{PSII} for both mutants were significantly lower than WT_{At} (Table S4). NPQ for both *npq* mutants were lower than the WT_{At} almost consistently throughout the day. Similarly to NPQ, SIF followed the diurnal pattern of solar irradiation, i.e. F760 was highest during the mid-day while lowest in the early morning and late afternoon. While this trend applies for all plant types, *npq* mutants had higher SIF emission than WT_{At} (Fig. 22c). Conversely, $F760_{yield}$ in WT_{At} showed high values in the morning and late afternoon while lowest during mid-day (Fig. 22d). $F760_{yield}$ in mutants were higher than WT_{At} but tends to decrease towards the end of the day (Fig. 22d). At the end of the day, this decrease coincides with significantly lower Φ_{PSII} as compared to WT_{At} (Table S4).

In the winter, Φ_{PSII} for all plant types immediately decreased as soon as the plants were exposed to cold conditions (Fig. 23a). At the end of the day, F_v/F_m decreased more than 2-fold lower than its initial value (Fig. 23a, marked with asterisk). While value of Φ_{PSII} dropped rapidly after cold exposure, NPQ gradually increased during the course of the day (Fig. 23b). In addition, *npq* mutants showed different levels of NPQ compared to WT_{At}. Accordingly, differences in F760 were also observed between mutants and WT_{At} but were only evident during the initial hours of cold exposure, until mid-day (Fig. 23c). Thereafter, F760 was quenched similarly to all plant types. Interestingly, F760 emission followed a similar diurnal trend of $F760_{yield}$, both being independent from the diurnal solar irradiation (Fig. 23c & 23d). Notably, the quenched state was sustained until second day in winter (Fig. 24e & 24f). When plants were transferred back to the glasshouse, F_v/F_m for all types slowly increased, indicating a recovery of PSII efficiency (Fig. 25).

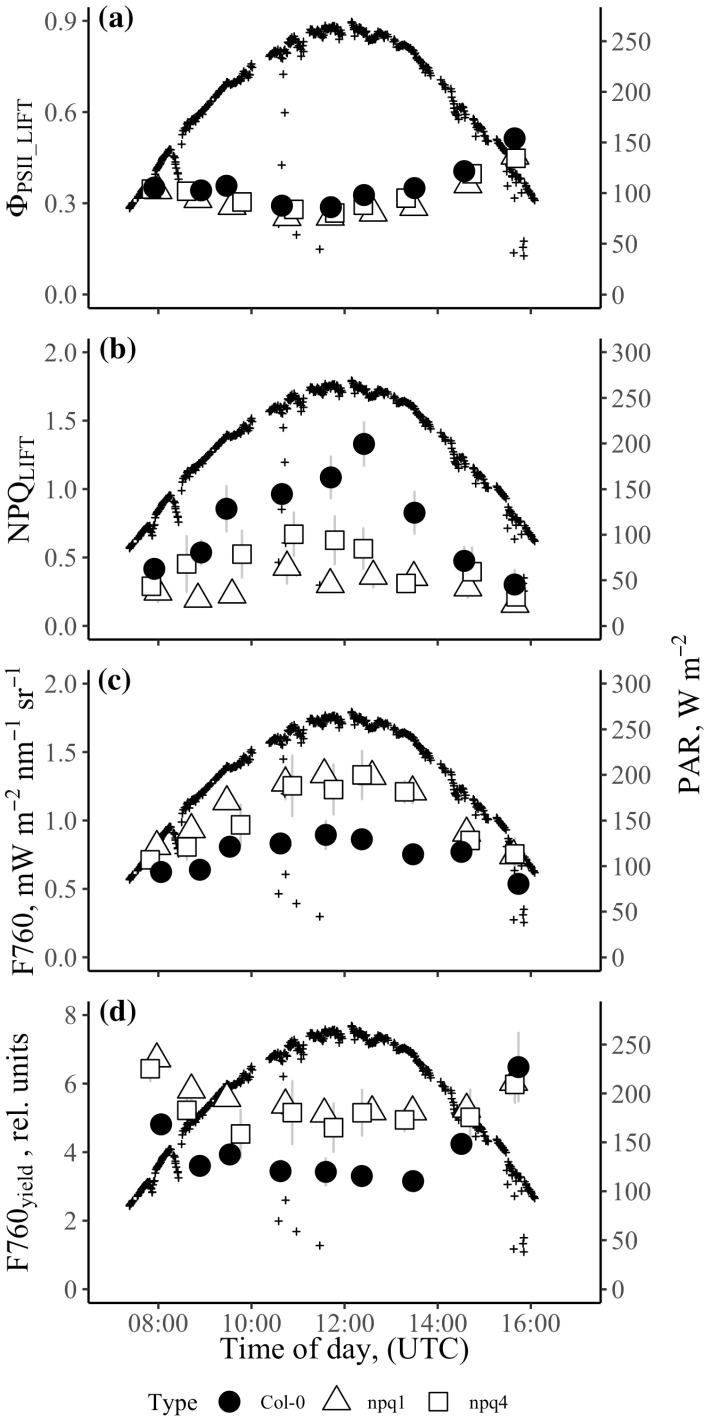

Fig. 22. Diurnal pattern of active and passive fluorescence parameters measured outdoors in the *Arabidopsis thaliana* wild type (WT_{At}) and non-photochemical quenching (NPQ)-deficient *npq* mutants during the day in summer. Points plotted on the left-hand y-axes are as follows: (**a**) effective quantum yield of photosystem II from light-induced fluorescence transients (LIFT) technique (Φ_{PSII_LIFT}); (**b**) non-photochemical quenching from LIFT technique (NPQ_{LIFT}); (**c**) solar-induced fluorescence emission at 760 nm (F760); and (**d**) solar-induced fluorescence yield at 760 nm ($F760_{yield}$). Photosynthetically active radiation (PAR) is plotted on the right-hand y-axis. Values are the average ± standard error of four plants from each plant type.

Image was taken from Figure 2 in Acebron, K., Matsubara, S., Jedmowski, C., Emin, D., Muller, O., & Rascher, U. Diurnal dynamics of non-photochemical quenching in Arabidopsis *npq* mutants assessed by solar-induced fluorescence and reflectance measurements in the field. *New Phytologist*. 05.Oct.2020

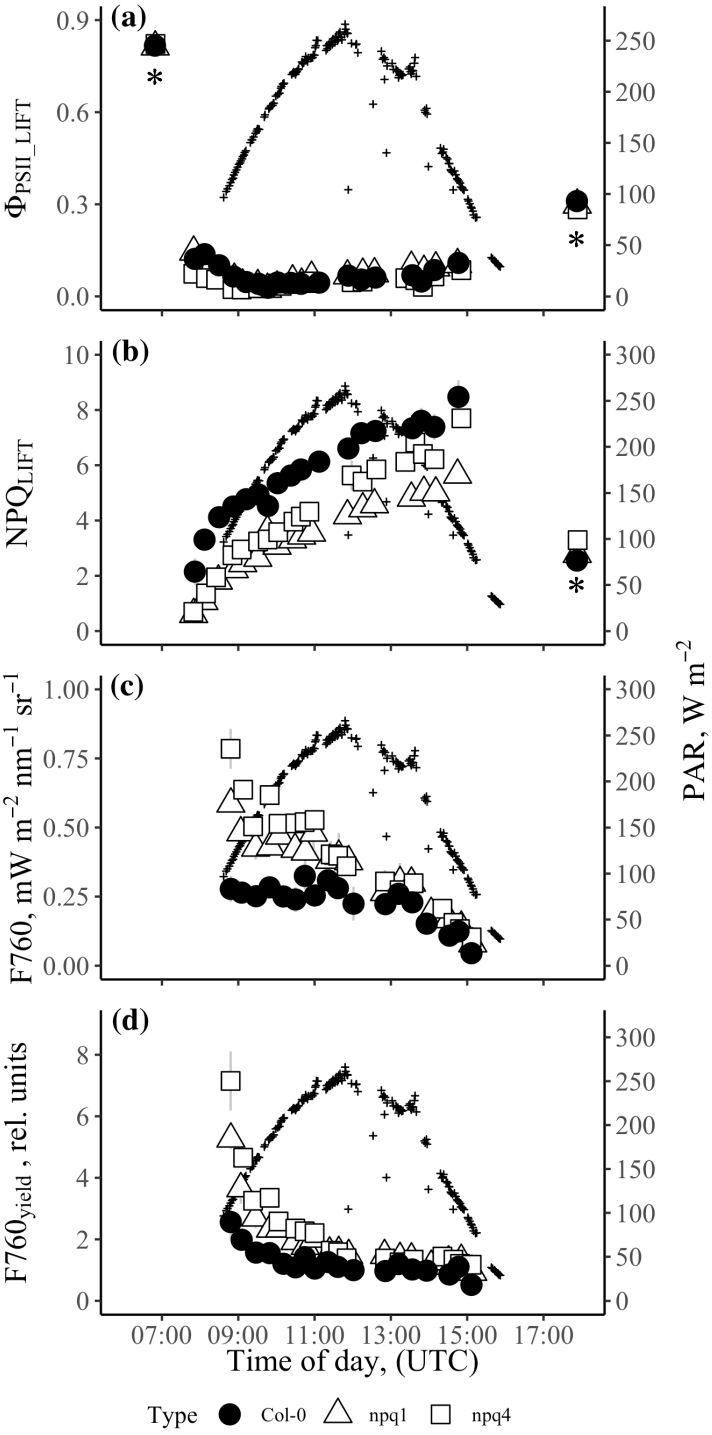

Fig. 23. Diurnal pattern of active and passive fluorescence parameters measured outdoors in the *Arabidopsis thaliana* wild type (WT_{At}) and non-photochemical quenching (NPQ)-deficient *npq* mutants when exposed in a cold day for the first time, mimicking a winter spell effect on plants. Points plotted on the left-hand y-axes are (**a**) effective quantum yield of photosystem II from light-induced fluorescence transients (LIFT) technique (Φ_{PSII_LIFT}), (**b**) non-photochemical quenching from LIFT technique (NPQ_{LIFT}), (**c**) solar-induced fluorescence emission at 760 nm (F760) and (**d**) solar-induced fluorescence yield at 760 nm ($F760_{yield}$), while photosynthetically active radiation (PAR) is plotted on the right-hand y-axis. Data points with asterisks are measurements relating to dark-adapted plants in glasshouse conditions. Values are the average ± standard error of three plants from each plant type.

Image was taken from Figure 3 in Acebron, K., Matsubara, S., Jedmowski, C., Emin, D., Muller, O., & Rascher, U. Diurnal dynamics of non-photochemical quenching in Arabidopsis *npq* mutants assessed by solar-induced fluorescence and reflectance measurements in the field. *New Phytologist*. 05.Oct.2020

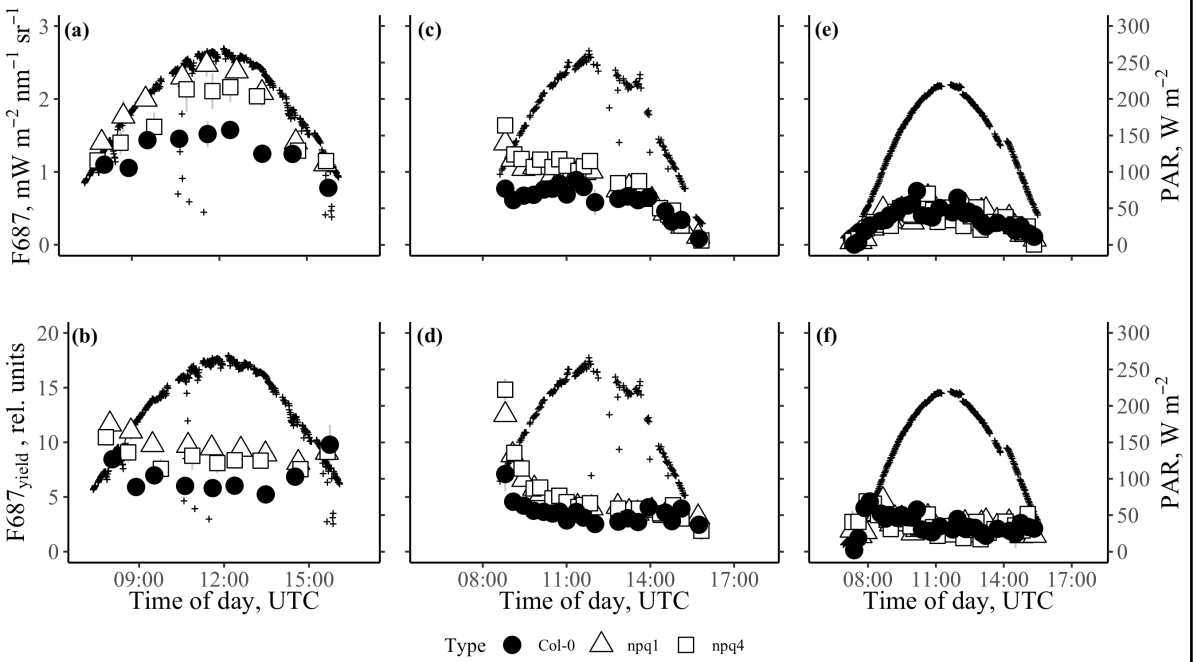

Fig. 24. Diurnal pattern of solar-induced fluorescence at 680 nm (**a, c, e,** F687) emission and (**b, d, f**; $F687_{yield}$) yield measured outdoors in the *Arabidopsis thaliana* wild type (WT_{At}) during (**a, b**) summer, and simulated cold spell in (**c, d**) day 1 and (**e, f**) day 2. Photosynthetically active radiation (PAR) is plotted on the right-hand y-axis. Data points with asterisks are measurements relating to dark-adapted plants in glasshouse conditions. Values are the average ± standard error of three to four plants from each plant type.

Image was taken from Figure S4 in Acebron, K., Matsubara, S., Jedmowski, C., Emin, D., Muller, O., & Rascher, U. Diurnal dynamics of non-photochemical quenching in Arabidopsis *npq* mutants assessed by solar-induced fluorescence and reflectance measurements in the field. *New Phytologist*. 05.Oct.2020

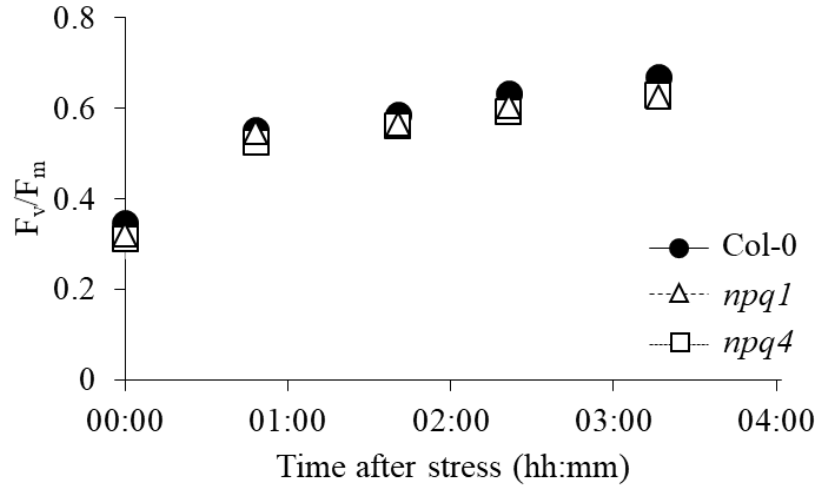

Fig. 25. Recovery of F_v/F_m measured in *Arabidopsis thaliana* Col-0 ecotype (WT_{At}), violaxanthin de-epoxidase (VDE)-deficient *npq1* mutant and PsbS-deficient *npq4* mutant after exposure for two days in cold winter. Values are the average ± standard error of three plants for each plant type.

Image was taken from Figure S5 in Acebron, K., Matsubara, S., Jedmowski, C., Emin, D., Muller, O., & Rascher, U. Diurnal dynamics of non-photochemical quenching in Arabidopsis *npq* mutants assessed by solar-induced fluorescence and reflectance measurements in the field. *New Phytologist*. 05.Oct.2020

3.4.3. Effect of Reduced NPQ Capacity on SIF Spectra

In an instantaneous leaf-level, *npq* mutants showed higher SIF_{yield} consistently at the two fluorescence peaks across the spectrum (Fig. 26a). In the field, strong correlation between F687 and F760 was observed in summer for all plant types (r = 0.95, Fig. 26b). Although I found similar relationship in winter day, more residuals were observed in first day with only r of 0.88 (Fig. 26c) while the correlation was weakest on the second day (r = 0.71, Fig. 26d).

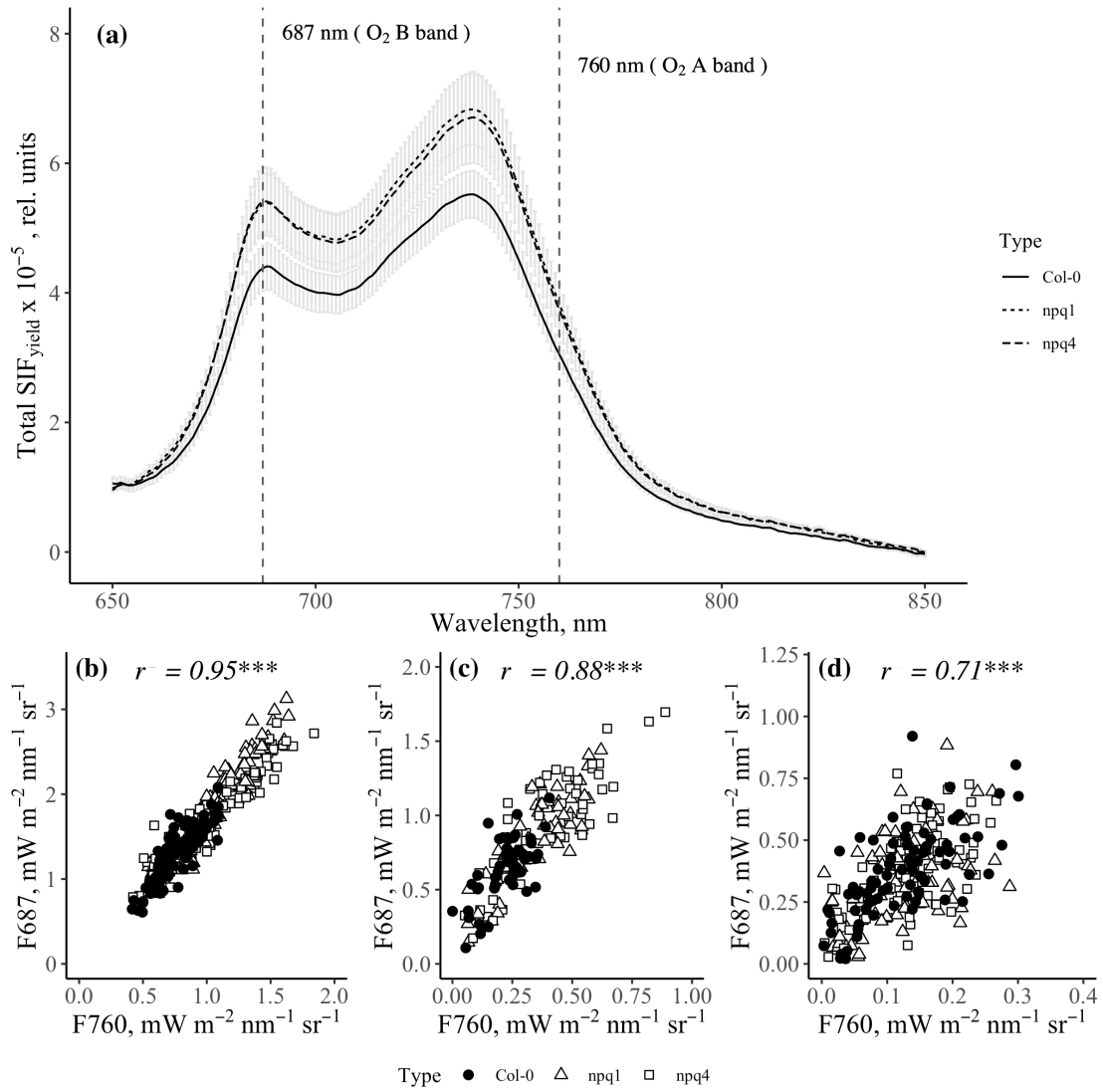

Fig. 26. Relationship between the two fluorescence peaks as affected by the mutation in non- photochemical quenching (NPQ), presented in full spectra of solar-induced fluorescence yield (SIF_{yield}), as well as solar-induced fluorescence retrieved in O_2A (F760) and O_2B (F687) absorption bands using the improved Fraunhofer Line Depth (iFLD) method. The graphs show the following: (**a**) total SIF_{yield} spectra measured in upwelling and downwelling emissions of a single leaf for each plant type; (**b**) correlation between F687 and F760, measured diurnally during the summer; (**c**) correlation between F687 and F760, measured diurnally during the cold winter on the first day of exposure; and (**d**) the second day of exposure. Values are the average ± standard error of four plants from each plant type. Pearson's correlation coefficients (*r*) are displayed at the top of each graph (***p-value < 0.001).

Image was taken from Figure 4 in Acebron, K., Matsubara, S., Jedmowski, C., Emin, D., Muller, O., & Rascher, U. Diurnal dynamics of non-photochemical quenching in Arabidopsis *npq* mutants assessed by solar-induced fluorescence and reflectance measurements in the field. *New Phytologist*. 05.Oct.2020

3.4.4. Analysis of Spectral Reflectance across the Visible Spectral Window

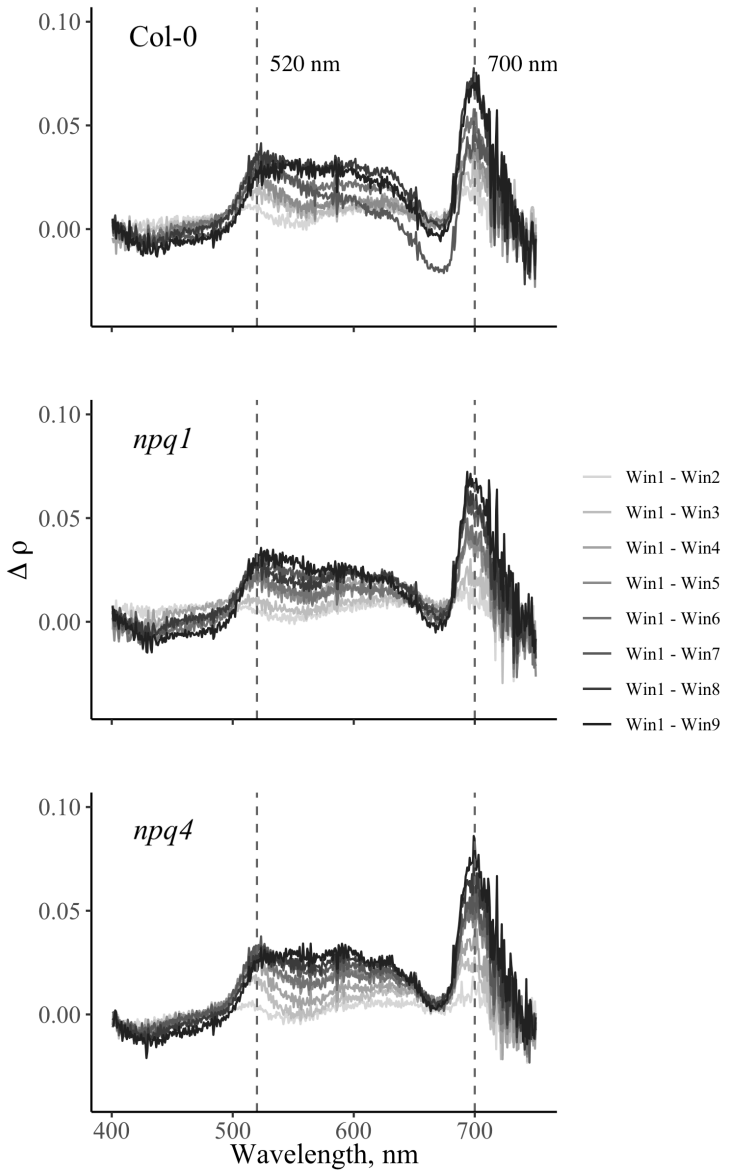

Fig. 27. Diurnal change in spectral reflectance ($\Delta\rho$) measured in *Arabidopsis thaliana* Col-0 wild type (WT_{At}), violaxanthin de-epoxidase (VDE)-deficient *npq1* mutant and PsbS-deficient *npq4* mutant in reference to the first measurement (Win1 - 7:34 to 8:15). Win2 - 8:20 to 9:07; Win3 - 9:13 to 10:00; Win4 - 10:24 to 11:07; Win5 - 11:16 to 11:56; Win6 - 12:09 to 12:55; Win7 - 13:04 to 13:50; Win8 - 4:06 to 15:04; Win9 - 15:17 to 16:04. Values are average of 3 to 4 plants per type.

This image was taken from Figure S6 in Acebron, K., Matsubara, S., Jedmowski, C., Emin, D., Muller, O., & Rascher, U. Diurnal dynamics of non-photochemical quenching in Arabidopsis *npq* mutants assessed by solar-induced fluorescence and reflectance measurements in the field. *New Phytologist*. 05.Oct.2020

There was a clear difference in ρ between WT_{At} and *npq1* characterised by two distinct peaks – one broadband signal peaking at 520 nm and a narrow range peaking at 700 nm (Fig. 28g). In contrast, the difference in ρ between WT_{At} and *npq4* was very subtle with a minor hump in 514 nm and 545 nm (Fig. 28h). I further investigated the diurnal changes in ρ measured in the summer day by conducting a cluster analysis. In all resolved cluster group, ρ

in WT_{At} and *npq4* were almost inseparable while majority of *npq1* were clustered together (Fig. 29). The major clustering found in the analysis were from WT_{At} and *npq4* measured from ~10:30 onwards (branch A, Fig. 29). Interestingly, the clustering also resolved ρ collected at different times of the day. In particular, there were clear separation of ρ data measured from morning, mid-day, and late afternoon within branch D (*npq1 cluster*) as well as in branch E (Col-0/*npq4* cluster).

Notably, both the difference in ρ between branch A and C in Fig. 31 were identical to the pattern of change in ρ ($\Delta\rho$) resolved as the difference between WT_{At} and *npq1* (Fig. 28g). Figs. 28d and 28f differentiated diurnal changes of ρ from mid-day to late afternoon which both had a broad peak centralised at 560 and a narrow peak at 700nm. Furthermore, the 700 nm peak observed was consistent, yet the magnitude was variable. In contrast, this peak was not observed in the difference between WT_{At} and *npq4* (Fig. 28h). The $\Delta\rho$ at different times of the day relative to the first measurement in the morning was peaking at 520 nm and 700 nm while the region from 520 nm to 650 nm is variable (Fig. 27). It is also worth noting that the 700 nm peak was consistently increasing from morning to afternoon for all plant types.

3.4.5. Effect of High Light Acclimation on the Spectral Reflectance of Arabidopsis *npq* Mutants

To investigate the difference in ρ between Arabidopsis plants grown in the glasshouse and in the field condition during summer, hyperspectral image of the plants was acquired using Specim IQ camera. Plants grown in the field (SA) were generally smaller than those grown in the glasshouse condition (Fig. 30a). Large variability in ρ in the range of 520 to 670 nm as well as from 720 to 1000 nm (Fig. 30b) was observed in all plants selected inside the hyperspectral image. The normalised difference vegetation index (NDVI) and red-edge inflection point (REIP) revealed that both *npq* mutants had significantly lower index values in SA plants compared to NSA plants, while WT_{At} did not seem to be affected (Fig. 30c – f). On the other hand, the PRI for all plant types were significantly reduced in SA plants compared to NSA plants (Fig. 30g & 30f). No significant difference in PRI were observed among plants grown in the glasshouse (NSA), while significant difference in response were observed in the field-grown plants (SA).

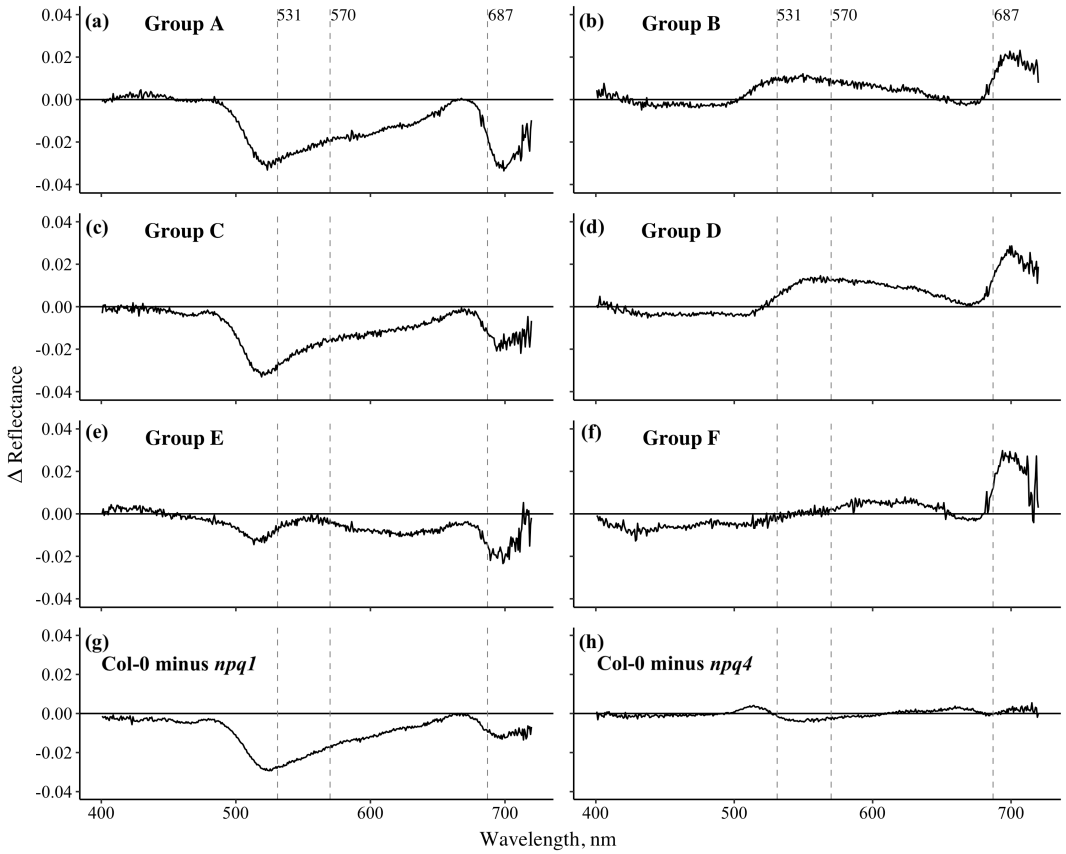

Fig. 28. Spectral characteristics of the difference in spectral reflectance (ρ) between two distinct sub-groupings resolved in the cluster analysis of summer data, as well as the ρ difference between the *Arabidopsis thaliana* wild type (WT_{At}) and non-photochemical quenching (NPQ)-deficient *npq* mutants. Data show two distinct peaks at ca 520 nm and ca. 700 nm, and are presented as follows: (**a**) measurement points identified with strong-minus-weak violaxanthin-antheraxanthin-zeaxanthin cycle (VAZ-cycle) activity; (**b**) mid-day minus late afternoon measurement within the violaxanthin de-epoxidase deficient *npq1* mutant cluster; (**c**) combined Columbia 0 (Col-0, WT_{At}) and PsbS-deficient *npq4* mutant reduced by *npq1* measurements, within the morning cluster; (**d**) measurements for mid-day minus late afternoon within strong VAZ activity; (**e**) 2nd to 3rd measurements less the 1st measurement within the morning cluster from both Col-0 or WT_{At} and *npq4*; (**f**) morning cluster minus *npq1* cluster within the weak VAZ activity; (**g**) all measurements in summer, during the day, for the Col-0 or WT_{At} minus mutant *npq1*; (**h**) all measurements in summer, during the day, for the Col-0 or WT_{At} minus mutant *npq4*. Horizontal dashes indicate reflectance used to calculate photochemical reflectance index (PRI) and solar-induced fluorescence (SIF) retrieval in O_2B absorption band.

Image was taken from Figure 7 in Acebron, K., Matsubara, S., Jedmowski, C., Emin, D., Muller, O., & Rascher, U. Diurnal dynamics of non-photochemical quenching in Arabidopsis *npq* mutants assessed by solar-induced fluorescence and reflectance measurements in the field. *New Phytologist*. 05.Oct.2020

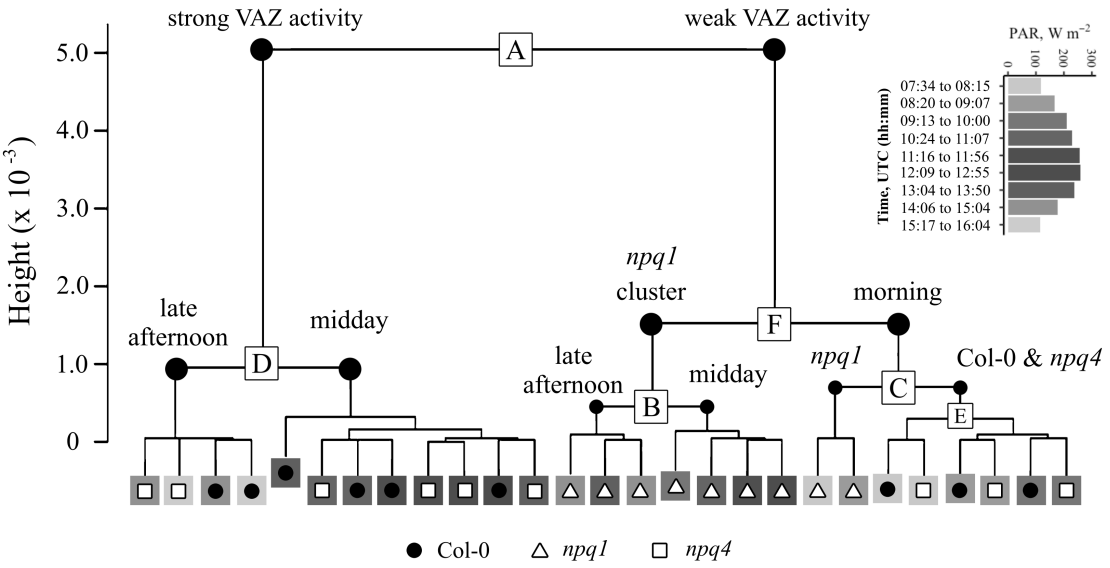

Fig. 29. Cluster analysis of spectral reflectance from 400 nm to 700 nm diurnally, measured during the day in summer, differentiating *Arabidopsis thaliana* violaxanthin de-epoxidase (VDE)-deficient *npq1* mutant from the wild type (WT_{At}) but not PsbS-deficient *npq4* mutant. Temporal groupings within plant types were also resolved from morning, mid-day and afternoon measurements. The time range of each measurement window and average light intensity are shown on the upper right-hand side of the figure. Letters indicate the point of separation of spectral reflectance, which was used as the basis for calculating the difference in reflectance ($\Delta\rho$) previously shown in Fig. 28.

Image was taken from Figure 8 in Acebron, K., Matsubara, S., Jedmowski, C., Emin, D., Muller, O., & Rascher, U. Diurnal dynamics of non-photochemical quenching in Arabidopsis *npq* mutants assessed by solar-induced fluorescence and reflectance measurements in the field. *New Phytologist*. 05.Oct.2020

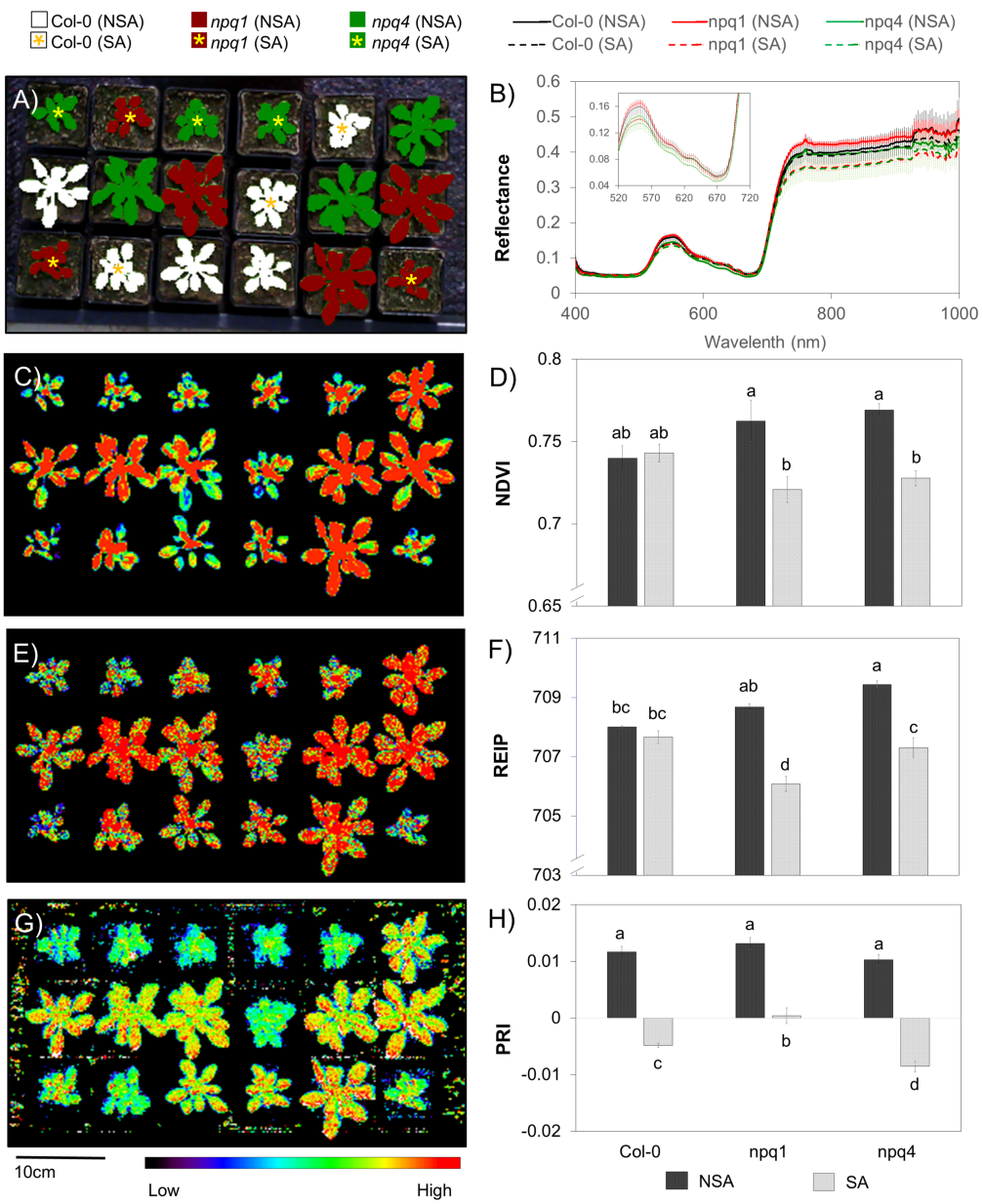

Fig 30. Differences observed between non-stress acclimated (NSA) and stress acclimated (SA) *Arabidopsis thaliana* Col-0 wild type (WT_{At}) and NPQ-deficient mutants (*npq1* and *npq4*) as shown by computed spectral ratios. Left panel shows the false-colour images of selected ROIs (**a**); NDVI (**c**); REIP (**e**); and PRI (**g**) computed from spectral information captured by the Specim IQ camera. Right panel shows the computed means ± standard errors of reflectance values (**b**); NDVI (**d**); REIP (**f**); and PRI (**h**) from three individual plants randomly distributed in the imaging frame. Different letters indicate significant differences based on LSD method (α=0.05).

Image was taken from Figure 6 in Behmann, J., Acebron, K., Emin, D., Bennertz, S., Matsubara, S., Thomas, S., ... & Mahlein, A. K. (2018). Specim IQ: evaluation of a new, miniaturized handheld hyperspectral camera and its application for plant phenotyping and disease detection. *Sensors*, *18*(2), 441. 2.Feb.2018

3.4.6. Measuring the Diurnal Dynamics of PRI in the Wild Type and *npq* Mutants in the Field Condition

In the summer, WT_{At} and *npq4* had similar diurnal trend of PRI while *npq1* was slightly sustained throughout the day (Fig. 31a). In winter, cold-naive WT_{At} plants had more stable PRI from the morning then decreased in the late afternoon (Fig. 31b). In the case of *npq1*, PRI was higher than WT_{At} in the morning then slightly increased, followed by a an abrupt decrease towards the end of the day. While, *npq4* had intermediate value between WT_{At} and *npq1*. On the second day, all plants had identical PRI trend that was following the diurnal course of solar irradiance (Fig. 31c).

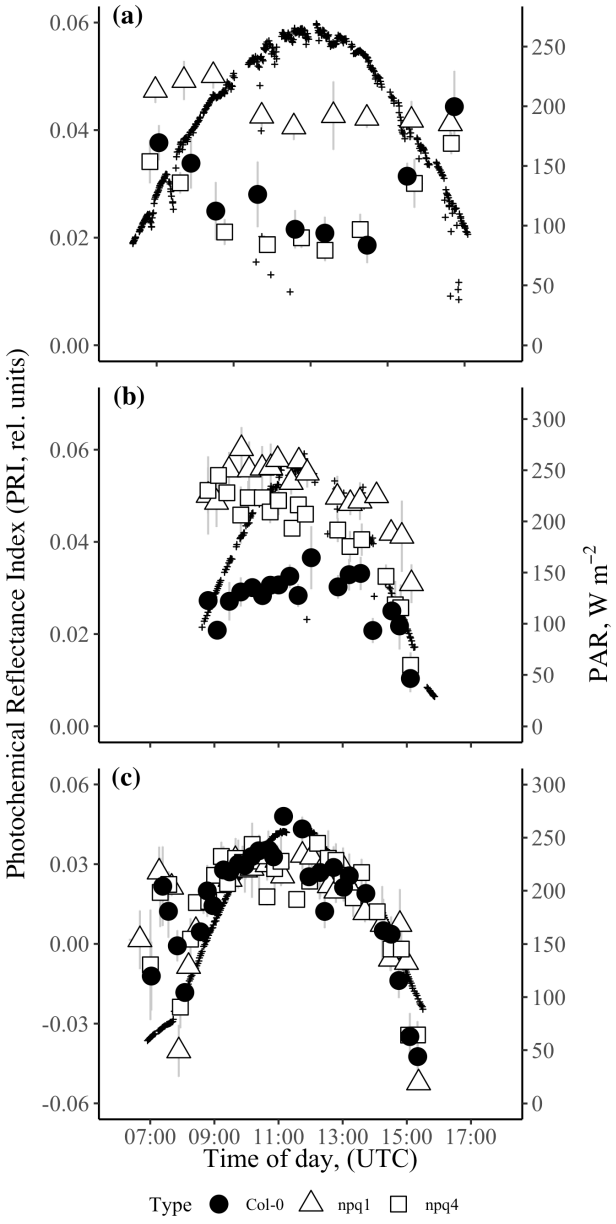

Fig. 31. Diurnal pattern of the photochemical reflectance index (PRI) measured in *Arabidopsis thaliana* wild type (WT_{At}), violaxanthin de-epoxidase (VDE)-deficient (*npq1*) and PsbS-deficient (*npq4*) mutants during one summer day and two winter days. The graphs show data points collected as follows: (**a**) during the day in summer, (**b**) on the first day and (**c**) on the second day of exposure in the cold. Values are the average ± standard error of three to four plants per genotype.

Image was taken from Figure 5 in Acebron, K., Matsubara, S., Jedmowski, C., Emin, D., Muller, O., & Rascher, U. Diurnal dynamics of non-photochemical quenching in Arabidopsis *npq* mutants assessed by solar-induced fluorescence and reflectance measurements in the field. *New Phytologist*. 05.Oct.2020

Diurnal measurement of PRI and NPQ in the summer, showed clear inverse relationship similarly in both WT_{At} and *npq* mutants, although WT_{At} reached higher NPQ than the mutants (Fig. 32, top graph). In contrast, the inverse relationship of PRI and NPQ became less distinct in winter. While WT_{At} had higher NPQ and lower PRI, mutants had lower NPQ and higher PRI (Fig. 32, bottom graph).

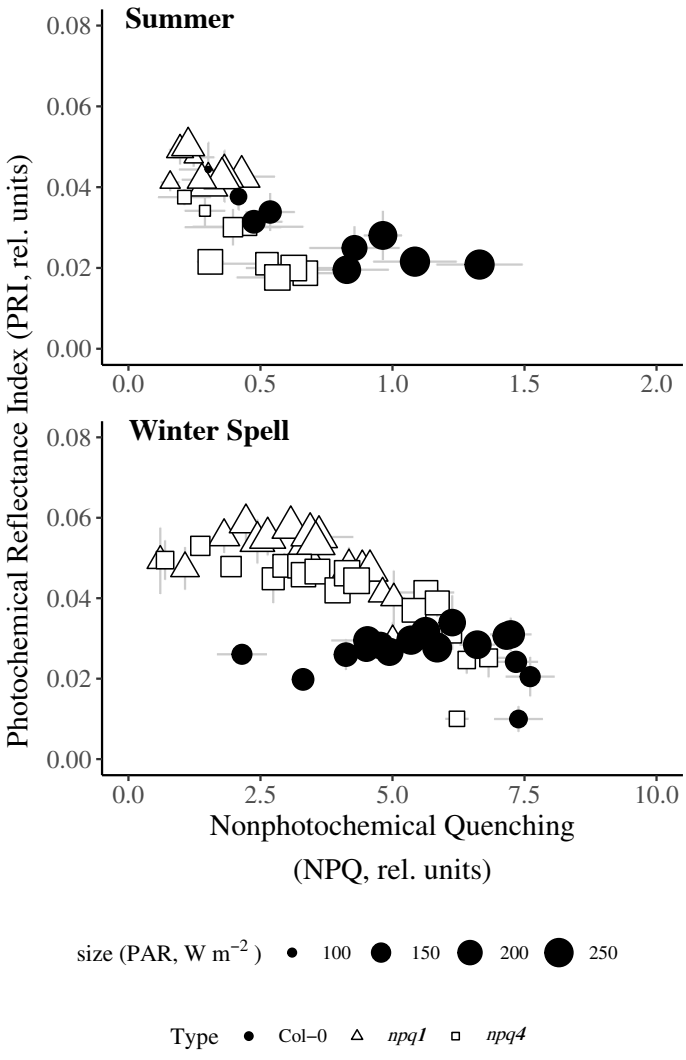

Fig. 32. Relationships between non-photochemical quenching (NPQ) and photochemical reflectance index (PRI), measured in *Arabidopsis thaliana* wild type (WT_{At}), violaxanthin de-epoxidase (VDE)-deficient (*npq1*) mutant and PsbS-deficient (*npq4*) mutant diurnally in summer and winter spell. Points are the average ± standard error of three to four plants from each type, repeatedly measured throughout the day. The size of the points shows the level of the incoming photosynthetically active radiation (PAR).

Image was taken from Figure 6 in Acebron, K., Matsubara, S., Jedmowski, C., Emin, D., Muller, O., & Rascher, U. Diurnal dynamics of non-photochemical quenching in Arabidopsis *npq* mutants assessed by solar-induced fluorescence and reflectance measurements in the field. *New Phytologist*. 05.Oct.2020

3.4.7. Relationship of $F760_{yield}$ to Φ_{PSII}, NPQ and PRI

For WT_{At} plants, $F760_{yield}$ was directly related to Φ_{PSII} but inversely related to NPQ during summer day (Fig. 33a & 33c). The correlation of determination of $F760_{yield}$ to Φ_{PSII} was slightly higher than to NPQ (Table 3). In mutants, $F760_{yield}$ was directly related to Φ_{PSII} only in the morning, then became independent from Φ_{PSII} towards the afternoon. Furthermore, $F760_{yield}$ had a curvilinear relationship with NPQ in both mutants. Contrastingly in winter, $F760_{yield}$ in all plant types was directly related to Φ_{PSII} only in the morning then became inversely related in the afternoon (Fig. 33b**)**. In contrast, $F760_{yield}$ had a strong but non-linear inverse relationship with NPQ (r = 0.88) throughout the whole day in winter for all plant types (Fig. 33d).

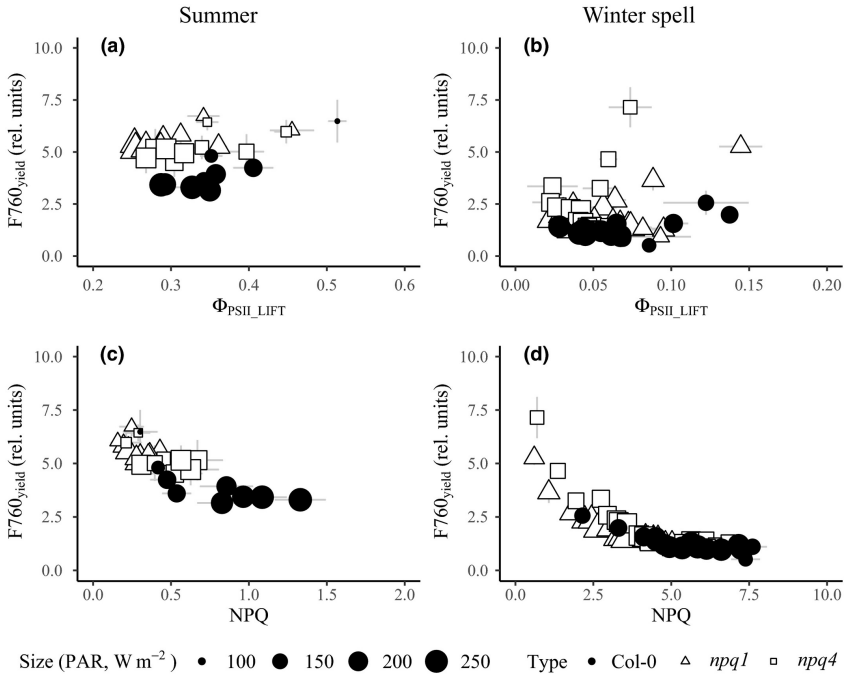

Fig. 33. Relationships between solar-induced fluorescence (SIF) and active fluorescence parameters: solar-induced fluorescence yield at 760 nm $F760_{yield}$ vs effective quantum yield of photosystem II from light-induced fluorescence transients (LIFT) technique Φ_{PSII_LIFT} during (**a**) summer and, (**b**) winter spell, as well as $F760_{yield}$ vs non-photochemical quenching (NPQ) during (**c**) summer, and (**d**) winter spell. Points are average ± standard error measured diurnally on *Arabidopsis thaliana* wild type (WT_{At}) and *npq* mutants. The size of the points shows the development through the course of the day.

Image was taken from Figure 9 in Acebron, K., Matsubara, S., Jedmowski, C., Emin, D., Muller, O., & Rascher, U. Diurnal dynamics of non-photochemical quenching in Arabidopsis *npq* mutants assessed by solar-induced fluorescence and reflectance measurements in the field. *New Phytologist*. 05.Oct.2020

The correlation between $F760_{yield}$ and PRI was higher in the summer than in winter day (Table 3). $F760_{yield}$ was directly related to PRI in WT_{At} but not distinctly in both mutants during summer (Fig. 34, top). In winter, $F760_{yield}$ and PRI had a direct but non-linear relationship with level of saturation differs across plant types (Fig. 34, bottom). The correlation coefficients are summarised in Table 3.

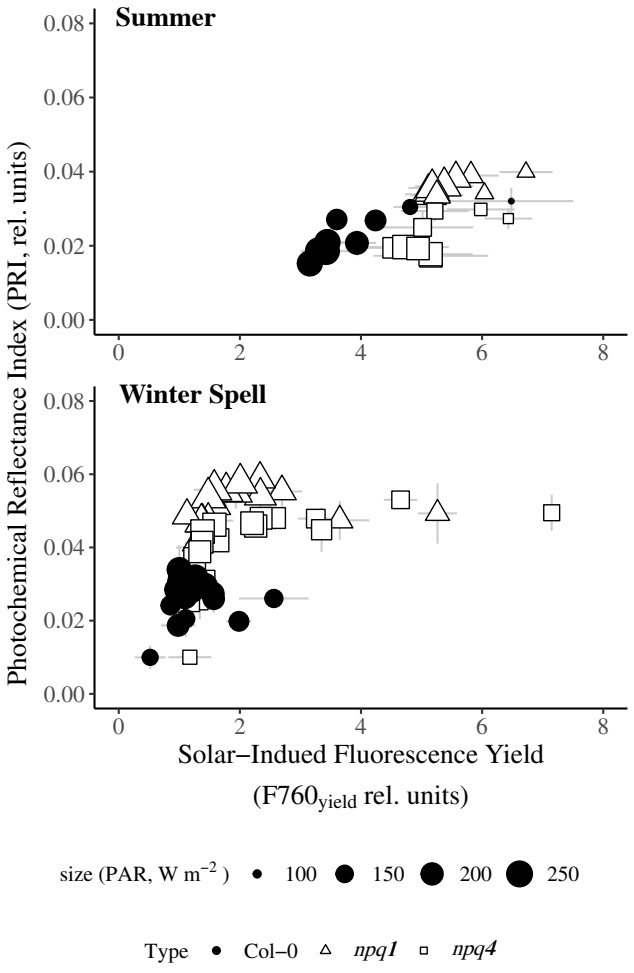

Fig. 34. Relationships between solar-induced fluorescence (SIF) and photochemical reflectance index (PRI), diurnally measured during the day in summer and winter spell, in the *Arabidopsis thaliana* wild type (WT_{At}) and *npq* mutants. Points are the average ± standard error of three to four plants. The size of the points shows the level of incoming photosynthetically active radiation (PAR).

Image was taken from Figure 10 in Acebron, K., Matsubara, S., Jedmowski, C., Emin, D., Muller, O., & Rascher, U. Diurnal dynamics of non-photochemical quenching in Arabidopsis *npq* mutants assessed by solar-induced fluorescence and reflectance measurements in the field. *New Phytologist*. 05.Oct.2020

Table 3. Correlation coefficients between $F760_{yield}$ and NPQ, and Φ_{PSII} and PRI.

	Summer			Winter		
	$F760_{yield}$ vs NPQ	$F760_{yield}$ vs Φ_{PSII}	$F760_{yield}$ vs PRI	$F760_{yield}$ vs NPQ	$F760_{yield}$ vs Φ_{PSII}	$F760_{yield}$ vs PRI
Col-0	-0.74^{*}	0.88^{**}	0.83^{**}	-0.78^{***}	0.05^{ns}	0.80^{***}
npq1	-0.58^{ns}	0.55^{ns}	0.67^{*}	-0.86^{***}	0.11^{ns}	0.72^{***}
npq4	-0.64^{ns}	0.55^{ns}	0.65^{ns}	-0.87^{***}	0.13^{ns}	0.75^{***}
All points	-0.83^{***}	0.29^{ns}	0.67^{***}	-0.79^{***}	-0.05^{ns}	0.72^{***}

Test of significance: ^{ns}not significant ($p > 0.05$), $^{*}p < 0.05$, $^{**}p$, 0.01, $^{***}p<0.001$

Partial results of this presented work have been published as Table 1 in: Acebron, K., Matsubara, S., Jedmowski, C., Emin, D., Muller, O., & Rascher, U. Diurnal dynamics of non-photochemical quenching in Arabidopsis *npq* mutants assessed by solar-induced fluorescence and reflectance measurements in the field. *New Phytologist*. 05.Oct.2020

3.5. NPQ of Cassava Assessed by Non-Invasive Measurements of SIF and Spectral Reflectance

Cassava plants grown in the glasshouse had different photosynthetic capacity compared to that grown in the field. Plants in the glasshouse had slightly higher Φ_{PSII}, NPQ and *A*, while lower F_{yield} was observed compared to field grown plants. Moreover, glasshouse plants had more dynamic Φ_{PSII}, NPQ, *A* and g_{sw} under fluctuating light compared to field-grown plants (Fig. 35). On the other hand, stomatal conductance (g_{sw}) in field-grown plants was almost stable throughout the fluctuating light protocol.

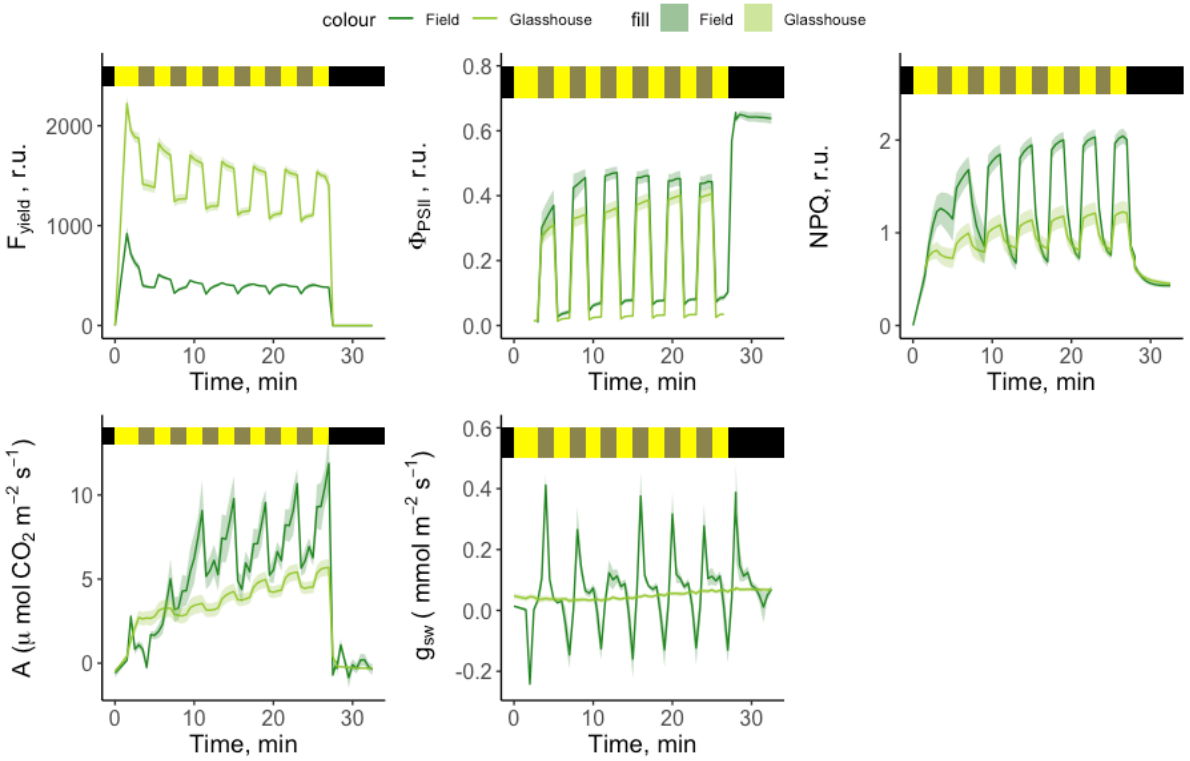

Fig. 35. Comparison of leaf-level fluorescence and gas-exchange between cassava plants grown in the glasshouse (light green) and in the field (dark green). Graph shows fluorescence yield (F_{yield}), effective quantum yield of photosystem II (Φ_{PSII}), non-photochemical quenching (NPQ), CO_2 assimilation rate (A) and stomatal conductance (g_{sw}) traced during fluctuating light. Single leaf for each plant was measured in a leaf cuvette (LI-6800) changing actinic illumination from 2,000 (light yellow) to 200 (dark yellow) µmol m^{-2} s^{-1} lasting 2 mins each to complete a cycle and a total of 6.5 cycles followed by 6 minutes of dark measurements. Values are average and standard error of 4 plants per type. CO_2 level was set to 400 ppm, leaf temperature at 27°C, relative humidity at 45%, flow rate at 600 µmol s^{-1}, and leaf vapour pressure deficit (VpdL) at 2.0.

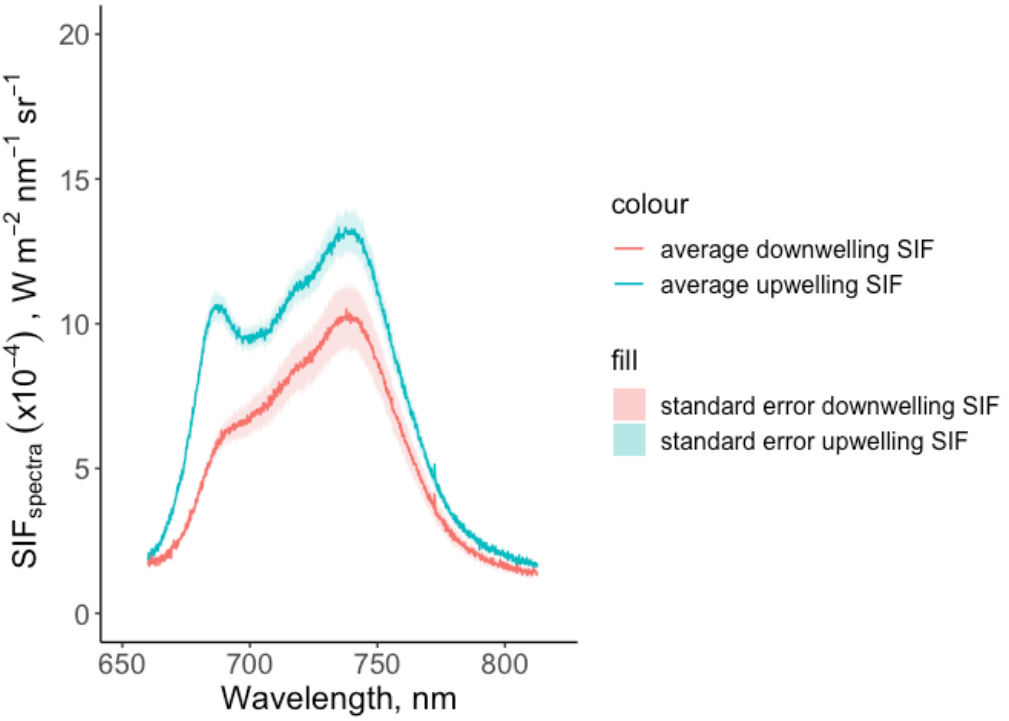

Fig. 36. Upward and downward emission spectra of solar-induced fluorescence (SIF) acquired at leaf-level from cassava wild type. Plants investigated were grown in the glasshouse and exposed in the clear sky outdoor condition for the first time. Measurements of SIF spectra were acquired using a modified FluoWat combined with FLOX system (see setup in Fig. 7). Values are average and standard error of four plants.

Solar-induced fluorescence emission was stronger on the adaxial side of the leaf where upwelling radiance was quantified along with reflected radiance, compared to the abaxial side where downwelling radiance was measured along with transmittance (Fig. 36). The upwelling SIF was characterised by two peaks; one in ca. 680 nm and the second at the ca 740 nm region. In contrast, the downwelling SIF had less shoulder at 680 nm but the 740 nm peak was still prominent.

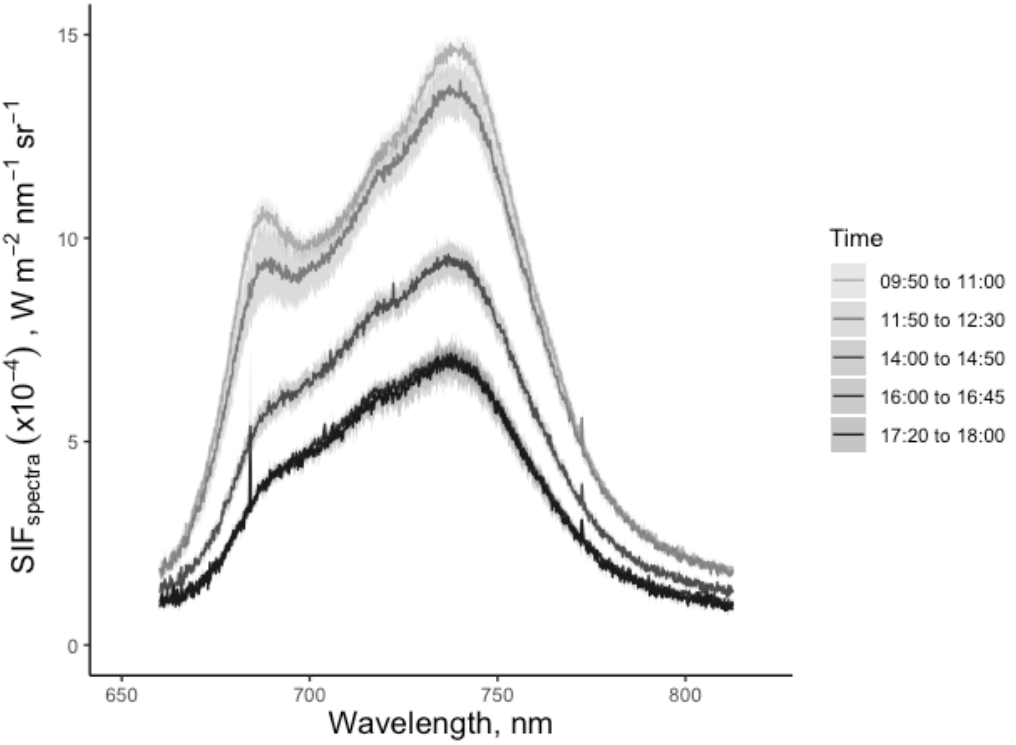

Fig. 37. Diurnal changes in the emission spectra of solar-induced fluorescence (SIF) from cassava cultivars. Plants grown in glasshouse were exposed to clear sky outdoor condition on the previous day prior to diurnal measurement resulting to slightly photo-inhibited plants. Data shows average and standard error of single leaf from four plants for each measurement window.

Solar-induced fluorescence emission was highest in the morning when the plants were exposed to outdoor condition (Fig. 37). Then, SIF emission gradually decreased towards the end of the day. This decrease seemed to be linear but the peak at 680 nm was clearly disappeared. Comparison of plants showed a ~ 55% decrease in F_v/F_m for those exposed in the field and those that were retained in the glasshouse.

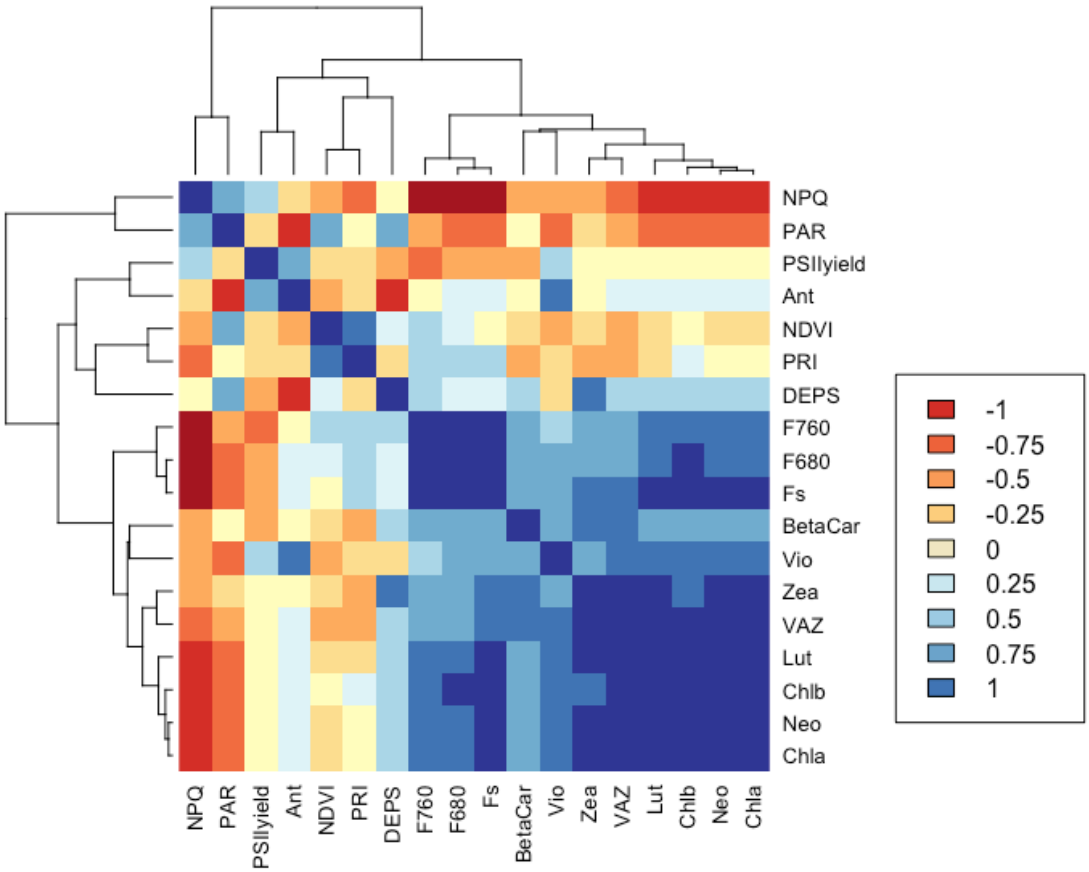

Fig. 38. Clustered display of the correlation coefficients derived among fluorescence parameters, vegetation indices and pigment composition. Data were acquired in cassava plants grown in the glasshouse and taken out in the field condition after 1 day of pre-acclimation. Colors indicate the degree of correlation, while the branches represent height and degree of similarity computed as a Eucledian distance between two parameters. Red color indicates negative correlation, while blue colour indicates positive correlation and yellow to no correlation. Parameters show non-photochemical quenching (NPQ), photosynthetically active radiation (PAR), effective quantum yield of photosystem II ($PSII_{yield}$), level of antheraxanthin (Ant), normalised difference vegetation index (NDVI), photochemical reflectance index (PRI), de-epoxidation state (DEPS), solar-induced fluorescence at 760 nm (F760), solar-induced fluorescence at 680 nm (F680), steady-state fluorescence from pulse-amplitude modulation technique (Fs), level of beta-carotene (BetaCar), level of violaxanthin (Vio), level of zeaxanthin (Zea), total violaxanthin, antheraxanthin and zeaxanthin pool (VAZ), level of lutein (Lut), level of chlorophyll *b* (Chl *b*), level of neoxanthin (Neo) and level of chlorophyll *a* (Chl *a*).

NPQ and PAR were clustered together while Φ_{PSII} was separated together with PRI, NDVI, DEPS and the level of antheraxanthin (Fig. 38). Interestingly, fluorescence parameters were grouped separately from the previous two clusters, while most of the pigment data were clustered together. NPQ had a strong negative correlation with F760, F680 and F_s from PAM, as well as with lutein, Chl *a* and *b* and neoxanthin, but a weaker

negative correlation with PRI (Fig. 38). In contrast, NPQ had a positive correlation with PAR and a much weaker positive correlation with Φ_{PSII}. Notably, NPQ had almost no relationship with DEPS. While, PRI had weak to almost no relationship with level of V or Z. PAR had a strong negative relationship with level of antheraxanthin. And, both of the passively retrieved fluorescence (F760 and F680) had strong positive relationship with F_{yield} retrieved from PAM. Φ_{PSII} had almost no correlation with Z, total VAZ, lutein, Chl *a* and *b* and neoxanthin while slight positive correlation was observed with V and slight negative correlation with beta-carotene.

4. DISCUSSION

In this thesis, I investigated the photosynthetic regulation of different plant species by looking at the the dynamic changes in PSII efficiency and NPQ at leaf level, both indoor (semi-controlled) and outdoor conditions. I have used different fluorescence techniques (i.e. PAM, LIFT, SIF) and later combined them with ρ measurements in order to bridge the knowledge gap between remote sensing signals and photosynthetic regulation in the field. By doing so, I resolved the dynamic changes in SIF in terms of photochemical and non-photochemical energy use diurnally at different seasons. First, I showed that Chl-deficient soybean mutant had reduced NPQ which was exacerbated under stressed condition. Consequently, the reduction in NPQ increased internal fluorescence yield (Φ_f) but the lower Chl concentration in the mutant leaves resulted to lower apparent F_{yield} (or brightness). This discrepancy indicates a strong influence of factors in between photosystem and leaf level that may affect how fluorescence photons escape the leaf surface. Moreover, despite no significant effect of Chl-deficiency in Φ_{PSII} and photochemical quenching (qP) parameter, the fraction of open reaction centre (qL) and ETR were shown to be lower in Chl-deficient mutant in a similar manner. Taken altogether, these observations are useful in modelling photosynthetic response of plants under fluctuating light using SIF data. Second, empirical associations among F_{yield}, PSII efficiency and NPQ at leaf level showed the relative strengths of either PSII photochemistry and NPQ to lower F_{yield} as affected by leaf status (e.g. age, location relative to the canopy, and the amount of light received and absorbed). These were examined in order to realise the energy balance inside the leaf and throughout the whole plant canopy. Third, Arabidopsis *npq* mutants were investigated indoor and outdoor diurnally during a summer day and simulated cold spell during winter in order to investigate the effect of different NPQ mechanisms on SIF and ρ. Results showed a similar increase in SIF for both NPQ-deficient mutants despite different mechanisms of NPQ affected. Furthermore, SIF was gradually quenching equally for all plant types as soon as photoinhibition was being developed, masking the previously observed effect of NPQ mutation on SIF. Cluster analysis of ρ revealed clear separation of *npq1* from both the wild type and *npq4*, indicating sensitivity of ρ signal to VAZ cycle and not in PsbS-mediated conformational change in the LHCII antenna system. Lastly, the strategies for SIF and PRI measurements were tested in cassava leaves in order to test the robustness of the remote sensing techniques in interpreting photosynthetic regulation. Afterwards, a summarised response of photochemical and non-

photochemical energy use at leaf level is hereby laid out to discuss the potential use and limitations of SIF and PRI on estimating photosynthesis from a single leaf to the canopy, regional and global scales.

4.1. Dark-to-Light Transition in Leaves

In the absence of light, NPQ, especially qE component, is relaxed; while the reaction centres are re-oxidised – that is, open to accept energy for initial charge separation. When dark-adapted leaves were exposed again to light, F_{yield} would gradually decrease due to increasing qP and NPQ (Fig. 13 & 14). This phenomenon is most commonly referred to as the 'Kautsky effect' (Kautsky et al., 1960). After exposing the leaves to steady for a long time (but low light), the steady-state F_{yield} was achieved with the maximum PSII efficiency (Fig. 13, 14 & 21). Havaux et al. (1990) provided evidence that the steady-state modulated F_{yield} represents a bioenergetic homeostasis. This is particularly noteworthy in the context of understanding dynamic changes in photosynthesis using SIF as previous works has related SIF to steady-state F_{yield} signal (van der Tol et al., 2014; Ač et al., 2015). In this experiment, the induction phase was examined because this may give complementary information on the response of NPQ, PSII efficiency and SIF during the dynamic changes in light intensity in the field.

During the induction phase, the ETR and NPQ increased simultaneously although not linearly (Fig. 18a & S4b). This non-linearity could be explained by various independent molecular events in the LHCII antenna that could act as competing energy sink for APAR. For instance, NPQ saturated quicker than qP (Fig. 14a–c). Using Arabidopsis *npq* mutants, I have shown that the fast induction in NPQ during dark-to-light transition was mainly governed by the activity of PsbS protein, while conversion of V to Z in the VAZ cycle contributes to the slower induction of NPQ (see comparative response of Arabidopsis *npq1* and *npq4* mutant in Fig. 21c). This is consistent from the previous study of the mechanistic function of qE to qP (Weis & Berry, 1987) as well as after characterising the response of the same Arabidopsis mutants exposed at different light intensities (Ikeuchi et al., 2016). Although Dall'Osto et al. (2014) previously demonstrated the contribution of chloroplast

movement in the quenching component of *npq4*, I did not observe a pattern in SIF that may have been ascribed to the photo-relocation of the chloroplasts.

The ETR based on fluorescence is a linear function of the incident light, Φ_{PSII}, α, and F_{II}. (Eqn. 11). During the induction phase, the increase in ETR was tightly linked with increased in qP, qL and qN parameters (Fig. 14a–d). While it is a common practice that α and F_{II} in estimating ETR from ChlF is assumed to be always constant, I have shown that the product of α and FII was dynamically responding during photosynthetic induction (Fig. 17). This result showed a clear evidence that the amount of light absorption (and potentially the σ_{PSII}) has a temporal variability which may significantly affect ETR regulation under fluctuating light in the field. Furthermore, Fig. 16 showed how the current model of fluorescence-based ETR can diverge significantly from that estimated using gas-exchange. This divergence was more striking in Chl-deficient soybean mutant during the induction phase, providing much stronger proof on the significant role of α and F_{II} on ETR. Taking all these observations together, it is therefore important to pair SIF measurements in the field condition with active fluorescence measurement strategies such as the LIFT, as well as gas-exchange, to further dissect changes that is related to photochemical and non-photochemical events.

I have shown that Chl-deficient mutant had lower capacity for NPQ (Fig. 13, 14c & Table 2). And this was exacerbated under stressed condition (Fig. 15). Because Chl-deficient mutant had lower amount of light absorbed, it probably required less rate for regulated thermal dissipation of excess energy. However, in turn, the lower NPQ in mutant resulted to higher rate of fluorescence emission (higher Φ_f) although the apparent F_{yield} was evidently lower than the wild type. This discrepancy strongly suggest significant factors that may change our perception of F_{yield} between photosystem and leaf level. Since the reduced NPQ in mutant resulted to higher Φ_f than the wild type, this balanced the effect towards PSII photochemistry. In turn, no remarkable difference in PSII efficiency was observed between Chl-deficient mutant and green wild type. Further analysis showed that qL in mutant was also lower indicating reduced connectivities between PSII units (Fig. 14b). This observation was in parallel to the lower ETR in the mutant (Fig. 14d & 14e), suggesting a possible causation of the former to the latter parameter. Furthermore, the reduced qL may also provide explanation on lower NPQ capacity in mutant that resulted to higher Φ_f. If this

corroborates in terms of the physical models, this will provide deeper insights on the regulatory balance between F_{yield} and NPQ as the amount of light absorbed is adapting as well as the corresponding adjustments in the PSII efficiency.

4.2. NPQ and PSII Efficiency under Fluctuating Light: Competing or Complementing?

Because photosynthesis in the field is always in non steady-state, studying the response of NPQ and PSII efficiency under fluctuating light is integral. The mechanistic control of NPQ on photosynthetic efficiency fundamentally lies on the LHCII antenna, which changes its mode from light-harvesting to energy-dissipating after experiencing excess light. Despite the prominent positive relationship between NPQ and PSII operating efficiency during the induction phase, this relationship shifted to inverse when NPQ had reached maximum rate (Fig. 15 & 18) suggesting that PSII efficiency had a certain degree of independence from NPQ components. On the other hand, PSII efficiency and qI share molecular properties that is extended out of the light-harvesting antenna – PSII core – and thus can be regarded as non-mutually exclusive events. While qE component, together with accumulation of reduction of PSII, may function to regulate net photochemistry (Weis & Berry, 1987), qI evidently controls PSII efficiency that could likely lead to reduced CO_2 assimilation. Even though Φ_{PSII} had a direct relationship to Φ_{CO2}, I observed that this is not always linear. To illustrate, the relationship between Φ_{PSII} and Φ_{CO2} in WT_{Sb} showed a direct and linear correlation while non-linear correlation is observed in Chl-deficient soybean mutant (Fig. S4c). Since the effect of Chl-deficiency in Φ_{PSII} was almost negligible but more significant decreased in NPQ (Fig. 13, Table 2), the non-linearity between Φ_{PSII} and Φ_{CO2} observed in Chl-deficient mutant may be partially explained by the reduced photoprotection in the mutant (Table 2).

In both soybean and cassava measurements, it was clear that NPQ increases as soon as the light intensity was changed from low to high, while PSII efficiency was decreased (Fig. 15 & 35). In contrast, NPQ decreased gradually, while PSII efficiency increased almost instantly, as light level was decreased (see insert in Fig. 15**)**. Because of the pH-dependent activation of the PsbS, NPQ (mainly qE component) responded fast during this transition. The quicker increase in NPQ (as compared to increase in PSII efficiency) as a response to

increase in light intensity led to the hypothesis that NPQ may provide a photoprotective role in PSII during excess light. Demmig-Adams et al. (1995) showed that increasing NPQ with decreased Φ_{PSII} was associated with the epoxidised state of the xanthophyll pigments. Yet it is not clear on the exact mechanism of Z in protecting PSII (e.g. quenching Chls vs scavenging ROS), this provided a stronger evidence to support the hypothesis that NPQ protects PSII reaction centre. However, when light intensity changes from high to low (naturally occurs in the under-storey of plant canopies or cloud passing), NPQ decreases in a slower rate due to slower reconversion of Z to V. This slow reaction drives all absorbed energy to be dissipated as heat, instead of gaining efficiency for PSII photochemistry for a higher electron transport (Kromdijk et al., 2016). On one hand, Zhu et al. (2004) showed that delay in recovery in photoprotection reduced daily carbon gain from ~6 to 30% when leaf response was modelled under fluctuating light. On the other hand, Long et al. (2005) have predicted an increase in radiation conversion efficiency of 15% if the recovery of photoprotection is sped up. In fact, it was evidently shown by Kromdijk et al. (2016) that by increasing PsbS and VDE in tobacco plants, rapid relaxation of NPQ was achieved during the transition from high to low light. Consequently, this created an advantage in the field condition where light fluctuations are more common and thus increase the biomass yield in tobacco by 15%. However, a separate study by Garcia-Molina & Leister (2020) revealed otherwise – resulting to an impaired biomass accumulation in a model plant Arabidopsis. Thus, it is fundamental to investigate if the nature of NPQ is either competing or complementing in terms of cumulative carbon gain from leaf to plant level. In modelling the response of larger homogeneous field, a more relevant question is to ask which sink is more energetically attractive for the dissipation of absorbed energy at leaf (i.e. the electron transport chain or different mechanisms of NPQ)?

4.3. Relation of F_{yield} to PSII Efficiency and NPQ

The tripartite relationship among F_{yield}, PSII efficiency and NPQ is dynamically changing with incident light, making it difficult to assess intrinsic changes in F_{yield} in the field. For example, a decrease in F_{yield} could mean three events: (1) increase in both NPQ and PSII efficiency during light induction (Figs. 13, 14 & 21), (2) decrease in NPQ while increase in PSII efficiency as a consequence of decrease in incident light (Figs. 15 & 35) or

(3) increase in NPQ and decrease in PSII efficiency during photoinhibition, caused by high light (Fig. 23). NPQ and PSII efficiency could either be directly or inversely related depending on the physiological status of the leaf, thus complicating the interpretation of F_{yield}. In this thesis, I showed that the direct relationship between NPQ and PSII efficiency could be achieved from dark to light transition during induction, while inverse relationship was mostly observed in light-adapted leaf during light fluctuations, and upon reaching a local maximal rate (Fig. 15). In controlled measurement, light adaptation is always interpreted as a steady-state condition which is not true in the field scenario. In the under-storey of plant canopies, the level of NPQ was usually low due to low incident light that the leaves receive (Figs. 18 and S5). However, more uncertainty on this relationship may occur if the leaves were old enough to perform functional photosynthesis. For instance, the low NPQ measured at the base leaves of cassava plants was associated by either low or high PSII efficiency, respectively, in the case of tall and small plant canopy (Fig. S5). Consequently, F_{yield} at the base leaf of a tall cassava plant was high, while F_{yield} was low in a small plant. This was because small plants tend to cast less shadows at the base leaves, thus exposing the leaves to higher light that might have eventually quenched F_{yield}. Yet, the difference in Φ_{PSII} seem to be more defined by the relative age of the leaf.

Younger and healthier leaves on top of plant canopy received more light which consequently reduced Φ_{PSII} but increased NPQ. As a result, the F_{yield} was quenched. Previous work already showed that the Chl-deficient mutant had reduced fAPAR (Sakowska et al. 2018). In Fig. 18, the correlation between NPQ and Φ_{PSII} measured at leaf level had a more curvature in WT_{Sb} than that of Chl-deficient mutant. Similar to high light scenario in Fig. 18, the leaf of WT_{Sb} had higher NPQ (at higher light and F_{yield}) during low Φ_{PSII}. As soon as the F_{yield} decreased (also because light intensity was changed from 780 to 520 μmol m^{-2} s^{-1}), Φ_{PSII} increased with decreasing NPQ. Here (Fig. 14), measurements of qP and qL confirmed that the increase in Φ_{PSII} quenched F_{yield} until ca 30 mins, which was longer than the time it took to saturate qN. Gu et al. (2019) suggested that qL parameter would provide better interpretation on the role of photochemical quenching on F_{yield} (Gu et al., 2019). This observation is critical in linking steady-state F_{yield} to photosynthesis (particularly ETR) and the feedback effect of NPQ towards reaching homeostasis dynamics in cellular and leaf level.

Under clear sky, light intensity changes gradually which, in turn, changed the balance between photochemical and non-photochemical energy use (Fig. 23a–b). In rapidly fluctuating light, the changes in photosynthetic efficiency and NPQ shows a rapid response to changing light level, despite the lag on the relaxation of NPQ from changing high to low light. Apparently, the delay in NPQ response to fluctuating light was magnified in both Chl-deficient soybean mutant under drought-stressed as well as cassava plants grown in the field, suggesting that the delayed response of NPQ is a function of stress (Fig. 15 & 35).

4.4. How Dynamic is the Link between SIF and Photosynthesis in the Field?

Availability of resources in the field is constantly changing (i.e. limiting or excess light for photosynthesis). Likewise, and consequently, SIF emission in the field is as dynamic as incoming irradiation (Figs. 22–24). Despite extensive research, it is still largely unknown how much change in SIF emission is actually due to, or related to, the regulation of photosynthesis in the field scenario. To tackle this, it is important to realise how dynamic and what mechanisms of NPQ affect the SIF – photosynthesis relationship.

Leaves quickly adapt to changes in light intensity such that the energy balance results to maximised productivity in proportion to the availability of other inputs (such as water, CO_2 and nutrients) and least damage to the plant from photo-oxidation. This is palpable because of two reasons: (1) plant parts grow and develop (e.g. leaves, roots, stems and seeds are all potential sink for photosynthates), and (2) the presence of NPQ mechanisms that is constantly adjusted in order to protect leaves from photodamage. The role of NPQ in regulating the energy balance in the leaf (also linking fluorescence to photosynthesis) exists in the range of short-, medium- and long-term response of plant to environment. Both the qE and qZ component of NPQ have been shown to be actively involved in protecting PSII during light fluctuations – an example of a short-term regulation of NPQ towards fluorescence—photosynthesis relationship (Fig. 15). Whereas qI (but also associated with qZ) component of NPQ have been shown to regulate energy dissipation in seasonal acclimation, particularly in overwintering species – an example of a medium- to long-term regulation of NPQ. Here, I have shown that F760 is slightly more correlated to Φ_{PSII} during summer but much more to NPQ when WT_{At} plants were exposed to cold stress during

simulated winter spell (Table 3). Therefore, in the context of large-scale monitoring of terrestrial photosynthesis and energy budget, the extent of which qE and qZ modulates the link between fluorescence and photosynthesis under non-stressful events should be taken into account. While qZ and qI should be considered in stressful conditions. Clearly, NPQ plays a significant role in regulating biomass accumulation in plants likely due to altering the energy balance during changing light (Kromdijk et al., 2016; Garcia-Molina & Leister, 2020). Nevertheless, since these studies have somewhat contradicting results, a clearer evidence has to be laid out in order to mark what role does NPQ have in biomass accumulation under constantly changing light in the field. SIF method, combined with ρ measurements at larger scales, can be used to fill this gap (see subchapter in relating ρ to NPQ).

In Arabidopsis results, it was shown that SIF is almost equivalent to the steady-state F_{yield}. Also, Zarco-Tejada et al. (2013) showed that steady-state F_{yield} is significantly related to net photosynthesis. However, it is false to assume that SIF is equivalent to steady-state photosynthesis as this consequently falsify the fact that photosynthesis is always at non steady-state. Because of logistical limitations, SIF measurement on top of canopy and airborne systems are automatically integrated signal providing an instantaneous snapshot of fluorescence emission. Yet, the coupling of fluorescence with photosynthesis lies not just on the NPQ activity but also on the synchronised recording of light absorbed by photosynthetic system. In fact, gathering of SIF images from the aircraft during HyPlant campaign (Rascher et al., 2015; Pinto et al., 2020) would take several minutes to complete where environmental factors are expected to change from the beginning to the end of campaign. Nevertheless, since SIF measurement is coupled with ρ measurement, synchronise estimation of APAR is possible. Normalising the SIF with APAR in order to eliminate contribution of changing light have been shown to relate to the internal status of the plant (or leaves) (Figs. 22–24). On the other hand, continuous monitoring of SIF using optical fibres automatically integrates the signal spatially. Understanding how SIF signals are integrated at different spatial and temporal domain would provide more light on how different plant species regulate photosynthesis and NPQ in their natural ecological niche. In Arabidopsis study, the effect of the molecular nature of NPQ mutation was clearly evident at leaf level (Fig. 25a). This result supports the idea that LHCII antenna is an extension of a classical solid-state physics where properties at leaf level are explained by the properties of its molecular components. It is thus

important to develop methodologies of retrieving integrated SIF signals at larger spatial domain (from airborne and satellite sensors) as well as long temporal observations (seasonal regulations) that can integrate APAR or the dose of light absorbed.

Box 1. Description of the effect of NPQ mechanisms on active and passive fluorescence signal

(The discussion was originally published and paraphrased from the Discussion section (p. 11) from Acebron, K., Matsubara, S., Jedmowski, C., Emin, D., Muller, O., & Rascher, U. Diurnal dynamics of non-photochemical quenching in Arabidopsis *npq* mutants assessed by solar-induced fluorescence and reflectance measurements in the field. *New Phytologist*. 05.Oct.2020)

"We have shown the consequence of a deficiency of PsbS and Z for active and passive fluorescence signals at leaf level. We tested this in various environmental conditions ranging from a controlled indoor setup to diurnal field conditions in summer and winter. PsbS and Z play a key role in the onset of rapidly inducible and reversible qE, and in sustained NPQ in winter (Verhoeven, 2014). As a control case, we first characterised the kinetics of NPQ induction in low light. Absence of Z in the *npq1* mutant reduced the extent of NPQ, but quick induction of NPQ upon illumination was observed as a result of functional PsbS protein (Fig. 21c). On the other hand, the *npq4* mutant showed a slower increase in NPQ, which was effected by the interconversion of pigments in the VAZ cycle upon absence of the PsbS protein. Our results consistently showed a similar increase in F_{yield} for both *npq* mutants measured in indoor and outdoor conditions (Figs. 21a, 22c, 23c), but this was less pronounced in LIFT measurement outdoors (Fig. S7). This increase was also consistently visible at the two fluorescence peaks which also suggest that the ratio between F_{760} and F_{680} is unaffected by changes in NPQ (Fig. 26). Although state-transitions may affect this ratio, we did not include this in our study as this NPQ event only occurs in low light levels which is considered less relevant in remote sensing (sensu Porcar-Castell et al., 2014). Nevertheless, in winter, the strength of the correlation between the two fluorescence peaks decreased, which was probably due to a smaller signal-to-noise ratio when SIF was fully quenched, as opposed to the strong flux of reflected radiance (Fig. 25c)."

4.5. SIF and its Relation to Intrinsic F_{yield} and APAR

SIF is a passive fluorescence emission that is highly linked to light intensity and photosynthetic light use. Its importance on understanding the plant traits ranges from photosystem level to ecosystem level, especially *in vivo* and *in situ*. Its emission kinetics is largely controlled by photochemical and non-photochemical energy use while its detection is highly determined by a range of biophysical factors (for review, see Porcar-Castell et al. 2014; Mohammed et al., 2019). Since SIF is also highly dependent on the prevailing light intensity, quantification of the fAPAR is compulsory to derive precise estimate of SIF_{yield}. This is possible when SIF retrieval is coupled with ρ measurement. Yet, there is always a caveat on accurate measurement of APAR. Nevertheless, the better the estimate of APAR, the closer is SIF_{yield} (or apparent F_{yield}) to internal F_{yield}. Wong et al. (2020) proposed that the relationship between apparent F_{yield} (brightness) and internal F_{yield} (quantum yield of fluorophores to emit fluorescence photon) is through the efficiency of energy transfer (i.e $\Phi_{ovl} = \eta \times \Phi_{int}$, such that the Φ_{ovl} is the apparent F_{yield}). In the case of photosynthetic light harvesting systems, SIF_{yield} is equivalent to the Φ_{ovl}, while the Φ_{int} is the internal F_{yield} and η is the efficiency of energy transfer in the photosynthetic system. Thus, if SIF_{yield} and internal F_{yield} are known, we can therefore derive η which I hypothesise to be related to the total efficiency of all the energy transfer that may occur at leaf or canopy level. This (η) includes, albeit crudely, the efficiency in excitonic energy transfer in the LHCII antenna, the electron transport chain, chloroplasts movement, and reabsorption of fluorescence photon and its effect on quantum efficiency of the PSII at leaf and/or in plant canopy. Therefore, retrieving SIF_{yield} at different spatial and temporal domain will likely provide link to other plant traits that can be used to discern the quantum yield of a healthy from stressed plants. SIF_{yield} from a leaf is more regulated by biochemical changes than SIF_{yield} retrieved on top of canopy due to the influence of complex structure to the escape of fluorescence photon (Dechant et al., 2020). Nevertheless, the canopy structure can also provide a glimpse for overall plant health. In Arabidopsis data, we have shown a very close relationship between SIF_{yield} and F_{yield} from PAM or LIFT. This is because of the relatively simple canopy structure of Arabidopsis plant which makes it ideal to study the effect of photochemical and non-photochemical energy use in SIF under field conditions. A detailed description of this study is found in Box 1.

Although our current technology makes it unrealistic to retrieve internal F_{yield} and that the PSII efficiency, while the NPQ activity in the thylakoid membrane is dynamically adjusting in the field, both of the energy sinks for fluorescence emission can be assumed constant (especially in the case of healthy leaf) when viewed in cellular (or chloroplastic) level where homeostasis can be achieved. In reality, constant adaptation of leaf to varying environmental conditions may also be resource intensive. Different signalling pathways, maintenance of the enzymatic activities in the Calvin cycle, reduction-oxidation reactions, regeneration of ADP and $NADP^+$, formation of reactive oxygen species and the scavenging of these species, source-sink balance especially that of starch loading, etc. entails the use of cellular resources that can potentially lead to feedback effect on the rate of fluorescence emission. Havaux et al. (1991) concluded with strong evidence that steady-state fluorescence is a product of homeostasis system for radiative energy dissipation but only in non-stressed and fully developed leaves. This opens opportunity to use dynamic features of SIF_{yield} in order to properly estimate APAR rather than energy balance in a healthy leaf. In fact, in rice canopies, SIF_{yield} is shown to be more related to changes in APAR than in photosynthesis during diurnal observations with half-hour resolution (Yang et al., 2018). On canopy level, $F687_{yield}$ and $F760_{yield}$ will differ because fluorescence photons at 687 nm are reabsorbed and can be further used for photochemistry or NPQ. Yang et al. (2020) had recently establish a new reflectance index (FCVI) which can quantify the effect of light absorption and SIF scattering (albeit not individually) on far-red SIF at canopy scale. Since utilising SIF as a parameter in modelling plant productivity have been shown to simplify the light-dependent reaction of photosynthesis (Gu et al., 2019), light-use efficiency can be elucidated at larger scales especially when paired with PRI and APAR to determine the net effect between NPQ and photosynthesis. To bridge cellular response to leaf level SIF observations, it is therefore worth exploring the concept of cellular homeostasis and its link to SIF emission by integrating fluorescence measurements that exploit the frequency domain (personal communication with Ladislav Nedbal) related to the dynamic relationship between ETR and NPQ. In addition, Poorter et al. (2010; 2019) have introduced the light dose response curve for different traits under a wide range of environmental factor in order to normalise experimental observations across different origins. Together, it may be possible to use information from SIF signal to estimate the fAPAR in order to relate the dose when scaling up productivity and enable quantitative and comparative analyses at larger scales (e.g. comparing the growth of two monocropping systems at similar and different environments).

4.6. PRI and its Relation to NPQ: How to Measure Reflectance to Quantify Changes in NPQ?

Relating ChlF to NPQ needs maximal F_{yield} from dark- (F_m) and light-adapted (F'_m) states using saturating flashes in active fluorometers. The components of NPQ can be resolved through their relaxation kinetics during leaf darkening. In remote sensing, changes in ρ can indicate changes in the VAZ cycle, which can be a reliable index of de-epoxidation states of the xanthophyll pigments. In Fig. 33, I have shown that SIF was linearly related to the PRI in summer (important in the case of wild type plants which naturally exist in the field). Weak and non-linear correlations were only found to occur during cold spell in the winter, when the diurnal trend of the PRI and SIF was suspected to be influenced by the development of qI that was accompanied by changes in other leaf pigments. Although there are various NPQ mechanisms, the VAZ cycle plays a major role in regulating the extent of NPQ (Jahns & Holzwarth, 2012). Adams and Demmig-Adams (in press) mention that 'For plants in nature, no increases in NPQ or decreases in PSII efficiency in response to excess light have thus been observed in the absence of a corresponding level of Z + A.' This poses a vital consideration in terms of whether tracking Z alone is a reliable measure of NPQ activity in field conditions.

The PRI is related to NPQ at leaf level (Peñuelas et al., 1995; Gamon et al., 1997; Evain et al., 2004; Rahimzadeh-Bajgiran, 2012; Alonso et al., 2017; Kohzuma & Hikosaka, 2018). In this thesis, this knowledge was extended by observing the diurnal response of WT_{At} and mutant plants in field conditions (Fig. 31a). Despite the lack of PsbS for qE induction and low NPQ in the *npq4* mutant (Fig. 21c & 23b), the PRI was similar to that of the WT_{At}, indicating a functional VAZ cycle, but this was not the case with *npq1*. Interconversion of V to Z via A is a somewhat slower process and is constantly adapting to incident light. Without VDE, *npq1* could not convert V to Z, so the PRI was nearly stable throughout the day except for a slight decline towards in the afternoon. Kohzuma & Hikosaka (2018) have previously reported a change in the PRI depending on *in situ* lumen pH, upon infusing leaf discs with a pH-controlled buffer. Hence, the slight decline in PRI observed in *npq1* mutant was probably due to a build-up of luminal pH as the light intensity increased. Müller et al. (2001) reported that qE is known to rapidly induce and relax. Despite constantly yet gradually changing light intensity diurnally – which might have emphasised

the differences in qE between the WT_{At} and *npq4* mutants in the field – there was no difference in ρ and the PRI (Figs. 28h, 29, 31a). I therefore conclude that conformational change cannot be detected by ρ at higher spatial and temporal sampling. While this conclusion may seem to contradict what was recently reported by van Wittenberghe et al. (2019), this discrepancy might be due to differences in how $\Delta\rho$ was traced. In particular, van Wittenberghe and the co-workers traced $\Delta\rho$ for a maximum of 10 min after actinic illumination, while I monitored $\Delta\rho$ throughout the entire day with ~45-min intervals. Although cluster analysis also showed temporal change in ρ, independent of VAZ activity (Fig. 29, branches B and D), it appears that this was due to gradually reduced ρ at 700 nm, probably resulting from Chl breakdown (Fig. 27). Nevertheless, clustering clearly separated *npq1* from both WT_{At} and *npq4* mutants strongly suggests that plant ρ is only sensitive to VAZ cycle but not to PsbS-mediated heat dissipation (Fig. 29).

The PRI showed clear linkage with NPQ in the summer and dissociation from NPQ during winter spell. Albeit uneven, an overall decline in the PRI was observed during cold spell in the winter, and this is likely to have been due to pigment breakdown during cold acclimation (Fig. 31b). Previous studies have shown that the challenge of linking the PRI to sustained NPQ lies in overwintering species when Z accumulation is compounded by changes in other pigments (Busch et al., 2009). Here, I have shown that 531 nm is sensitive to changes during the VAZ interconversion (Fig 28a). By comparing the PRI calculated in other spectral regions (Fig. S6), 570 nm showed itself to be a fairly reliable reference band for the PRI (Fig. 31). The PRI on the second day in winter followed light intensity, which was probably a consequence of the changing angle of the sun (Fig. 31c). This suggests that some consideration needs to be given to the effect of leaf albedo and pigment pools when scaling up the PRI both temporally and spatially. Changes in the PRI associated with dark conditions or low levels of light would facilitate quantification of pigment changes in a fixed space for remote-sensing applications. Nevertheless, the PRI should be parameterised on pigment changes during winter and the functional lutein cycle.

Since Z also plays a role in qE while PsbS and Z have similar quenching strength, tracking Z can, therefore, potentially measure the relative role of qE and qZ in SIF quenching. Despite the fact that low luminal pH and PsbS trigger NPQ, I have shown (by tracking the PRI in field conditions) a high correlation with NPQ (Fig. 32), while SIF and

NPQ were found to have an inverse relationship (Figs. 33c, d). High correlation of SIF_{yield} and the PRI in summer (but not winter) suggests that accounting for NPQ using the PRI is limited in summer conditions.

4.7. Diurnal Dynamics of SIF and PRI Tracks NPQ Activity in the Field

The field measurements conducted in Arabidopsis during summer revealed how dynamic is the relationship among NPQ, Φ_{PSII}, $F760_{yield}$ and PRI in the WT_{At} and *npq* mutants (Fig. 22d). Here, I showed that aside from the increase in $F760_{yield}$ for both *npq* mutants, the diurnal trend was different from the WT_{At}. At the end of the day, both *npq* mutants had lower $F760_{yield}$ than the WT_{At}, which was coupled with lower Φ_{PSII} (Table S4). As the *npq* mutants had been shown to be more prone to high levels of light (Havaux & Niyogi, 1999; Li et al., 2002), the diurnal trend of $F760_{yield}$ therefore reflected the development of photoinhibition. Specifically, $F760_{yield}$ of the WT_{At} was found to recover, while the mutants had lower $F760_{yield}$ compared to the initial value in the morning. Since it was postulated that a decrease in $F760_{yield}$ during conditions of high light levels was due to the onset of qI, I further tested this hypothesis by extending the experiment in the winter to induce photoinhibition. By placing the plants outside to experience cold and high light levels, SIF quenched equally for all plant types, proving the onset of qI (Fig. 23), which retained on the second day of exposure to cold (Fig. 24). The reduced F_v/F_m and its slow recovery in the glasshouse (Fig. 25) strongly suggest damage in the PSII during winter conditions and its repair inside the glasshouse.

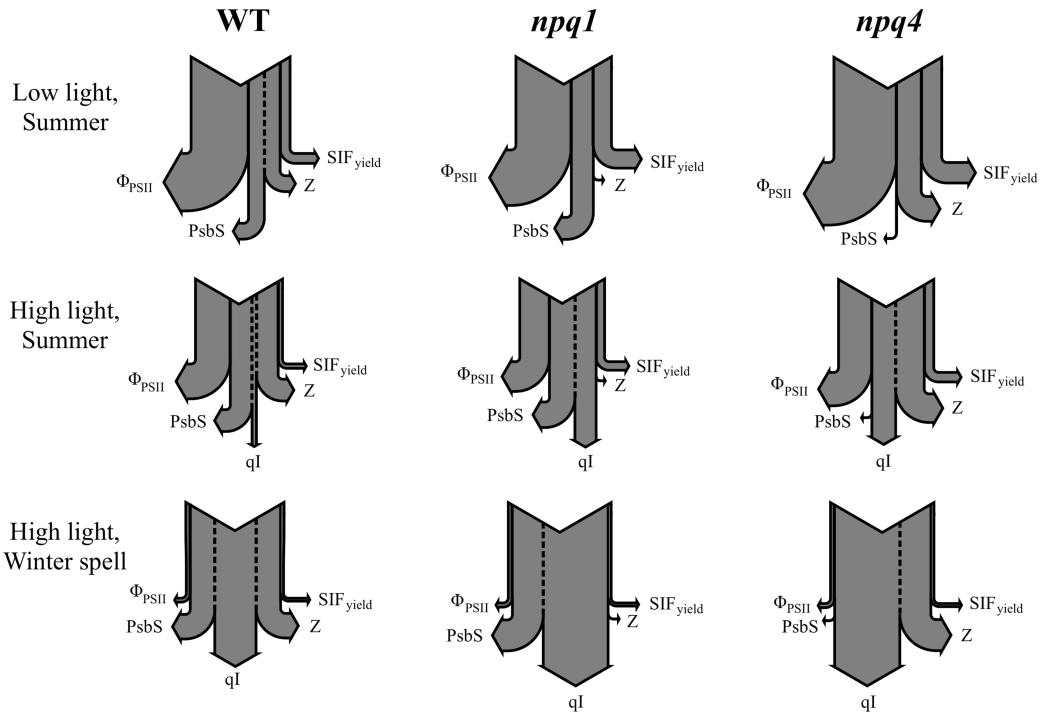

Fig. 39. Schematic representation illustrating the major quenching pathways of absorbed light energy in *Arabidopsis thaliana* wild type (WT_{At}) plants and in the violaxanthin de-epoxidase (VDE)-deficient *npq1* and PsbS-deficient *npq4* mutants under low and high light on a summer or a cold spell. The relative size of each pathway is either based on the observations during the diurnal field experiment (for SIF_{yield} – solar-induced fluorescence yield, and Φ_{PSII} – effective quantum yield of PSII) or estimated by the comparison between WT_{At} and the mutants (for PsbS – PsbS-dependent quenching, Z – zeaxanthin-dependent quenching and qI – photoinhibitory quenching). Since the quantum yield is not known for the non-photochemical quenching (NPQ)-related pathways, the width of the pathways does not correspond to their relative contributions. For simplicity, non-regulated energy dissipation is assumed to be similar in the three genotypes under all conditions, and thus not depicted in this summary.

Image was taken from Figure 11 in Acebron, K., Matsubara, S., Jedmowski, C., Emin, D., Muller, O., & Rascher, U. Diurnal dynamics of non-photochemical quenching in Arabidopsis *npq* mutants assessed by solar-induced fluorescence and reflectance measurements in the field. *New Phytologist*. 05.Oct.2020

I also showed that a decrease in SIF was always related to an increase in NPQ, but was also associated with a decrease in PSII efficiency to varying degrees (I summarised this response in Fig. 39). The degree of relationship greatly depended on the prevailing environmental conditions. In the WT_{At}, $F760_{yield}$ was found to be slightly more correlated to

Φ_{PSII} than NPQ during summer (Table 3). Conversely, $F760_{yield}$ was more correlated to NPQ than Φ_{PSII} in winter, which was predominantly qI (Fig. 33d). This relationship was also consistent with that in cassava plants which developed qI after diurnally exposing the plants in the field (Fig. 38). In contrast, this observation was markedly different when fluorescence quenching was observed on a dark-adapted leaf – that is fluorescence quenching is explained by Kautsky effect (Kautsky et al., 1960), driven by the increase in both NPQ and PSII efficiency (Figs. 21b, d). Interestingly, SIF spectra measured in cassava leaves at the end of the day clearly lacked the peak at 680 nm suggesting a loss of signal from the PSII core (Fig. 37). Note that these cassava plants were also photoinhibited as evidenced by decrease in F_v/F_m. In contrary, when Arabidopsis were exposed in cold spell, the development of photoinhibition did not seem to affect the ratio of F760 to F680 (Figs. 23c, 24c and 26c). More recently, van Wittenberghe et al. (2020) showed also no remarkable change in the ratio of F760 to F680 when they traced fluorescence emission spectra in *Morus alba* L. as transitioned from dark to high light within 3 mins. Together, it is likely that the reduction in F680 signal in cassava plants is due to reabsorption of fluorescence photon as the chloroplast stacked together and moved to the lateral side of the cell to avoid excess light. Further studies has to be done on this behaviour in order to verify the relationship between chloroplast movement and SIF emission profile.

Using the SCOPE model, van der Tol et al. (2014) demonstrated that the relative light saturation of PSII affect the relationship between fluorescence and photosynthesis. This response could be due to high light conditions, when Z tends to accumulate. Although van der Tol et al. (2014) showed a strong link between light saturation and rate constant for NPQ, this relationship was purely empirical and did not establish mechanistically the effect of each of the known NPQ components. The methods I conducted in this thesis have filled this gap using *npq* mutants and have experimentally shown the extent to which PsbS, Z and qI modulate SIF emission diurnally in stressed and unstressed conditions (Fig. 39). Different NPQ kinetics represent different physiological mechanisms – for instance, the NPQ kinetics involving PsbS and VAZ cycle (Fig. 21c). Both *npq* mutants appeared to have a similar effect to SIF_{yield} indicating that the extent of NPQ (but not the kinetics) affected diurnal SIF emission. Since our study was limited to the VAZ cycle, studying the effect of the lutein cycle on SIF and ρ will give a more holistic understanding of the influence of NPQ on ρ.

4.8. Opportunities in Relating SIF to GPP

The term "steady-state" can only be truly achieved under controlled conditions where environmental factors are fixed for a certain period of time. This is likely not the case in the field condition. Thus, understanding steady-state photosynthesis can only be used to *infer* true photosynthetic activity in the field. As the development of strategies to precisely retrieve APAR, SIF and SIF_{yield} from remote sensing platforms becomes more available, the availability of SIF data (with large spatial and temporal coverage) will enable researchers to understand photosynthetic regulation under natural environment. I proved that diurnal changes in SIF were not just due to changing light intensity but also to changing efficiency for PSII photochemistry as well as the level and mechanisms of NPQ involved (Fig. 21–24). This was due to the fact that the regulation in the balance between photochemistry and NPQ is consequently expressed in terms of changes in the pattern of ChlF emission (Fig. 18). Recently, Gu et al. (2019) showed that SIF simplified the modelling of complex photochemical process in the light-dependent reaction of photosynthesis. Overall, the data shown in this thesis provides a mechanistic evidence for a strong relation of SIF to GPP.

It is well established that SIF can estimate photosynthesis and GPP (Guanter et al., 2014; Gu et al., 2019). With the assumption that a homogeneous canopy is a single big leaf, modelling photosynthesis using SIF would require understanding how NPQ is linked to this relationship. Although ρ reflects only partial NPQ, a parallel survey of light and temperature can be added in numerical simulations to predict both the component and mechanism of NPQ involved. We therefore propose that the conceptual model summarised in Fig. 39 should be tested at canopy level and on different species, employing various NPQ strategies. Despite the complexity of canopy level photosynthesis in a dynamically fluctuating light, testing this model will guide future researchers on when and how the results of empirical experiments does not hold true to the leaf level model proposed in Fig. 39.

In contrast, Havaux et al. (1990) showed that steady-state fluorescence level in healthy leaves are more or less constant at different light intensity. As the SIF signal had always been related to steady-state F_{yield}, it now poses a question whether SIF represents a biological homeostasis in a healthy leaf. The conceptual relation of SIF to energy homeostasis in plant level may be further explored by exploring the spatial data on canopy scale. So far, a more direct role of NPQ in regulating the energy balance which is translated

to dormancy in plant growth is strongly evident in overwintering evergreen species where a clear down-regulation of photosynthesis is tightly linked to quenched F_{yield} (Fig. 23). Exploring whether SIF signal represents biological homeostasis in a healthy leaf requires generation of proper methodology on aggregating SIF signals from wide spatial and temporal samples. Also, discrimination of healthy and photoinhibited leaves can be aided if SIF measurement is paired with changes in PRI, to show relative Z accumulation (indicative of photoinhibition). The ratio of healthy to photoinhibited leaf in a plant can greatly improve the GPP estimates at the canopy level. Furthermore, relating this observation in different crop ideotypes would help breeders identify high performing genotypes in their breeding materials.

In spite of stressful environment that may limit the rate of photosynthesis in the field (e.g. high light, drought, cold), different plant species have developed strategies in order to survive, reproduce and create their own ecological niche, — a result of evolutionary pressure, natural selection and adaptation. To illustrate, adaptation of plants to decreasing CO_2 level resulted to the evolution of C4 type of photosynthesis from the ancestral C3 type (Sage, 2004). Because different types of photosynthesis (C3, C4 and CAM) uses different strategies to assimilate CO_2, understanding the link of SIF to the type of photosynthesis would give a more precise estimate of light use efficiency and GPP in regional and global scales (He et al., 2020). As C4 type of photosynthesis has significant advantage over C3 type with regards to crop grain yield and biomass production (Mitchell & Sheehy, 2006), it is important to parameterise SIF based on type of photosynthesis (Liu et al., 2017; Gu et al., 2019). Moreover, it is necessary to understand other limitations in photosynthesis at leaf level that has been explored in the model of von Caemmerer and Farquhar (1981), such as the V_{cmax} and the g_{sw}, which are also constantly adjusted under dynamic condition. Since SIF simplifies the light-dependent reactions (Gu et al., 2019), other abiotic events that can influence photosynthetic rates can be analysed by SIF. Both meta-analysis (Ac et al., 2015) and more targeted studies (e.g. Migliavacca et al., 2017; Watts et al., 2020) have shown strong evidence on the link of SIF to nutrient availability. This also gives opportunity to understand different modes for nutrient uptakes as it was argued that ecological niches can be developed due to the plasticity in the uptake of nutrients (e.g. case of phosphorus uptake investigated by Phoenix et al., 2020).

4.9. Future Perspectives

Photosynthesis is a complex network of molecular processes. Its measurement is usually expressed in terms of the rates and efficiencies of its component processes that have become a proxy for true photosynthesis. To list some examples, the carboxylation efficiency, PSII efficiency, rate of photosynthetic carbon uptake and the rate of electron transport. On the other hand, GPP provides an integrated measure of true photosynthesis (see Wohlfahrt & Gu, (2015) for its relation and many definitions of photosynthesis). Yet the integration do not necessarily disregard the overall function of photosynthesis, it provides less information of its dynamic regulation. And understanding the relation of photosynthesis to growth requires a robust measure of gross and net photosynthesis (and its interaction to environment) and growth rate.

Presently, researchers have identified key processes in photosynthesis that is predicted to increase the overall photosynthetic efficiency when improved. For example, strategies in developing Green Super Rice (Zhang 2007; Wing et al., 2018) proved thus far a promising direction by simultaneously identifying key traits for improved yield and resource use but phenotyping strategies is still a major bottleneck to identify functions of candidate genes. Furthermore, C3 to C4 conversion in rice crop (Mitchell & Sheehy, 2006), increasing recovery of photoprotection (Kromdijk et al., 2016), and increasing efficiency of Rubisco enzyme (Parry et al., 2013) are current efforts to achieve food security in the near future. These projects have been based on the fact that the target traits have strong evolutionary advantage, which made scientists to predict that enhancing the efficiency may lead to higher crop yield. For example, the evolution of C4 from a more primitive C3 type of photosynthesis occurs from at least 60 independent times (Sage, 2004) which strongly suggests that plant species in their natural systems may have already achieved an optimised photosynthesis to perform under seemingly stressful conditions in the field. Yet, a high efficiency does not always mean high rates, and vice versa. For example, a higher PSII efficiency under low light may have lower rates of electron transport compared to a lower PSII operating efficiency in high light (see discussion in Chapter 4.2). If the efficiencies for all processes for plant growth can be assumed to work in unity, then increasing the efficiency of one process may consequently and inadvertently decrease the efficiency of other processes. Thus, in the context of improving the efficiency for photoprotection, the efficiency for other energy-use (photochemistry and F_{yield}) may inevitably decrease – thus

benchmarking a new limitation for plant growth and development. This depends on the specific space and time where the measurement was conducted and when environment have direct effect on other physiological processes that are linked to photosynthesis. Therefore, optimising kinetics rather than absolute capacities may provide a better option for crop improvement.

In agricultural crops, photosynthesis and NPQ may have been inevitably selected already by long-term and rigorous selection by the farmers. To illustrate, in rice, different landraces have been shown to exhibit distinct differences in capacity for NPQ depending on where the landrace had been developed (Kasajima et al., 2011). This might have been brought about by the selection of farmers in their local environments. But to test whether NPQ adaptation has contributed (or how much has it contributed) to significantly improved photosynthesis or yield in modern varieties – is still a challenging task. It could be that improving photosynthetic efficency may only translate to higher yield when plant is grown in a highly controlled conditions in the greenhouse (personal communication with Shizue Matsubara). And yet most of the experimental results thus far have promising implications, most of it are either difficult to replicate in the field or only proven to improve photosynthesis in modelling or in measurements. Evidence is still scarce *in situ*. And SIF has a great potential to improve our understanding of dynamic regulation of photosynthesis and NPQ, which will enable us to address these research questions in the next decades.

Because light is mostly fluctuating under natural environment since the dawn of terrestrial plants, it is likely that leaves have adopted traits that optimise their contribution to overall plant productivity under fluctuating light condition. Recently, Arp et al (2020) showed strong evidence that light-harvesting system in plants had evolved to decrease the noisy input from light fluctuations such that the energy output for photosynthesis is minimally disturbed. This modelling study suggests that the absorption features of the Chls in plants are the result of evolution such that the energy utilisation is optimised and photosynthetic machinery is tolerant to dynamic changes in light intensity. On top of this are different NPQ mechanisms. Furthermore, the spectral quality of solar-radiation was suggested to impose a selection pressure in favour to Chl *b* as a main component of the light-harvesting complex to ensure safe and efficient use of solar energy in terrestrial plants (see discussion in Kume et al., 2018). This likely explain, albeit partially, why most of the

remotely-sensed ρ signal that is related to Chl content (e.g. NDVI, NIRv) is highly correlated to GPP (Badgley et al., 2017, Yang et al., 2018). However, we have shown here (Fig. 19) that changes in NDVI had independence to photosynthesis-related changes in SIF. With the development of tools to remotely sense SIF, it is therefore more appropriate to further tests these hypotheses in a global scale to prove the evolutionary advantage of plants and how they suspect to change through changing climate such as heat and increasing CO_2 levels.

Nevertheless, SIF is strongly dependent on light intensity (Fig. 22c). To separate functional-related traits from light dependency, it is imperative to normalise fluorescence emission by the fAPAR. While in this thesis, fAPAR in Arabidopsis measurement was only substituted by the reflectance-based APAR, SIF_{yield} estimates still accorded with that of PAM and FluoWat due to the close measurement distance and simple canopy of Arabidopsis plant. In remote sensing, SIF_{yield} is highly compounded by the structural effects. Therefore, future research should focus on further improving the estimation of fAPAR from leaf to canopy level, including the escape probability of fluorescence (Zeng et al., 2019).

At canopy level, fAPAR is largely driven by the complexity of the canopy structure. Leaf-area index and specific leaf area, leaf angle and leaf clumping will have a direct effect on ρ as well as with SIF. We have previously shown that $\Delta\rho$ at leaf level was influenced by pigment regulation and that such changes could be short-term (diurnal) and/or long-term (seasonal) responses in the field (Gamon & Berry, 2012). This, however, does not directly equate to canopy level as structural effects have been shown to have a bigger influence on the PRI than its physiological dynamics (Gamon et al., 1992; Gitelson et al., 2017). We suggest to quantify changes in the PRI by either removing the canopy effect, as proposed by Wu et al. (2015). The use of portable hyperspectral imaging sensors (Behmann et al., 2018) provide easy way to utilise PRI signal in crop phenotyping so to identify crop varieties with different NPQ strategy. The PRI can then be combined with SIF and fAPAR within a spatial domain, and the leaf signal can be scaled-up to the total canopy signal by radiative transfer modelling (see review from Mohammed et al., 2019). Pinto et al. (2016; 2020) have recently provided proof of concept that high-resolution imaging spectrometers could provide the spatial pattern of SIF in order to quantify photosynthetic functions at canopy level. Investigation of the influence of Z on PSII efficiency and its consequence for SIF emission is a promising direction, which will create new opportunities in testing hypotheses related to

the functional role of NPQ in canopy photosynthesis and productivity (Acebron et al., 2020). This should involve investigating the role of the xanthophyll cycle in regulating cellular homeostasis during stressful conditions.

Linking SIF to photosynthesis is not straightforward, but understanding NPQ kinetics will provide us deeper insights on the regulation of photosynthesis in the field by tracking the energy balance and its dynamic regulation across space and time. Because of the uncertainty of role of NPQ in regulating photosynthesis, the dependence of photosynthetic efficiency on the intrinsic efficiency of the PSII reaction centre was explored in this thesis in great depth. Knowing whether NPQ and PSII efficiency are mutually inclusive events, is vital to the understanding of the interplay of NPQ between PSII photochemistry and F_{yield}. Arguably, the perfect example of this behaviour is a natural phenomenon of photoinhibition which is tightly linked to the down-regulation of photosynthesis in the field. This should provide a basis to categorise leaves that are photoinhibited and healthy in order to identify its contribution to the overall plant productivity. Therefore, profiling SIF and PRI during plant growth can ultimately provide insights on the dilemma of plants – that is whether to grow or to defend, as previously discussed by Herms & Mattson in 1992.

5. BIBLIOGRAPHY

Aasen H, Van Wittenberghe S, Sabater Medina N, Damm A, Goulas Y, Wieneke S, Hueni A, Malenovský Z, Alonso L, Pacheco-Labrador J. 2019. Sun-induced chlorophyll fluorescence II: Review of passive measurement setups, protocols, and their application at the leaf to canopy level. *Remote Sensing*, **11**: 927.

Ač A, Malenovský Z, Olejníčková J, Gallé A, Rascher U, Mohammed G. 2015. Meta-analysis assessing potential of steady-state chlorophyll fluorescence for remote sensing detection of plant water, temperature and nitrogen stress. *Remote Sensing of Environment* **168**: 420–436.

Acebron K, Matsubara, S, Jedmowski C, Emin D, Muller O, Rascher U. 2020. Diurnal dynamics of non-photochemical quenching in Arabidopsis *npq* mutants assessed by solar-induced fluorescence and reflectance measurements in the field. *New Phytologist*. https://doi.org/10.1111/nph.16984.

Allakhverdiev SI, Tomo T, Shimada Y, Kindo H, Nagao R, Klimov VV, Mimuro M. 2010. Redox potential of pheophytin a in photosystem II of two cyanobacteria having the different special pair chlorophylls. *Proceedings of the National Academy of Sciences*, **107**: 3924–3929.

Allen JF. 2003. Cyclic, pseudocyclic and noncyclic photophosphorylation: new links in the chain. *Trends in plant science*, **8**: 15–19.

Alonso L, Gomez-Chova L, Vila-Frances J, Amoros-Lopez J, Guanter L, Calpe J, Moreno J. 2008. Improved Fraunhofer line discrimination method for vegetation fluorescence quantification. *IEEE Geoscience and Remote Sensing Letters* **5**: 620−624.

Alonso L, van Wittenberghe S, Amorós-López J, Vila-Francés J, Gómez-Chova L, Moreno J. 2017. Diurnal cycle relationships between passive fluorescence, PRI and NPQ of vegetation in a controlled stress experiment. *Remote Sensing* **9**: 770.

Aro EM, Virgin I, Andersson B. 1993. Photoinhibition of photosystem II. Inactivation, protein damage and turnover. *Biochimica et Biophysica Acta (BBA)-Bioenergetics* **1143**: 113−134.

Athanasiou K, Dyson BC, Webster RE, Johnson GN. 2010. Dynamic acclimation of photosynthesis increases plant fitness in changing environments. *Plant Physiology* **152**: 366–373.

Atherton J, Nicol CJ, Porcar-Castell A. 2016. Using spectral chlorophyll fluorescence and the photochemical reflectance index to predict physiological dynamics. *Remote Sensing of Environment* **176**: 17−30.

Barton CVM, North PRJ. 2001. Remote sensing of canopy light-use efficiency using the photochemical reflectance index: Model and sensitivity analysis. *Remote Sensing of Environment* **78:** 264–273.

Baker NR. 2008. Chlorophyll fluorescence: A probe of photosynthesis in vivo. *Annual Review of Plant Biology* **59**: 89–113.

Bassi R, Høyer-Hansen G, Barbato R, Giacometti GM, Simpson DJ. 1987. Chlorophyll-proteins of the photosystem II antenna system. *Journal of Biological Chemistry*, **262**: 13333–13341.

Behmann J, Acebron K, Emin D, Bennertz S, Matsubara S, Thomas S, Bohnenkamp D, Kuska MT, Jussila J, Salo H, Mahlein AK, Rascher U. 2018. Specim IQ: evaluation of a new, miniaturized handheld hyperspectral camera and its application for plant phenotyping and disease detection. *Sensors*, **18**: 441.

Bellafiore S, Barneche F, Peltier G, Rochaix JD. 2005. State transitions and light

adaptation require chloroplast thylakoid protein kinase STN7. *Nature* **433**: 892–895.

Bendall DS, Manasse RS. 1995. Cyclic photophosphorylation and electron transport. *Biochimica et Biophysica Acta (BBA)-Bioenergetics*, **1229**: 23–38.

Bertamini M, Nedunchezhian N. 2002. Leaf age effects on chlorophyll, Rubisco, photosynthetic electron transport activities and thylakoid membrane protein in field grown grapevine leaves. *Journal of Plant Physiology* **159**: 799–803.

Bertamini M, Nedunchezhian N. 2003. Photoinhibition of photosynthesis in mature and young leaves of grapevine (*Vitis vinifera* L.). *Plant Science* **164**: 635–44.

Bilger W, Björkman O. 1990. Role of the xanthophyll cycle in photoprotection elucidated by measurements of light-induced absorbance changes, fluorescence and photosynthesis in leaves of *Hedera canariensis*. *Photosynthesis Research **25***: 173−185.

Bilger W, Björkman O. 1994. Relationships among violaxanthin deepoxidation, thylakoid membrane conformation, and non-photochemical chlorophyll fluorescence quenching in leaves of cotton (*Gossypium hirsutum* L.). *Planta* **193**: 238–246.

Boardman NK. 1977. Comparative photosynthesis of sun and shade plants. *Annual Review of Plant Physiology* **28**: 355–77.

Busch F, Hüner NP, Ensminger I. 2009. Biochemical constraints limit the potential of the photochemical reflectance index as a predictor of effective quantum efficiency of photosynthesis during the winter-spring transition in Jack pine seedlings. *Functional Plant Biology* **36**: 1016−1026.

Buschmann, C. 1999. Thermal dissipation related to chlorophyll fluorescence and photosynthesis. *Bulg. J. Plant Physiol*, **25***:* 77– 88.

Butler WL. 1978. Energy distribution in the photochemical apparatus of photosynthesis, *Annual Review in Plant Physiology* **29**: 345–378.

Cailly AL, Rizza F, Genty B, Harbinson J. 1996. Fate of excitation at PS II in leaves. The non-photochemical side. Plant Physiol Biochemistry (special issue): **86**

Campbell BW, Mani D, Curtin SJ, Slattery RA, Michno JM, Ort DR, Schaus PJ, Palmer RG, Orf JH, Stupar RM. 2015. Identical substitutions in magnesium chelatase paralogs result in chlorophyll-deficient soybean mutants. *G3: Genes, Genomes, Genetics*, **5**: 123–131.

Chapin III FS. 1980. The mineral nutrition of wild plants. *Annual review of ecology and systematics* **11**: 233–260.

Cogliati S, Rossini M, Julitta T, Meroni M, Schickling A, Burkart A, Pinto F, Rascher U, Colombo, R. 2015. Continuous and long-term measurements of reflectance and sun-induced chlorophyll fluorescence by using novel automated field spectroscopy systems. *Remote Sensing of Environment* **164**: 270–281.

Dall'Osto L, Cazzaniga S, Wada M, Bassi R. 2014. On the origin of a slowly reversible fluorescence decay component in the Arabidopsis *npq4* mutant. *Philosophical Transactions of the Royal Society B: Biological Sciences* **369**: 1640.

Damm A, Elbers JAN, Erler A, Gioli B, Hamdi K, Hutjes R, Kosvancova M, Meroni M, Miglietta M, Moersch A, et al. 2010. Remote sensing of sun-induced fluorescence to improve modeling of diurnal courses of gross primary production (GPP). *Global Change Biology* **16**: 171–186.

Daumard F, Goulas Y, Champagne S, Fournier A, Ounis A, Olioso A, Moya I. 2012. Continuous monitoring of canopy level sun-induced chlorophyll fluorescence during the growth of a sorghum field. *IEEE Transactions on Geoscience and Remote Sensing*, **50**: 4292–4300.

Dechant B, Ryu Y, Badgley G, Zeng Y, Berry JA, Zhang Y, Goulas Y, Li Z, Zhang Q,

Kang M. 2020. Canopy structure explains the relationship between photosynthesis and sun-induced chlorophyll fluorescence in crops. *Remote Sensing of Environment* **241**: 111733.

Demmig-Adams B. 1990. Carotenoids and photoprotection in plants: a role for the xanthophyll zeaxanthin. *Biochimica et Biophysica Acta (BBA)-Bioenergetics* **1020**: 1–24.

Demmig-Adams B, Adams WW, Heber U, Neimanis S, Winter K, Krüger A, Czygan F-C, Bilger W, Björkman O. 1990. Inhibition of zeaxanthin formation and of rapid changes in radiationless energy dissipation by dithiothreitol in spinach leaves and chloroplasts. *Plant Physiology* **92**: 293–301.

Demmig-Adams B, Adams III WW. 1992. Photoprotection and other responses of plants to high light stress. *Annual Review of Plant Biology* **43**: 599–626.

Demmig-Adams B, Adams WI, Logan BA, Verhoeven AS. 1995. Xanthophyll cycle-dependent energy dissipation and flexible photosystem II efficiency in plants acclimated to light stress. *Functional Plant Biology* **22**: 249−260.

Demmig-Adams B, Adams III WW. 2006. Photoprotection in an ecological context: the remarkable complexity of thermal energy dissipation. *New Phytologist* **172**: 11−21.

Dietzel L, Bräutigam K, Pfannschmidt T. 2008. Photosynthetic acclimation: State transitions and adjustment of photosystem stoichiometry–functional relationships between short-term and long-term light quality acclimation in plants. *The FEBS journal* **275**: 1080–1088.

Diner BA, Petrouleas V, Wendoloski JJ. 1991. The iron-quinone electron-acceptor complex of photosystem II. *Physiologia Plantarum*, **81**: 423–436.

Drusch D, Moreno J, Bello UD, Franco R, Goulas Y, Huth A, Middleton EM, Mohammed G, Nedbal L, Rascher U, et al. 2016. The fluorescence explorer mission concept – ESA's earth explorer 8. *IEEE Transactions on Geoscience and Remote Sensing* **55**: 1273−1284.

Enriquez S, Borowitzka MA. 2010. The use of the fluorescence signal in studies of seagrasses and macroalgae. In Suggett DJ. (eds). Chlorophyll a fluorescence in aquatic sciences methods and applications. Dordrecht: *Springer*. pp. 197–208.

Evain S, Flexas J, Moya I. 2004. A new instrument for passive remote sensing: 2. Measurement of leaf and canopy reflectance changes at 531 nm and their relationship with photosynthesis and chlorophyll fluorescence. *Remote Sensing of Environment* **91**: 175−185.

Evrendilek F, Asher JB, Aydin M. 2008. Diurnal photosynthesis, water use efficiency and light use efficiency of wheat under Mediterranean field conditions. *Journal of Environmental Biology* **29**: 397–406.

Fajer J, Brune DC, Davis MS, Forman A, Spaulding LD. 1975. Primary charge separation in bacterial photosynthesis: oxidized chlorophylls and reduced pheophytin. *Proceedings of the National Academy of Sciences*, **72**: 4956–4960.

Farquhar GD, von Caemmerer SV, Berry JA. 1980. A biochemical model of photosynthetic CO_2 assimilation in leaves of C_3 species. *Planta*, **149**: 78–90.

Frankenberg C, Fisher JB, Worden J, Badgley G, Saatchi SS, Lee JE, Toon GC, Butz A, Jung M, Kuze A, et al. 2011. New global observations of the terrestrial carbon cycle from GOSAT: Patterns of plant fluorescence with gross primary productivity. *Geophysical Research Letters*. https://doi.org/10.1029/2011GL048738.

Gamon JA, Berry JA. 2012. Facultative and constitutive pigment effects on the photochemical reflectance index (PRI) in sun and shade conifer needles. *Israel Journal*

of Plant Sciences, **60**: 85−95.

Gamon JA, Field CB, Bilger W, Björkman O, Fredeen A, Peñuelas J. 1990. Remote sensing of the xanthophyll cycle and chlorophyll fluorescence in sunflower leaves and canopies. *Oecologia* **85**: 1−7.

Gamon JA, Peñuelas J, Field CB. 1992. A narrow-waveband spectral index that tracks diurnal changes in photosynthetic efficiency. *Remote Sensing of Environment* **41**: 35−44.

Gamon J, Serrano L, Surfus JS. 1997. The photochemical reflectance index: an optical indicator of photosynthetic radiation-use efficiency across species, functional types, and nutrient levels. *Oecologia* **112**: 492−501.

Gamon JA, Surfus JS. 1999. Assessing leaf pigment content and activity with a reflectometer. *The New Phytologist* **143:** 105−117.

Garbulsky MF, Peñuelas J, Gamon J, Inoue Y, Filella I. 2011. The photochemical reflectance index (PRI) and the remote sensing of leaf, canopy and ecosystem radiation-use efficiencies: A review and meta-analysis. *Remote Sensing of Environment* **115:** 281−297.

Garcia-Molina A, Leister D. 2020. Accelerated relaxation of photoprotection impairs biomass accumulation in Arabidopsis. *Nature Plants* 1-4.

García-Plazaola JI, Matsubara S, Osmond CB. 2007. The lutein epoxide cycle in higher plants: its relationships to other xanthophyll cycles and possible functions. *Functional Plant Biology* **34**: 759−773.

Genty B, Briantais JM, Baker NR. 1989. The relationship between the quantum yield of photosynthetic electron transport and quenching of chlorophyll fluorescence. *Biochimica et Biophysica Acta (BBA)-General Subjects*, **990**: 87–92.

Gitelson AA, Gamon JA, Solovchenko A. 2017. Multiple drivers of seasonal change in PRI: Implications for photosynthesis 2. Stand level. *Remote Sensing of Environment* **190:** 198−206.

Givnish TJ. 1978. On the adaptive significance of compound leaves, with particular reference tropical trees. In: Tomlinson PB, Zimmermann MH (eds) Tropical trees as living systems. Cambridge University Press, Cambridge, pp 351–380.

Goulas Y, Fournier A, Daumard F, Champagne S, Ounis A, Marloie O, Moya I. 2016. Gross primary production of a wheat canopy relates stronger to far red than to red solar-induced chlorophyll fluorescence. *Remote Sensing*, **9**: 97.

Govindjee U. 2014. Non-photochemical quenching and energy dissipation in plants, algae and cyanobacteria (Vol. 40). Demmig-Adams B, Garab G, Adams III W. (Eds.). Dordrecht, The Netherlands: *Springer*.

Guanter L, Zhang Y, Jung M, Joiner J, Voigt M, Berry JA, Frankenberg C, Huete AR, Zarco-Tejada P, Lee J-E. 2014. Global and time-resolved monitoring of crop photosynthesis with chlorophyll fluorescence. *Proceedings of the National Academy of Sciences* **111**: E1327−E1333.

Gu L, Han J, Wood JD, Chang C, YY, Sun Y. 2019. Sun-induced Chl fluorescence and its importance for biophysical modeling of photosynthesis based on light reactions. *New Phytologist*, **223**: 1179–1191.

Harper JL. 1989. The value of a leaf. *Oecologia*, **80**: 53–58.

Havaux M, Niyogi KK. 1999. The violaxanthin cycle protects plants from photo-oxidative damage by more than one mechanism. *Proceedings of the National Academy of Sciences* **96**: 8762−8767.

He L, Magney T, Dutta D, Yin Y, Köhler P, Grossmann K, Stutz J, Dold C, Hatfield J,

Peng B, Frankenberg C. 2020. From the ground to space: Using solar-induced chlorophyll fluorescence to estimate crop productivity. *Geophysical Research Letters* **47**: e2020GL087474.

Herms DA, Mattson WJ. 1992. The dilemma of plants: to grow or defend. *The quarterly review of biology*, **67**: 283–335.

Hendrickson L, Furbank RT, Chow WS. 2004. A simple alternative approach to assessing the fate of absorbed light energy using chlorophyll fluorescence. *Photosynthesis research*, **82**: 73.

Hikosaka K, Noda HM. 2018. Modelling leaf CO_2 assimilation and photosystem II photochemistry from chlorophyll fluorescence and the photochemical reflectance index. *Plant Cell and Environment*. https://doi.org/10.1111/pce.13461

Hill R, Bendall FAY. 1960. Function of the two cytochrome components in chloroplasts: a working hypothesis. *Nature*, **186**: 136–137.

Horler DNH, Dockray M, Barber J. 1983. The red edge of plant leaf reflectance. *International journal of remote sensing*, **4**: 273–288.

Horton P. 2000. Prospects for crop improvement through the genetic manipulation of photosynthesis: morphological and biochemical aspects of light capture. *Journal of experimental botany*, **51**: 475–485.

Horton P, Johnson MP, Perez-Bueno ML, Kiss AZ, Ruban AV. 2008. Photosynthetic acclimation: Does the dynamic structure and macro-organisation of photosystem II in higher plant grana membranes regulate light harvesting states?. *The FEBS journal* **275**: 1069–1079.

Horton P, Ruban AV, Rees D, Pascal AA, Noctor G, Young AJ. 1991. Control of the light-harvesting function of chloroplast membranes by aggregation of the LHCII chlorophyll-protein complex. *FEBS Letters* **292**: 1−4.

Horton P, Ruban AV, Walters RG. 1994. Regulation of light harvesting in green plants (indication by nonphotochemical quenching of chlorophyll fluorescence). *Plant Physiology*, **106**: 415–420.

Ikeuchi M, Sato F, Endo T. 2016. Allocation of absorbed light energy in photosystem II in NPQ mutants of Arabidopsis. *Plant and Cell Physiology*, **57**: 1484–1494.

Jackson RD, Slater PN, Pinter Jr PJ. 1983. Discrimination of growth and water stress in wheat by various vegetation indices through clear and turbid atmospheres. *Remote sensing of environment*, **13**: 187–208.

Jahns P, Holzwarth AR. 2012. The role of the xanthophyll cycle and of lutein in photoprotection of photosystem II. *Biochimica et Biophysica Acta (BBA)-Bioenergetics* **1817**: 182−193.

Jia H, Liggins JR, Chow WS. 2012. Acclimation of leaves to low light produces large grana: the origin of the predominant attractive force at work. *Philosophical Transactions of the Royal Society B: Biological Sciences.* **367**: 3494–3502.

Johnson MP, Davison PA, Ruban AV, Horton P. 2008. The xanthophyll cycle pool size controls the kinetics of non-photochemical quenching in *Arabidopsis thaliana*. *FEBS letters*, *582*(2), 262–266.

Joiner J, Yoshida Y, Vasilkov AP, Middleton EM. 2011. First observations of global and seasonal terrestrial chlorophyll fluorescence from space. *Biogeosciences* **8**: 637−651.

Joiner J, Yoshida Y, Vasilkov AP, Schaefer K, Jung M, Guanter L, Zhang Y, Garrity S, Middleton EM, Huemmrich KF, Gu L, Belelli Marchesini L. 2014. The seasonal cycle of satellite chlorophyll fluorescence observations and its relationship to vegetation phenology and ecosystem atmosphere carbon exchange. *Remote Sensing of*

Environment, **152**: 375–391.

Kasahara M, Kagawa T, Oikawa K, Suetsugu N, Miyao M, Wada M. 2002. Chloroplast avoidance movement reduces photo damage in plants. *Nature* **420**: 829-832.

Kasajima I, Ebana K, Yamamoto T, Takahara K, Yano M, Kawai-Yamada M, Uchimiya H. 2011. Molecular distinction in genetic regulation of nonphotochemical quenching in rice. *Proceedings of the National Academy of Sciences* **108**: 13835–13840.

Kasajima I, Takahara K, Kawai-Yamada M, Uchimiya H. 2009. Estimation of the relative sizes of rate constants for chlorophyll de-excitation processes through comparison of inverse fluorescence intensities. *Plant and cell physiology*, **50**: 1600–1616.

Kautsky H, Appel W, Amann H. 1960. Chlorophyllfluorescenz und Kohlensaureassimilation. *Biochem. Z.* **33**: 277—292.

Keller B, Vass I, Matsubara S, Paul K, Jedmowski C, Pieruschka R, Nedbal L, Rascher U, Muller O. 2019. Maximum fluorescence and electron transport kinetics determined by light-induced fluorescence transients (LIFT) for photosynthesis phenotyping. *Photosynthesis Research* **140**: 221−233.

Kitajima M, Butler WL. 1975. Quenching of chlorophyll fluorescence and primary photochemistry in chloroplasts by dibromothymoquinone. *Biochimica et Biophysica Acta (BBA)-Bioenergetics*, **376**: 105–115.

Kitajima K, Mulkey SS, Samaniego M, Wright SJ. 2002. Decline of photosynthetic capacity with leaf age and position in two tropical pioneer tree species. *American Journal of Botany* **89**: 1925–32.

Kohzuma K, Hikosaka K. 2018. Physiological validation of photochemical reflectance index (PRI) as a photosynthetic parameter using *Arabidopsis thaliana* mutants. *Biochemical and Biophysical Research Communications* **498**: 52−57.

Kolber Z, Klimov D, Ananyev G, Rascher U, Berry J, Osmond B. 2005. Measuring photosynthetic parameters at a distance: Laser induced fluorescence transient (LIFT) method for remote measurements of photosynthesis in terrestrial vegetation. *Photosynthesis Research* **84**: 121–29.

Kolber ZS, Prasil O, Falkowski PG. 1998. Measurements of variable fluorescence using FRR technique: Defining methodology and experimental protocols. *Biochim. Biophys. Acta* **1367**: 88−106.

Krall JP, Edwards GE. 1992. Relationship between photosystem II activity and CO2 fixation in leaves. *Physiologia Plantarum*, **86**: 180–187.

Kramer DM, Johnson G, Kiirats O, Edwards GE. 2004. New fluorescence parameters for the determination of Q A redox state and excitation energy fluxes. *Photosynthesis research*, **79**: 209.

Krause GH. 1973. The high-energy state of the thylakoid system as indicated by chlorophyll fluorescence and chloroplast shrinkage. *Biochimica et Biophysica Acta (BBA)-Bioenergetics* **292**: 715−728.

Krause GH. 1988. Photoinhibition of photosynthesis. An evaluation of damaging and protective mechanisms. *Physiologia Plantarum* **74**: 566−574.

Krause GH, Vernotte C, Briantais J-M. 1982. Photoinduced quenching of chlorophyll fluorescence in intact chloroplasts and algae. Resolution into two components. Biochim. Biophys. Acta **679**: 116–24.

Krause GH, Weis E. 1991. Chlorophyll fluorescence and photosynthesis: the basics. *Annual Review of Plant Biology* **42**: 313−349.

Kromdijk J, Głowacka K, Leonelli L, Gabilly ST, Iwai M, Niyogi KK, Long SP. 2016.

Improving photosynthesis and crop productivity by accelerating recovery from photoprotection. *Science* **354**: 857–861.

Kume A, Akitsu T, Nasahara KN. 2018. Why is chlorophyll b only used in light-harvesting systems?. *Journal of Plant research*, **131**: 961–972.

Li XP, Björkman O, Shih C, Grossman AR, Rosenquist M, Jansson S, Niyogi KK. 2000. A pigment-binding protein essential for regulation of photosynthetic light harvesting. *Nature* **403**: 391−395.

Li XP, Müller-Moulé P, Gilmore AM, Niyogi KK. 2002. PsbS-dependent enhancement of feedback de-excitation protects photosystem II from photoinhibition. *Proceedings of the National Academy of Sciences* **99**: 15222−15227.

Li XP, Gilmore AM, Caffarri S, Bassi R, Golan T, Kramer D, Niyogi KK. 2004. Regulation of photosynthetic light harvesting involves intrathylakoid lumen pH sensing by the PsbS protein. *Journal of Biological Chemistry* **279**: 22866–22874.

Lichtenthaler HK, Ač A, Marek MV, Kalina J, Urban O. 2007a. Differences in pigment composition, photosynthetic rates and chlorophyll fluorescence images of sun and shade leaves of four tree species. *Plant Physiology and Biochemistry* **45**: 577–88.

Lichtenthaler HK, Babani F, Langsdorf G. 2007b. Chlorophyll fluorescence imaging of photosynthetic activity in sun and shade leaves of trees. *Photosynthesis Research*, **93**: 235.

Liu L, Guan L, Liu X. 2017. Directly estimating diurnal changes in GPP for C3 and C4 crops using far-red sun-induced chlorophyll fluorescence. *Agricultural and Forest Meteorology* **232:** 1–9.

Liu X, Liu L, Zhang S, Zhou X. 2015. New spectral fitting method for full-spectrum solar-induced chlorophyll fluorescence retrieval based on principal components analysis. *Remote Sensing*, **7**: 10626-10645.

Long SP, Humphries S, Falkowski PG. 1994. Photoinhibition of photosynthesis in nature. *Annual review of plant biology* **45**: 633–662.

Lu X, Liu Z, Zhao F, Tang J. 2020. Comparison of total emitted solar-induced chlorophyll fluorescence (SIF) and top-of-canopy (TOC) SIF in estimating photosynthesis. *Remote Sensing of Environment* **251:** 112083.

Magney TS, Frankenberg C, Fisher JB, Sun Y, North GB, Davis TS, Kornfeld A, Siebke K. 2017. Connecting active to passive fluorescence with photosynthesis: A method for evaluating remote sensing measurements of Chl fluorescence. *New Phytologist* **215**: 1594−1608.

Magney TS, Frankenberg C, Köhler P, North G, Davis TS, Dold C, Dutta D, Fisher JB, Grossmann K, Harrington A, et al. 2019. Disentangling changes in the spectral shape of chlorophyll fluorescence: Implications for remote sensing of photosynthesis. *Journal of Geophysical Research: Biogeosciences*, **124**: 1491−1507.

Maguire AJ, Eitel JU, Griffin KL, Magney TS, Long RA, Vierling LA, Schmiege SC, Jennewein JS, Weygint WA, Boelman NT, Bruner SG. 2020. On the functional relationship between fluorescence and photochemical yields in complex evergreen needleleaf canopies. *Geophysical Research Letters* **47**: e2020GL087858.

Malkin S, Fork DC. 1981. Photosynthetic units of sun and shade plants. *Plant Physiology* **67**: 580–83.

Maxwell K, Johnson GN. 2000. Chlorophyll fluorescence − a practical guide. *Journal of Experimental Botany* **51:** 659−668.

McEvoy JP, Brudvig GW. 2006. Water-splitting chemistry of photosystem II. *Chemical reviews*, **106**: 4455–4483.

Meroni M, Busetto L, Colombo R, Guanter L, Moreno J, Verhoef W. 2010. Performance of spectral fitting methods for vegetation fluorescence quantification. *Remote Sensing of Environment*, **114**: 363–374.

Migliavacca M, Perez-Priego O, Rossini M, El-Madany TS, Moreno G, van der Tol C, Rascher U, Berninger A, Bessenbacher V, Burkart A, et al. 2017. Plant functional traits and canopy structure control the relationship between photosynthetic CO_2 uptake and far-red sun-induced fluorescence in a Mediterranean grassland under different nutrient availability. *New Phytologist* **214:** 1078−1091.

Mitchell PL, Sheehy JE. 2006. Supercharging rice photosynthesis to increase yield. *The New Phytologist*, **171:** 688-693.

Mohammed GH, Colombo R, Middleton EM, Rascher U, van der Tol C, Nedbal L, Goulas Y, Pérez-Priego O, Damm A, Meroni M, et al. 2019. Remote sensing of solar-induced chlorophyll fluorescence (SIF) in vegetation: 50 years of progress. *Remote sensing of environment* **231**: 111177.

Mohotti AJ, Lawlor DW. 2002. Diurnal variation of photosynthesis and photoinhibition in tea: effects of irradiance and nitrogen supply during growth in the field. Journal of Experimental Botany **53**: 313–22.

Müller P, Li XP, Niyogi KK. 2001. Non-photochemical quenching. A response to excess light energy. *Plant Physiology* **125**: 1558−1566.

Murchie EH, Kefauver S, Araus JL, Muller O, Rascher U, Flood PJ, Lawson T. 2018. Measuring the dynamic photosynthome. *Annals of botany*, **122**: 207–220.

Murchie EH, Niyogi KK. 2011. Manipulation of photoprotection to improve plant photosynthesis. *Plant Physiology* **155**: 86–92.

Nichol CJ, Rascher U, Matsubara S, Osmond B. 2006. Assessing photosynthetic efficiency in an experimental mangrove canopy using remote sensing and chlorophyll fluorescence. *Trees* **20**: 9.

Niyogi KK, Björkman O, Grossman AR. 1997. Genetic dissection of xanthophyll-dependent photo protection in algae and plants. 8th International Conference on Arabidopsis Research.

Niyogi KK, Grossman AR, Björkman O. 1998. Arabidopsis mutants define a central role for the xanthophyll cycle in the regulation of photosynthetic energy conversion. *The Plant Cell* **10**: 1121−1134.

Nobel PS. 1976. Photosynthetic rates of sun versus shade leaves of *Hyptis Emoryi* Torr. *Plant Physiology* **58**: 218–23.

Osmond B, Chow WS, Wyber R, Zavafer A, Keller B, Pogson BJ, Robinson SA. 2017. Relative functional and optical absorption cross-sections of PSII and other photosynthetic parameters monitored in situ, at a distance with a time resolution of a few seconds, using a prototype light-induced fluorescence transient (LIFT) device. *Functional Plant Biology* **44**: 985−1006.

Öquist G, Huner NP. 2003. Photosynthesis of overwintering evergreen plants. *Annual Review of Plant Biology* **54**: 329−355.

Owens TG, Shreve AP, Albrecht AC. 1992. Dynamics and mechanism of singlet energy transfer between carotenoids and chlorophylls: light harvesting and non-photochemical fluorescence quenching. In N. Murata (Ed.), *Research in Photosynthesis* **4**: 179–186. Kluwer Academic, Dordrecht, The Netherlands.

Paillotin G. 1976. Capture frequency of excitations and energy transfer between photosynthetic units in the photosystem II. *Journal of theoretical biology*, **58**: 219–235.

Parry MA, Andralojc PJ, Scales JC, Salvucci ME, Carmo-Silva AE, Alonso H, Whitney

SM. 2013. Rubisco activity and regulation as targets for crop improvement. *Journal of Experimental Botany*, **64**: 717–730.

Peñuelas J, Filella I, Gamon JA. 1995. Assessment of photosynthetic radiation-use efficiency with spectral reflectance. *New Phytologist* **131**: 291−296.

Peñuelas J, Garbulsky MF, Filella I. 2011. Photochemical reflectance index (PRI) and remote sensing of plant CO_2 uptake. *New Phytologist* **191**: 596–599.

Pieruschka R, Albrecht H, Muller O, Berry JA, Klimov D, Kolber ZS, Malenovsky Z, Rascher U. 2014. Daily and seasonal dynamics of remotely sensed photosynthetic efficiency in tree canopies. *Tree physiology*, **34**: 674–685.

Pinto F, Damm A, Schickling A, Panigada C, Cogliati S, Müller-Linow M, Balvora A, Rascher U. 2016. Sun-induced chlorophyll fluorescence from high-resolution imaging spectroscopy data to quantify spatio-temporal patterns of photosynthetic function in crop canopies. *Plant, Cell & Environment* **39:** 1500−1512.

Pinto F, Celesti M, Acebron K, Alberti G, Cogliati S, Colombo R, Radoslaw J, Matsubara S, Miglietta F, Palombo A, et al. 2020. Dynamics of sun-induced chlorophyll fluorescence and reflectance to detect stress-induced variations in canopy photosynthesis. *Plant, Cell & Environment* **43**: 1637−1654.

Poorter H, Niinemets Ü, Walter A, Fiorani F, Schurr, U. 2010. A method to construct dose–response curves for a wide range of environmental factors and plant traits by means of a meta-analysis of phenotypic data. *Journal of Experimental Botany*, **61:** 2043–2055.

Poorter H, Niinemets Ü, Ntagkas N, Siebenkäs A, Mäenpää M, Matsubara S, Pons T. 2019. A meta-analysis of plant responses to light intensity for 70 traits ranging from molecules to whole plant performance. *New Phytologist* **223:** 1073–1105.

Porcar-Castell A, Tyystjärvi E, Atherton J, van der Tol C, Flexas J, Pfündel EE, Moreno J, Frankenberg C, Berry JA. 2014. Linking chlorophyll and fluorescence to photosynthesis for remote sensing applications: mechanisms and challenges. *Journal of Experimental Botany* **65:** 4065−4095.

Powles SB. 1984. Photoinhibition of photosynthesis induced by visible light. *Annual review of plant physiology* **35**: 15–44.

Quick WP, Horton P. 1984. Studies on the induction of chlorophyll fluorescence in barley protoplasts. II. Resolution of fluorescence quenching by redox state and the transthylakoid pH gradient. *Proceedings of the Royal society of London. Series B. Biological sciences* **220**: 371–382.

R Core Team 2013. R: A language and environment for statistical computing. *R Foundation for Statistical Computing*, Vienna, Austria. URL http://www.R-project.org/.

Rahimzadeh-Bajgiran P, Munehiro M, Omasa K. 2012. Relationships between the photochemical reflectance index (PRI) and chlorophyll fluorescence parameters and plant pigment indices at different leaf-growth stages. *Photosynthesis Research* **113**: 261−271.

Raines CA. 2003. The Calvin cycle revisited. *Photosynthesis research*, **75**: 1–10.

Rascher U, Agati G, Alonso L, Cecchi G, Champagne S, Colombo R, Damm A, Daumard F, de Miguel E, Fernandez G, et al. 2009. CEFLES2: the remote sensing component to quantify photosynthetic efficiency from the leaf to the region by measuring sun-induced fluorescence in the oxygen absorption bands. *Biogeosciences*, **6**: 1181–1198.

Rascher U, Alonso L, Burkart A, Cilia C, Cogliati S, Colombo R, Damm A, Drusch M, Guanter L, Hanus J, et al. 2015. Sun-induced fluorescence – a new probe of

photosynthesis: First maps from the imaging spectrometer HyPlant. *Global Change Biology* **21**: 4673−4684.

Rascher U, Nedbal L. 2006. Dynamics of photosynthesis in fluctuating light. *Current opinion in plant biology*, **9**: 671–678.

Roach T, Krieger-Liszkay A. 2012. The role of the PsbS protein in the protection of photosystems I and II against high light in *Arabidopsis thaliana. Biochimica et Biophysica Acta (BBA) - Bioenergetics* **1817**: 2158–65.

Roháček K. 2010. Method for resolution and quantification of components of the non-photochemical quenching (q N). *Photosynthesis research*, **105**: 101–113.

Rossini M, Meroni M, Celesti M, Cogliati S, Julitta T, Panigada C, Rascher U, van der Tol C, Colombo R. 2016. Analysis of red and far-red sun-induced chlorophyll fluorescence and their ratio in different canopies based on observed and modeled data. *Remote Sensing* **8**: 412.

Rossini M, Meroni M, Migliavacca M, Manca G, Cogliati S, Busetto L, Picchi V, Cescatti A, Seufert G, Colombo R. 2010. High resolution field spectroscopy measurements for estimating gross ecosystem production in a rice field. *Agricultural and Forest Meteorology* **150**: 1283–1296.

Rossini M, Nedbal L, Guanter L, Ač A, Alonso L, Burkart A, Cogliati S, Colombo R, Damm A, Drusch M, et al. 2015. Red and far-red sun-induced chlorophyll fluorescence as a measure of plant photosynthesis. *Geophysical Research Letters* **42:** 1632−1639.

Ruban AV. 2016. Non-photochemical chlorophyll fluorescence quenching: mechanism and effectiveness in protecting plants from photodamage. *Plant Physiology* **170**: 1903−1916.

Ruban AV. 2017. Quantifying the efficiency of photoprotection. Philosophical Transactions of the Royal Society B: Biological Sciences, **372**: 20160393.

Ruban AV, Murchie EH. 2012. Assessing the photoprotective effectiveness of non-photochemical chlorophyll fluorescence quenching: a new approach. *Biochimica et Biophysica Acta (BBA)-Bioenergetics*, **1817**: 977–982.

Sakowska K, Alberti G, Genesio L, Peressotti A, Delle Vedove G, Gianelle D, Colombo R, et al. 2018. Leaf and canopy photosynthesis of a chlorophyll deficient soybean mutant. *Plant, cell & environment*, **41**: 1427–1437.

Sage RF. 2004. The evolution of C4 photosynthesis. *New phytologist* **161:** 341–370.

Savitzky A, Golay MJ. 1964. Smoothing and differentiation of data by simplified least squares procedures. *Analytical chemistry*, **36**: 1627–1639.

Schickling A, Matveeva M, Damm A, Schween JH, Wahner A, Graf A, Crewell S, Rascher U. 2016. Combining sun-induced chlorophyll fluorescence and photochemical reflectance index improves diurnal modeling of gross primary productivity. *Remote Sensing* **8**: 574.

Schreiber U. 1986. Detection of rapid induction kinetics with a new type of high-frequency modulated chlorophyll fluorometer. In *Current topics in photosynthesis* (pp. 259-270). Springer, Dordrecht.

Schreiber U, Schliwa U. 1987. A solid-state, portable instrument for measurement of chlorophyll luminescence induction in plants. *Photosynthesis research*, **11**: 173–182.

Schreiber U, Schliwa U, Bilger W. 1986. Continuous recording of photochemical and non-photochemical chlorophyll fluorescence quenching with a new type of modulation fluorometer. *Photosynthesis research*, **10**: 51–62.

Schurr U, Walter A, Rascher U. 2006. Functional dynamics of plant growth and

photosynthesis–from steady-state to dynamics–from homogeneity to heterogeneity. *Plant, Cell & Environment* ***29****:* 340−352.

Şener M, Strümpfer J, Hsin J, Chandler D, Scheuring S, Hunter CN, Schulten K. 2011. Förster energy transfer theory as reflected in the structures of photosynthetic light-harvesting systems. *ChemPhysChem*, **12**: 518–531.

Shevela D, Björn LO. 2017. Evolution of the Z-scheme of photosynthesis: a perspective. *Photosynthesis Research*, **133**: 5-15.

Stirbet A. 2013. Excitonic connectivity between photosystem II units: what is it, and how to measure it?. *Photosynthesis research*, **116**: 189–214.

Sukenik A, Bennett J, Falkowski P. 1987. Light-saturated photosynthesis—limitation by electron transport or carbon fixation?. *Biochimica et Biophysica Acta (BBA)-Bioenergetics*, **891**: 205–215.

Thayer SS, Björkman O. 1990. Leaf xanthophyll content and composition in sun and shade determined by HPLC. *Photosynthesis research*, 23: 331–343.

van der Tol C, Berry JA, Campbell PKE, Rascher U. 2014. Models of fluorescence and photosynthesis for interpreting measurements of solar-induced chlorophyll fluorescence. *Journal of Geophysical Research*: *Biogeosciences* **119**: 2312−2327.

van der Tol C, Vilfan N, Dauwe D, Cendrero-Mateo MP, Yang P. 2019. The scattering and re-absorption of red and near-infrared chlorophyll fluorescence in the models Fluspect and SCOPE. *Remote sensing of environment*, **232**: 111292.

van Kooten O, Snel JF. 1990. The use of chlorophyll fluorescence nomenclature in plant stress physiology. *Photosynthesis research*, **25**: 147–150.

van Wittenberghe S, Alonso L, Verrelst J, Hermans I, Delegido J, Veroustraete F, Valcke R, Moreno J, Samson R. 2013. Upward and downward solar-induced chlorophyll fluorescence yield indices of four tree species as indicators of traffic pollution in Valencia. *Environmental Pollution* **173**: 29−37.

van Wittenberghe S, Alonso L, Malenovský Z, Moreno J. 2019. In vivo photoprotection mechanisms observed from leaf spectral-absorbance changes showing VIS–NIR slow-induced conformational pigment bed changes. *Photosynthesis Research* **142**: 283−305.

van Wittenberghe S, Laparra V, García-Plazaola JI, Fernández-Marín B, Porcar-Castell A, Moreno J. 2020. Combined dynamics of the 500-600 nm leaf absorption and chlorophyll fluorescence changes in vivo: evidence for the multifunctional energy quenching role of xanthophylls. *Biochimica et Biophysica Acta (BBA)-Bioenergetics*, 148351.

Verhoeven A. 2014. Sustained energy dissipation in winter evergreens. *New Phytologist* **201**: 57−65.

Verrelst J, van der Tol C, Magnani F, Sabater N, Rivera JP, Mohammed G, Moreno J. 2016. Evaluating the predictive power of sun-induced chlorophyll fluorescence to estimate net photosynthesis of vegetation canopies: A SCOPE modeling study. *Remote Sensing of Environment* **176**: 139−151.

Vilfan N, van der Tol C, Verhoef W. 2019. Estimating photosynthetic capacity from leaf reflectance and Chl fluorescence by coupling radiative transfer to a model for photosynthesis. *New Phytologist* **223**: 487−500.

von Caemmerer SV, Farquhar GD. 1981. Some relationships between the biochemistry of photosynthesis and the gas exchange of leaves. *Planta*, **153**: 376–387.

Walker BJ, Ort DR. 2015. Improved method for measuring the apparent CO2 photocompensation point resolves the impact of multiple internal conductances to CO2 to net gas exchange. *Plant, Cell & Environment*, **38**: 2462–2474.

Walters RG. 2005. Towards an understanding of photosynthetic acclimation. *Journal of experimental botany* **56**: 435–447.

Walters RG, Rogers JJ, Shephard F, Horton P. 1999. Acclimation of *Arabidopsis thaliana* to the light environment: the role of photoreceptors. *Planta* **209**: 517–527.

Watt MS, Buddenbaum H, Leonardo EMC, Estarija HJC, Bown HE, Gomez-Gallego M, Hartley R, Massam P, Wright L, Zarco-Tejada PJ. 2020. Using hyperspectral plant traits linked to photosynthetic efficiency to assess N and P partition. *ISPRS Journal of Photogrammetry and Remote Sensing* **169:** 406–420.

Weis E, Berry JA. 1987. Quantum efficiency of photosystem II in relation to 'energy'-dependent quenching of chlorophyll fluorescence. *Biochimica et Biophysica Acta (BBA)-Bioenergetics*, **894**: 198–208.

Wieneke S, Ahrends H, Damm A, Pinto F, Stadler A, Rossini M, Rascher U. 2016. Airborne based spectroscopy of red and far-red sun-induced chlorophyll fluorescence: Implications for improved estimates of gross primary productivity. *Remote Sensing of Environment*, **184**: 654–667.

Wohlfahrt G, Gu L. 2015. The many meanings of gross photosynthesis and their implication for photosynthesis research from leaf to globe. *Plant, cell & environment*, **38**: 2500.

Wong CY, Gamon JA. 2015. Three causes of variation in the photochemical reflectance index (PRI) in evergreen conifers. *New Phytologist* **206**: 187−195.

Wong KL, Bünzli JCG, Tanner PA. 2020. Quantum yield and brightness. *Journal of Luminescence*, 117256.

Wu C, Huang W, Yang Q, Xie Q. 2015. Improved estimation of light-use efficiency by removal of canopy structural effect from the photochemical reflectance index (PRI). *Agriculture, Ecosystems & Environment* **199:** 333−338.

Wunder T, Liu Q, Aseeva E, Bonardi V, Leister D, Pribil M. 2013. Control of STN7 transcript abundance and transient STN7 dimerisation are involved in the regulation of STN7 activity. *Planta* **237**: 541–558.

Yamamoto HY, Bugos RC, Hieber AD. 1999. Biochemistry and molecular biology of the zanthophyll cycle. In The Photochemistry of Carotenoids, ed. Frank HA, Young AJK, Britton G, Cogdell RJ, pp. 293–303. Dordrecht, The Netherlands: Kluwer Academic Publishers.

Yang K, Ryu Y, Dechant B, Berry JA, Hwang Y, Jiang C, Kang M, Kim J, Kimm H, Kornfeld A, Yang X. 2018. Sun-induced chlorophyll fluorescence is more strongly related to absorbed light than to photosynthesis at half-hourly resolution in a rice paddy. *Remote Sensing of Environment* **216:** 658–673.

Yang P, van der Tol C, Campbell PK, Middleton EM. 2020. Fluorescence Correction Vegetation Index (FCVI): A physically based reflectance index to separate physiological and non-physiological information in far-red sun-induced chlorophyll fluorescence. *Remote sensing of environment* **240:** 111676.

Yang X, Tang J, Mustard JF, Lee JE, Rossini M, Joiner J, Munger JW, Kornfeld A, Richardson AD. 2015. Solar-induced chlorophyll fluorescence that correlates with canopy photosynthesis on diurnal and seasonal scales in a temperate deciduous forest. *Geophysical Research Letters* **42**: 2977−2987.

Yun JI, Taylor SE. 1986. Adaptive implications of leaf thickness for sun- and shade-grown *Abutilon theophrasti*. *Ecology* 67: 1314–18.

Zarco-Tejada PJ, Catalina A, González MR, Martín P. 2013. Relationships between net photosynthesis and steady-state chlorophyll fluorescence retrieved from airborne

hyperspectral imagery. *Remote Sensing of Environment* **136:** 247–258.

Zarco-Tejada PJ, Miller JR, Mohammed GH, Noland TL, Sampson PH. 2000. Chlorophyll fluorescence effects on vegetation-apparent reflectance: II laboratory and airborne canopy-level measurements with hyperspectral data. *Remote Sensing of Environment* **74**: 596–608.

Zhang Q. 2007. Strategies for developing green super rice. *Proceedings of the national Academy of Sciences*, **104**: 16402–16409.

Zeng Y, Badgley G, Dechant B, Ryu Y, Chen M, Berry JA. 2019. A practical approach for estimating the escape ratio of near-infrared solar-induced chlorophyll fluorescence. *Remote Sensing of Environment* **232**: 111209.

6. PUBLICATIONS

1. First publication (Behmann et al., 2018)

Specim IQ: Evaluation of a New, Miniaturized Handheld Hyperspectral Camera and Its Application for Plant Phenotyping and Disease Detection

Jan Behmann, Kelvin Acebron, Dzhaner Emin, Simon Bennertz, Shizue Matsubara, Stefan Thomas, David Bohnenkamp, Matheus T. Kuska, Jouni Joussila, Harri Salo, Anne-Katrin Mahlein, Uwe Rascher

Journal: Sensors (2018) 18: 441

DOI: 10.3390/s18020441

Status: Published on 2 February 2018

Contribution: Design 30%, Experimentation 50%, Analysis 50%, Publication work 20%

I was involved in testing the portable hyperspectral camera (Specim IQ) on *Arabidopsis thaliana npq* mutants, analysed the data and wrote the section of the manuscript describing the results. I was also partially involved in the overall design of the the experiment and the manuscript.

2. Second publication (Pinto et al., 2020)

Dynamics of sun-induced chlorophyll fluorescence and reflectance to detect stress-induced variations in canopy photosynthesis

Francisco Pinto, Marco Celesti, Kelvin Acebron, Giorgio Alberti, Sergio Cogliati, Roberto Colombo, Radoslaw Jusczcak, Shizue Matsubara, Franco Miglietta, Angelo Palombo, Cinzia Panigada, Stefano Pignatti, Micol Rossini, Karolina Sakowska, Anke Schickling, Dirk Schüttemeyer, Marcin Stróżecki, Marin Tudoroiu, Uwe Rascher

Journal: Plant, Cell and Environment (2020) 43: 1637 – 1654

DOI: 10.1111/pce.13754

Status: Published on 13 March 2020

Contribution: Experimentation 10%, Analysis 10%, Publication work (5%)

I conducted an independent confirmatory experiments that validate the main results of the manuscript. Then I was involved in refining the claims in the manuscript.

3. Third publication (Acebron et al., 2020)

Diurnal dynamics of nonphotochemical quenching in Arabidopsis *npq* mutants assessed by solar-induced fluorescence and reflectance measurements in the field

Kelvin Acebron, Shizue Matsubara, Christoph Jedmowski, Dzhaner Emin, Onno Muller, Uwe Rascher

Journal: New Phytologist (2020) 229: 2104 – 2119

DOI: 10.1111/nph.16984

Status: Published on 05 October 2020

Contribution: Design 90%, Experimentation 100%, Analysis 95%, Publication work 90%

This work is the main component of my PhD thesis. I originally designed the experiments with initial input from Shizue Matsubara, Uwe Rascher and Onno Muller. I also performed all the experiments in the laboratory, greenhouse and field condition. I analysed and interpret all the data with inputs from S. Matsubara and U. Rascher. I wrote the manuscript with guidance of U.Rascher and critical review from S.Matsubara.

4. Fourth publication (Acebron et al., 2021)

Photosynthetic Induction of Chlorophyll-Deficient Soybean (*Glycine max* L.) Mutant

Kelvin Acebron, Nicole Salvatori, Shizue Matsubara, Onno Muller, Alessandro Peressotti, Uwe Rascher, Giorgio Alberti

Journal: Photosynthesis Research

Status: to be submitted

Contribution: Design 50%, Experimentation 50%, Analysis 50%, Publication work 60%

This work is in collaboration with Nicole Salvatori and Giorgio Alberti. I designed most of the gas-exchange and fluorescence protocol with inputs from Shizue Matsubara and Giorgio Alberti. I also analysed and interpret the data together with N. Salvatori. I wrote majority of the manuscript with significant inputs from N. Salvatori.

7. ACKNOWLEDGEMENTS

First of all, I would like to express my sincerest appreciation to Prof. Uwe Rascher for being my Doctorvater. Thank you Uwe for your patience during my adjustment periods in the institute, for your guidance during my stay in Germany and for believing that I can finish my PhD.

I also would like to acknowledge other Professors and Scientists in the institute who are very approachable and welcoming when it comes to scientific discussion. Many thanks to Shizue Matsubara for being the critic of my work and ideas. Thanks also to Ladislav Nedbal and Hendrik Poorter who had been very open for discussion and provided words of encouragement. Without them, the quality of my research output would have not improved. Many thanks to Onno Muller especially for the opportunity for me to be involved in the CASS project. Thanks to all the members of the shoot group (especially: Nils Müller, Verena Trinkel, Michael Quarten, Christoph Jedmowski, MaPi Cendrero-Pilar, Andreas Burkhart, and Bastian Siegmann) who helped me in logistical and technical issues during my experiments as well as to some members of IBG-2 (Prof. Ingar Janzik, Beate, and Kathy) who helped with administration and maintenance of my plants.

I would like to thank my fellow Phd students at the IBG-2 for the social events as well as giving a healthy environment for a good scientific practice. Thank you as well to Vikas Pingle and Simon Bennertz for helping me during my first year at the IBG-2. Especial thanks to Anh Banh, Beat Keller and Paola Puggioni for scientific discussions we had regarding NPQ, to Vitalij Dombinov and Lisa Mau for joining me in the *Shut up and Write* sessions especially during the COVID lockdown, to Yannik Müllers for editing my *Zusammenfassung*, and to Nicolas Zendonadi for editing mainly the materials and method section of my thesis. Also thanks to Nicole Savlatori and Giorgio Alberti from University of Udine who were very integral on the development of soybean research.

I would also like to extend my appreciation to other groups who I found very useful for me to maintain my sanity while I do my PhD. Particularly, my basketball group, CrossFit group, Zirkeltraining, IBG-2 dinner nights, badminton, lunch group, '*safety issues'* band, writing group, and journal club. Our regular meetings enabled me to plan my week with good balance for work, recreations and social events.

Most especially, I would like to dedicate my Phd work to my family and friends in the Philippines who I dearly missed during the pursuit of my PhD endeavour. Thank you for your constant moral support especially to my parents who were always there to support me unconditionally. I am also most grateful to have found real friends during my stay in Germany and help me cope up with cultural differences in social dynamics as well as in scientific practices. Cheers to people who I truly met: Bogdan, Martino, Dzhaner, Marco, Inez, Lucy, Vera, Theresa and Nileena, – without you, my life in Germany would have been dull and boring.

Lastly, I would like to give my special thanks to Anca Macovei and Robert Coe who inspired me to pursue research and to be genuinely interested in scientific career. My thanks also is extended to Dr Paul Quick who gave me solid foundation on chlorophyll fluorescence as well as the proper conduct in scientific research.

8. SUPPLEMENTARY MATERIALS

Table S1. Area of the curve for each efficiency illustrated in Fig. 13.

	Φ_f	Φ_D	Φ_{PSII}	Φ_{NPQ}
Constant light				
Wild type	3.48 ± 0.03[a]	11.66 ± 0.03[a]	23.46 ± 0.08[a]	26.84 ± 0.08[a]
Mutant	10.77 ± 0.02[b]	9.57 ± 0.02[a]	25.44 ± 0.07[a]	19.55 ± 0.05[b]
Fluctuating light				
Wild type	3.62 ± 0.03[a]	11.63 ± 0.03[a]	22.86 ± 0.09[a]	26.55 ± 0.10[a]
Mutant	9.97 ± 0.03[b]	9.76 ± 0.02[a]	26.21 ± 0.06[a]	18.73 ± 0.06[a]

Different letters indicate statistical difference at $\alpha = 0.05$

Table S2. F_v/F_m before and after 1-hr of photosynthetic induction comparing wild type and mutant grown in either fluctuating or non-fluctuating light.

Type	F_v/F_m before protocol	F_v/F_m after protocol	Decline
Induction using constant light and grown in non-fluctuating light			
Wild type	0.808 ± 0.006	0.583 ± 0.023	29.5 ± 0.5 %
Mutant	0.827 ± 0.013	0.583 ± 0.010	27.8 ± 2.4 %
Induction using constant light and grown in fluctuating light			
Wild type	0.816 ± 0.011	0.555 ± 0.024	32.1 ± 1.4 %
Mutant	0.822 ± 0.009	0.565 ± 0.010	31.8 ± 2.1 %
Induction using fluctuating light and grown in non-fluctuating light			
Wild type	0.808 ± 0.007	0.551 ± 0.013	31.8 ± 1.3 %
Mutant	0.826 ± 0.010	0.586 ± 0.024	29.1 ± 2.9 %
Induction using fluctuating light and grown in fluctuating light			
Wild type	0.811 ± 0.011	0.541 ± 0.029	33.4 ± 2.7 %
Mutant	0.822 ± 0.009	0.549 ± 0.010	33.2 ± 0.4 %
Mean for all conditions			
Wild type	0.810 ± 0.002	0.557 ± 0.009	31.3 ± 1.2 %
Mutant	0.824 ± 0.001	0.570 ± 0.009	30.8 ± 0.9 %

All mean comparisons showed no significant differences using the student's t-test.

Table S3. Differences in photoprotective index and photochemical yield during dark between wild type and Chl-deficient mutant grown and measured in either fluctuating or non-fluctuating light.

	PI	qPd
Plants grown in non-fluctuating light and measured during constant light		
Mutant	0.787 ± 0.003	0.952 ± 0.002
Wild type	0.862 ± 0.004	0.919 ± 0.006
Plants grown in fluctuating light and measured during constant light		
Mutant	0.799 ± 0.005	0.936 ± 0.003
Wild type	0.811 ± 0.009	0.906 ± 0.007
Plants grown in non-fluctuating light and measured during fluctuating light		
Mutant	0.794 ± 0.005	0.955 ± 0.002
Wild type	0.827 ± 0.004	0.906 ± 0.005
Plants grown in fluctuating light and measured during fluctuating light		
Mutant	0.778 ± .004	0.932 ± 0.004
Wild type	0.812 ± 0.004	0.884 ± 0.010

Table S4. SIF_{yield} and Φ_{PSII} during the morning, mid-day and afternoon, measured for all Arabidopsis plant types. This table was presented as Table S2 in: Acebron, K., Matsubara, S., Jedmowski, C., Emin, D., Muller, O., & Rascher, U. Diurnal dynamics of non-photochemical quenching in Arabidopsis *npq* mutants assessed by solar-induced fluorescence and reflectance measurements in the field. *New Phytologist*. 05.Oct.2020

Window	**Col-0**		***npq1***		***npq4***	
	SIF_{yield}	**Φ_{PSII}**	**SIF_{yield}**	**Φ_{PSII}**	**SIF_{yield}**	**Φ_{PSII}**
Morning	4.62 ± 0.23	0.35 ± 0.01	6.51 ± 0.43	0.34^{ns} ± 0.02	6.30 ± 0.37	0.35^{ns} ± 0.01
Mid-day	3.23 ± 0.21	0.32 ± 0.02	4.87 ± 0.01	0.27^{**} ± 0.01	6.51 ± 2.17	0.29^{*} ± 0.01
Afternoon	5.30 ± 1.21	0.51 ± 0.01	4.88 ± 0.10	0.46^{**} ± 0.03	4.85 ± 0.50	0.45^{**} ± 0.02

Test of significance to compare mutant versus wild type: ^{ns}not significant, *0.05α; **0.01α

Table S5. Results of analysis of variance (ANOVA) in Arabidopsis measurements during light induction in controlled condition.

Sources of variation	SS	MS	df	F value	P value
			F_{PAM}		
Type	0.066931	0.033466	2	505.838	< 2.2e-16***
Time (after Induction)	0.209589	0.014971	14	226.283	< 2.2e-16***
Type*Time	0.022048	0.000787	28	11.902	< 2.2e-16***
			NPQ_{PAM}		
Type	58.974	29.4868	2	245.827	< 2.2e-16***
Time (after Induction)	34.934	2.4953	14	20.802	< 2.2e-16***
Type*Time	17.428	0.6224	28	5.189	3.25e-12***
			Φ_{PSII_PAM}		
Type	0.0103	0.00513	2	4.2413	0.01589*
Time (after Induction)	6.3858	0.45613	14	377.2176	< 2e-16***
Type*Time	0.0250	0.00089	28	0.7371	0.82845
			F_{LIFT}		
Type	9046271	4523135	2	2122.739	< 2.2e-16***
Time (after Induction)	15327052	1179004	13	553.315	< 2.2e-16***
Type*Time	2720437	104632	26	49.105	< 2.2e-16***
			NPQ_{LIFT}		
Type	47.878	23.9391	2	13663.43	< 2.2e-16***
Time (after Induction)	16.774	1.2903	13	736.46	< 2.2e-16***
Type*Time	8.123	0.3124	26	178.32	< 2.2e-16***
			Φ_{PSII_LIFT}		
Type	0.009397	0.0046985	2	227.805	< 2.2e-16***
Time (after Induction)	0.161348	0.0124114	13	601.757	< 2.2e-16***
Type*Time	0.013887	0.0005341	26	25.897	< 2.2e-16***

*Test of significance: < 0.001***, < 0.01**, < 0.05**

Table S6. Results of analysis of variance (ANOVA) in Arabidopsis experiment during outdoor measurements on a summer day.

Sources of variation	SS	MS	df	F value	P value
			SIF spectra		
Type	1.0610e-08	5.3044e-09	2	290.86	< 2.2e-16***
Wavelength	8.5403e-07	4.2702e-09	200	234.15	< 2.2e-16***
			F760		
Type	6.7160	3.3580	2	118.7806	< 2.2e-16***
Window	10.8072	1.3509	8	47.7847	< 2.2e-16***
Type*Window	1.5938	0.0996	16	3.5235	8.032e-06***
			F687		
Type	21.380	10.6902	2	153.5142	< 2.2e-16***
Window	42.277	5.2846	8	75.8888	< 2.2e-16***
Type*Window	6.074	0.3796	16	5.4514	3.392e-10***
			$F760_{yield}$		
Type	141.402	70.701	2	31.5900	3.577e-13***
Window	89.240	11.155	8	4.9842	8.195e-06***
Type*Window	75.857	4.741	16	2.1183	0.007741**
			$F687_{yield}$		
Type	444.68	222.341	2	44.6474	< 2.2e-16***
Window	289.34	36.167	8	7.2625	8.185e-09***
Type*Window	202.77	12.673	16	2.5448	0.001068**
			Φ_{PSII}		
Type	0.06253	0.031265	2	51.7550	< 2e-16***
Window	0.58826	0.073532	8	121.7221	< 2e-16***
Type*Window	0.01754	0.001096	16	1.8144	0.03224*
			NPQ		
Type	772.5	386.23	2	2.7400	0.067296
Window	2963.8	370.48	8	2.6282	0.009588**
Type*Window	5113.3	319.58	16	2.2671	0.004974**

*Test of significance: < 0.001***, < 0.01**, < 0.05**

Table S7. Results of analysis of variance (ANOVA) in Arabidopsis experiment during the first day of outdoor measurements on a winter spell.

Sources of variation	SS	MS	df	F value	P value
			F760		
Type	0.6660	0.33301	2	91.6952	< 2.2e-16***
Window	3.9274	0.21819	18	60.0779	< 2.2e-16***
Type*Window	0.6402	0.01778	36	4.8968	4.219e-11***
			F687		
Type	2.2428	1.12141	2	53.3861	< 2.2e-16***
Window	14.5093	0.80601	18	38.3715	< 2.2e-16***
Type*Window	2.3551	0.06542	36	3.1144	2.113e-06***
			$F760_{yield}$		
Type	28.91	14.4557	2	32.4765	1.337e-11***
Window	551.03	30.6128	18	68.7755	< 2.2e-16***
Type*Window	73.13	2.0314	36	4.5638	2.880e-10***
			$F687_{yield}$		
Type	108.43	54.216	2	34.7441	1.431e-12***
Window	923.26	51.292	18	32.8705	< 2.2e-16***
Type*Window	198.28	5.508	36	3.5297	1.434e-07***
			Φ_{PSII}		
Type	0.0293	0.01467	2	29.2694	2.208e-12***
Window	20.7835	1.03917	20	2072.8995	< 2.2e-16***
Type*Window	0.0299	0.00075	40	1.4905	0.03225*
			NPQ		
Type	806.5	403.26	2	14.1934	1.866e-06***
Window	8233.9	433.36	19	15.2527	< 2.2e-16***
Type*Window	3847.5	101.25	38	3.5636	2.680e-10***

*Test of significance: < 0.001***, < 0.01**, < 0.05**

Table S8. Results of analysis of variance (ANOVA) in Arabidopsis experiment during the second day of outdoor measurements on a winter spell.

Sources of variation	SS	MS	df	F value	P value
			F760		
Type	0.00218	0.001092	2	0.5624	0.5719
Window	1.19652	0.041259	29	21.2474	< 2e-16***
Type*Window	0.12804	0.002208	58	1.1368	0.2611
			F687		
Type	0.0206	0.010291	2	0.7458	0.475839
Window	6.6497	0.229301	29	16.6137	< 2.2e-16***
Type*Window	1.3086	0.022561	58	1.6350	0.007719**
			$F760_{yield}$		
Type	1.298	0.6489	2	0.8981	0.41023
Window	225.924	7.7905	29	10.7863	< 2e-16***
Type*Window	55.673	0.9599	58	1.3286	0.08208
			$F687_{yield}$		
Type	2.879	1.4397	2	0.5092	0.6018
Window	310.539	10.7082	29	3.7876	1.943e-08***
Type*Window	148.459	2.5596	58	0.9054	0.6641
			Φ_{PSII}		
Type	0.0351	0.01754	2	20.5450	1.623e-08***
Window	4.0611	0.40611	10	475.5970	< 2.2e-16***
Type*Window	0.0229	0.00115	20	1.3429	0.1573
			NPQ		
Type	131.93	65.966	2	340.477	< 2.2e-16***
Window	461.12	46.112	10	238.002	< 2.2e-16***
Type*Window	138.31	6.916	20	35.694	< 2.2e-16***

*Test of significance: < 0.001***, < 0.01**, < 0.05**

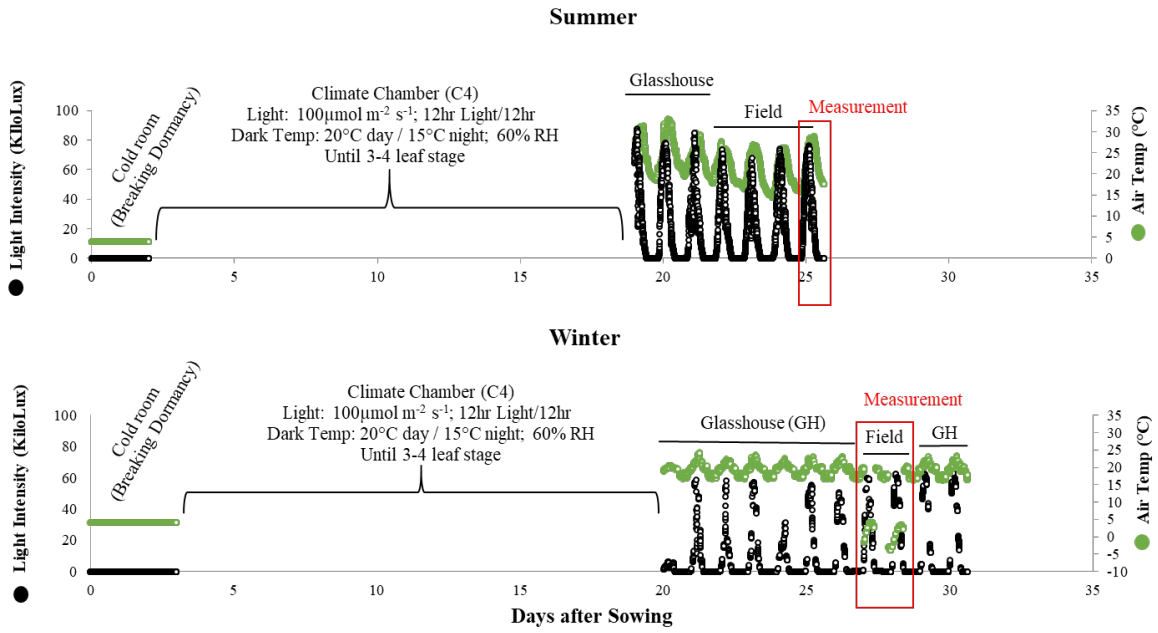

Fig. S1. Growing conditions of the Arabidopsis WT_{At} and *npq* mutants before field measurements in summer and winter conditions. Seeds were germinated inside the controlled climate chamber until ~ 20 days after sowing then transferred to the glasshouse to grow and field condition during measurement.

This image was borrowed from Figure S3 in: Acebron, K., Matsubara, S., Jedmowski, C., Emin, D., Muller, O., & Rascher, U. Diurnal dynamics of non-photochemical quenching in Arabidopsis *npq* mutants assessed by solar-induced fluorescence and reflectance measurements in the field. *New Phytologist*. 05.Oct.2020

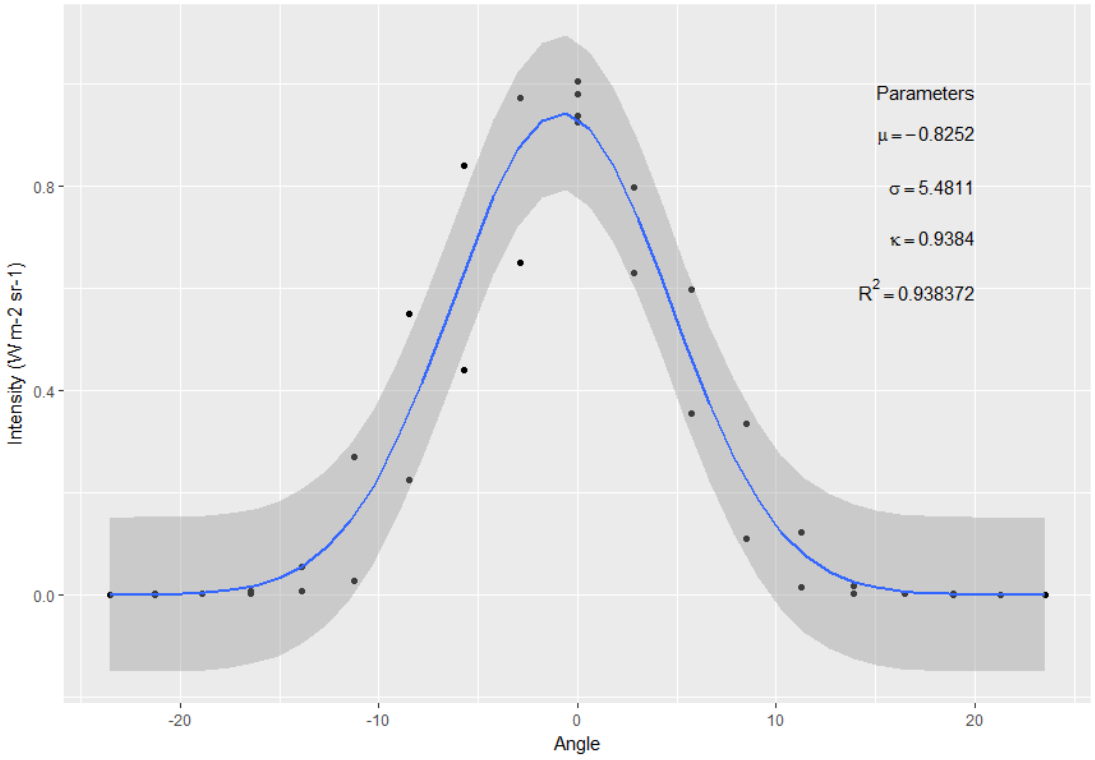

Fig. S2. Field of view of the Fluorescence Box (FLOX) instrument at 5 cm distance on top of the target.

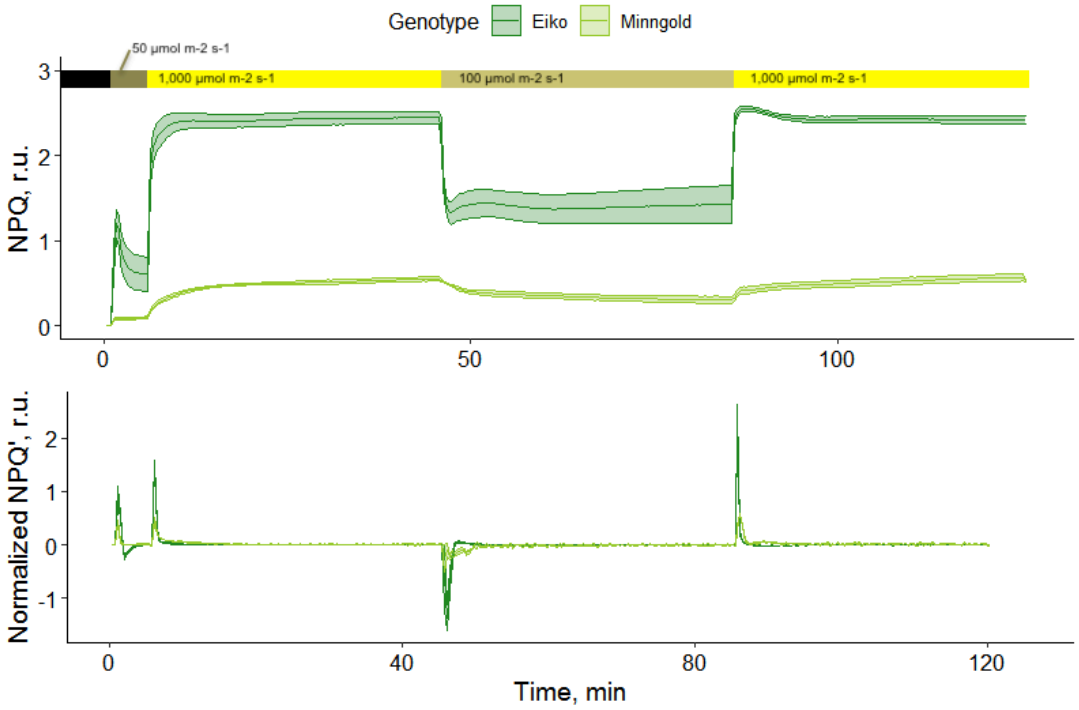

Fig. S3. Adjustments of non-photochemical quenching (NPQ) and the derivative of normalised NPQ during light intensity change comparing wild type (Eiko) and mutant (Minngold), measured after drought stress.

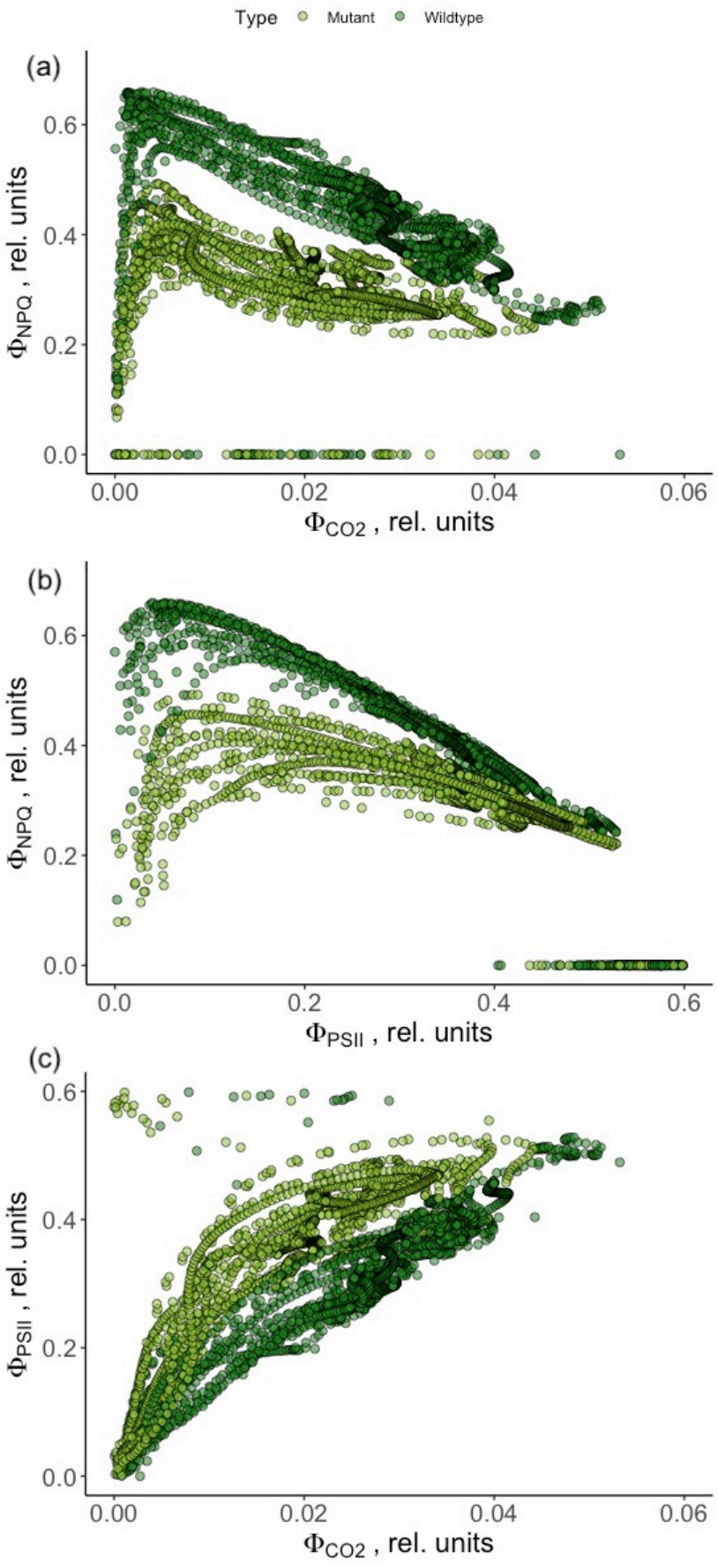

Fig. S4. Relationships between (a) Φ_{CO2} and Φ_{NPQ}, (b) Φ_{PSII} and Φ_{NPQ}, and (c) Φ_{CO2} and Φ_{PSII} during photosynthetic inductions using constant and fluctuating light conditions.

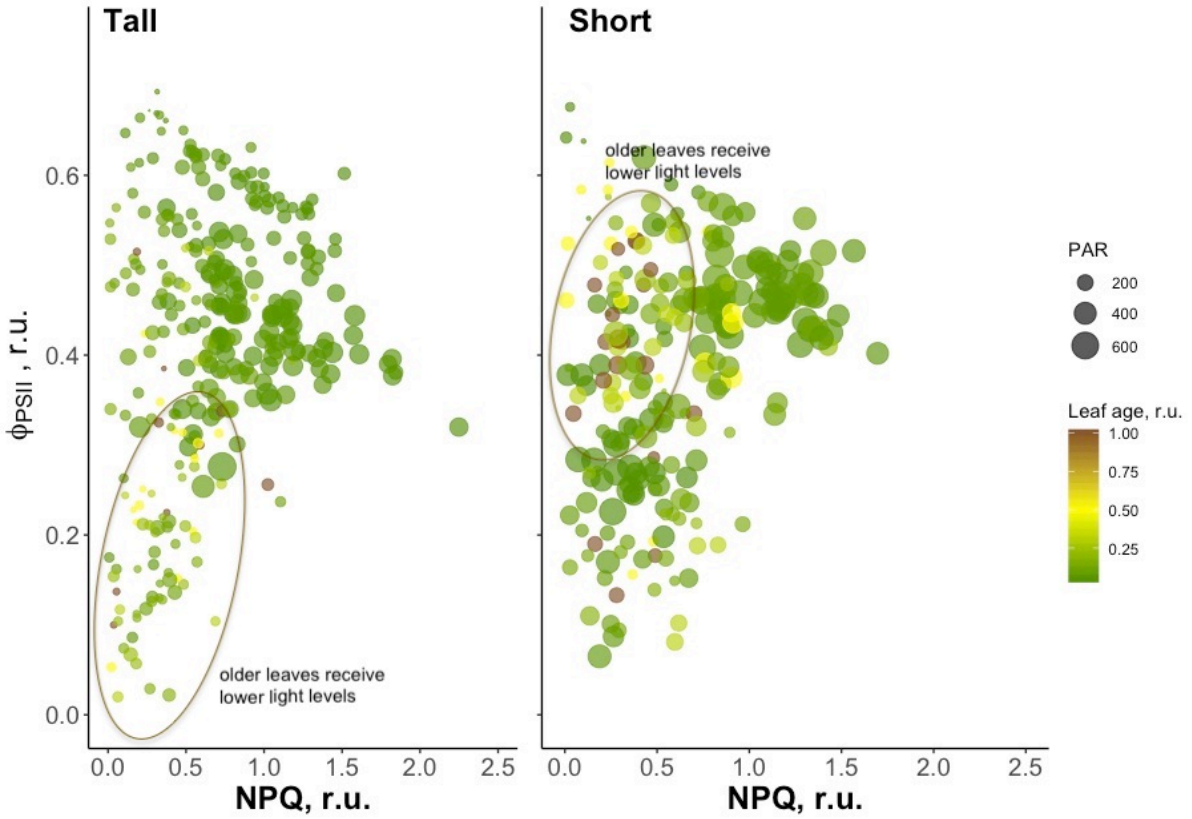

Fig. S5. Relationship between non-photochemical quenching (NPQ) and the efficiency of photosystem II (Φ_{PSII}) measured in individual leaf parts on a canopy of multiple cassava plants. Measurement was conducted inside the glasshouse using miniPAM (Walz, Germany) where the plants are grown and the leaves are undisturbed to its original angle and position inside the canopy. The size of each points represents the incoming photosynthetically active radiation (PAR) while the color gradient represents the relative age of the leaf (where 0.25 is young on top of canopy and 1.00 is old and on base of the canopy).

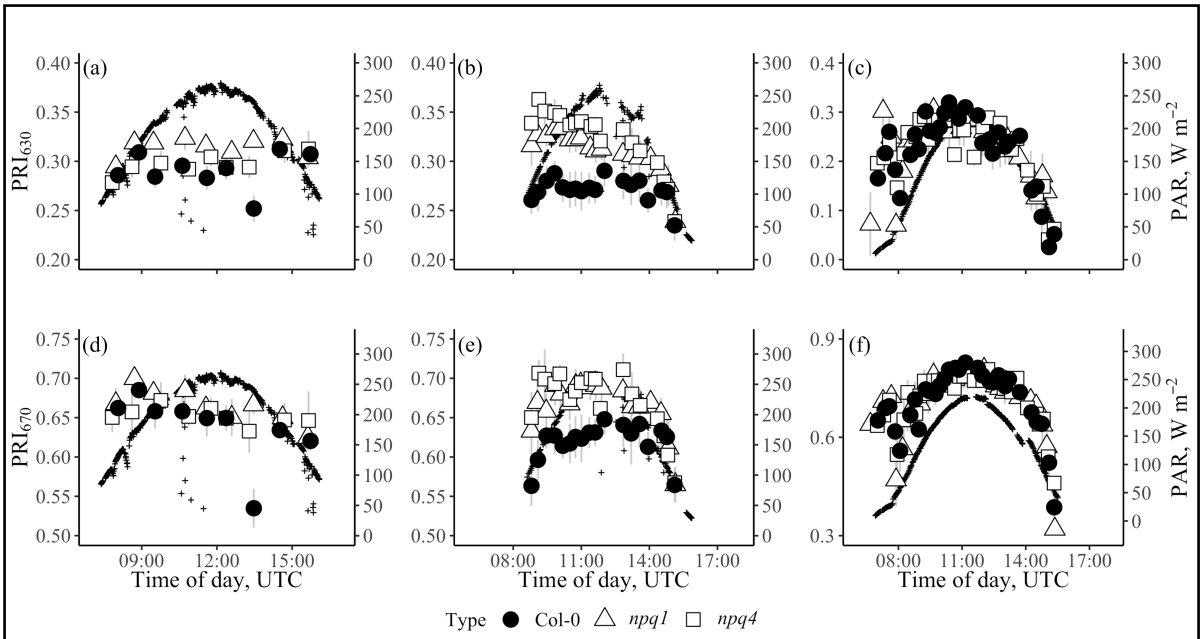

Fig. S6. Diurnal pattern of photochemical reflectance index (PRI) calculated using either (a, b, c) 630 nm or (d, e, f) 670 nm as reference band. Calculation for $PRI_{630} = (\rho_{531} - \rho_{630}) / (\rho_{531} + \rho_{630})$ and $PRI_{670} = (\rho_{531} - \rho_{670}) / (\rho_{531} + \rho_{670})$ where based on Gamon et al. (1992). Measurements were done in the (a, d) summer and winter spell during (b, e) day 1 and (c, f) day 2. Values are average ± the standard error of three to four plants per genotype.

This image is borrowed from Figure S8 in: Acebron, K., Matsubara, S., Jedmowski, C., Emin, D., Muller, O., & Rascher, U. Diurnal dynamics of non-photochemical quenching in Arabidopsis *npq* mutants assessed by solar-induced fluorescence and reflectance measurements in the field. *New Phytologist*. 05.Oct.2020

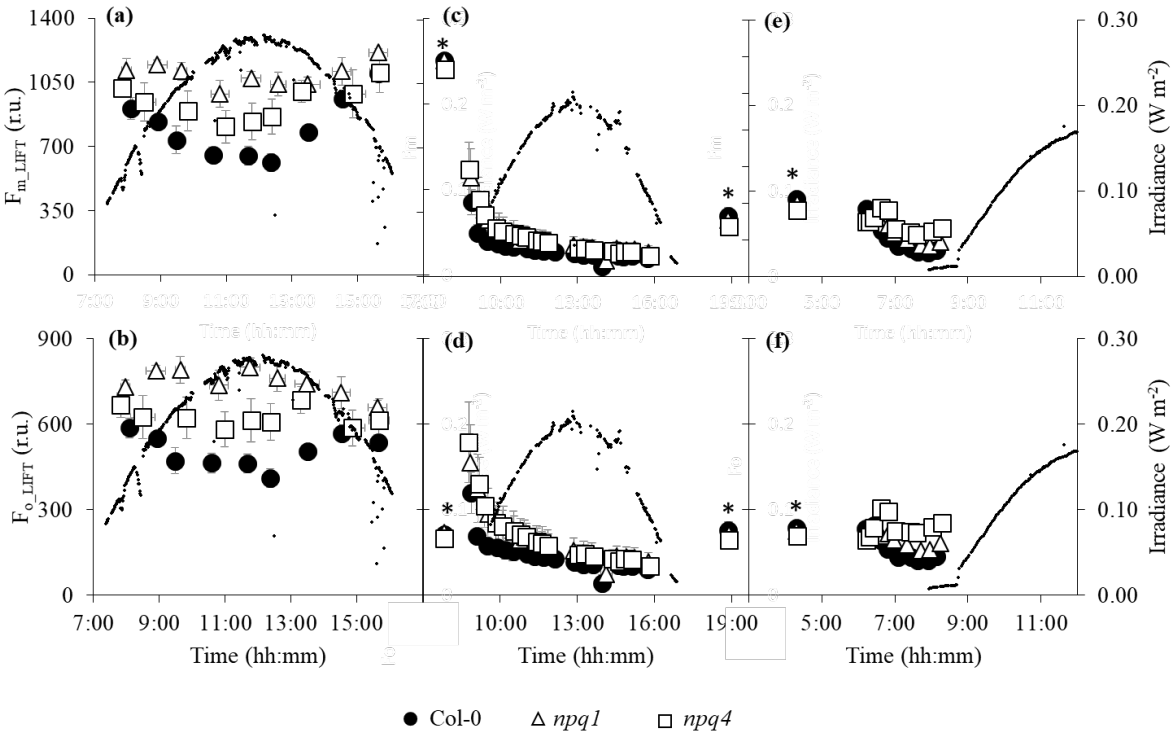

Fig. S7. Diurnal trend of active fluorescence parameters measured in summer (left side) and winter field conditions (middle panel relates to day 1; right side relates to day 2). Data points with asterisks are measurements relating to dark-adapted plants in glasshouse conditions.